NASA CONTRACTOR REPORT

NASA CR-2225

NASA CR-2225

ANALYSIS OF HELICOPTER MANEUVER-LOADS AND ROTOR-LOADS FLIGHT-TEST DATA

by Edward A. Beno

Prepared by
SIKORSKY AIRCRAFT DIVISION
UNITED AIRCRAFT CORPORATION
Stratford, Conn. 06602
for Langley Research Center

NATIONAL AERONAUTICS AND SPACE ADMINISTRATION • WASHINGTON, D. C. • MARCH 1973

1. Report No.	2. Government Accession No.	3. Recipient's Catalog No.
NASA CR-2225		

4. Title and Subtitle	5. Report Date
ANALYSIS OF HELICOPTER MANEUVER-LOADS AND ROTOR-LOADS FLIGHT-TEST DATA	March 1973
	6. Performing Organization Code
7. Author(s)	8. Performing Organization Report No.
Edward A. Beno	
	10. Work Unit No.
9. Performing Organization Name and Address	
Sikorsky Aircraft Division United Aircraft Corporation Stratford, CT	11. Contract or Grant No. NAS1-11049
	13. Type of Report and Period Covered
12. Sponsoring Agency Name and Address	Contractor Report
National Aeronautics and Space Administration Washington, D.C. 20546	14. Sponsoring Agency Code

15. Supplementary Notes

16. Abstract

A study was conducted in which available airload and blade response data for the NH-3A and CH-53A rotors were analyzed in an attempt to provide greater insight into the sources of rotor vibratory loads in both level and maneuvering flight. Primary emphasis in the study was placed on examining and understanding causes of high-frequency rotor control loads. Secondary objectives were (1) to examine the effect of number of rotor blades on hub vibratory shear forces and (2) to assess which of the many terms appearing in the hub vibratory shear force expression were of most significance.

17. Key Words (Suggested by Author(s))	18. Distribution Statement
Helicopter rotor Airloads Control loads Maneuver loads	Unclassified - Unlimited

19. Security Classif. (of this report)	20. Security Classif. (of this page)	21. No. of Pages	22. Price*
Unclassified	Unclassified	93	$3.00

*For sale by the National Technical Information Service, Springfield, Virginia 22151

TABLE OF CONTENTS

ANALYSIS OF HELICOPTER MANEUVER-LOADS AND ROTOR-LOADS FLIGHT-TEST DATA

By Edward A. Beno
Sikorsky Aircraft Division
United Aircraft Corporation

SUMMARY

A study was conducted in which available airload and blade response data for the NH-3A and CH-53A rotors were analyzed in an attempt to provide greater insight into the sources of rotor vibratory loads in both level and maneuvering flight. Primary emphasis in the study was placed on examining and understanding causes of high-frequency rotor control loads. Secondary objectives were (1) to examine the effect of number of rotor blades on hub vibratory shear forces and (2) to assess which of the many terms appearing in the hub vibratory shear force expressions were of most significance.

Although stall flutter is probably a major contributor to high-frequency control load oscillations when operating well above the knee of the control load curve, it was found for the less stalled conditions analyzed in this study that the principal high-frequency control load cause appears to be a forced dynamic response of the blade to the time varying aerodynamic moment. Other factors previously considered to be potentially important, such as moments induced by blade/tip-vortex interactions or blade bending, were generally small for the conditions studied.

Analysis of the hub vibratory shear forces indicated that the nondimensionalized force harmonics for the six-bladed rotor were generally higher than those for the five-bladed rotor. Care must be exercised in generalizing this result, however, inasmuch as detailed blade dynamic characteristics (e.g. natural frequencies) undoubtedly influence the comparison. Finally, a review of the equations used to compute hub vibratory forces from measurements of blade root dynamic response indicates that many of the dynamic correction terms due to motion of the hub, blade cuff, and instrumented blade segment can be neglected.

INTRODUCTION

One of the current problems facing helicopter rotor designers is the flight envelope limitations imposed by high-speed and maneuvering flight conditions where high vibratory control loads are encountered. Expansion of the envelope may be possible if the source or sources of these vibratory loads can be established and accurate methods validated for their prediction.

Previous investigators have studied this problem including analysis of the effects of stall flutter, rotor inflow, and unsteady aerodynamics. The

present study sought an explanation of the cause of the vibratory control loads measured on the NH-3A and the CH-53A, and the ability of available analytical methods to predict the measured blade response. References 1 and 2 have concluded that retreating blade oscillations can be the result of a complicated series of dynamic and aerodynamic events. Reference 3 postulated the source of high oscillatory control loads to be a wake-induced forced response of the torsional degree-of-freedom. Vortex crossings in the wake were shown to have a direct correspondence with measured retreating blade c_m oscillations. The study reported herein investigated torsional response utilizing in-flight data previously measured on the NH-3A and the CH-53A. Reference 4 describes the measurement program on the NH-3A. The CH-53A data were acquired during a previous flight test program funded by the Naval Air Systems Command under Contract NOw 63-0150-f, CO-40 (63-0150) and CO-40R1 (63-0150).

Included in the present study was an analysis of the measured maneuvering and high-speed blade azimuthal responses. Analysis was limited to a relatively few rotor revolutions of flight data. An understanding of the source of retreating blade torsional oscillations was sought and measured blade response was correlated with analytical calculations.

A secondary investigation covers an examination of the vibratory rotor loads on both the NH-3A and the CH-53A. Methods were sought from which the rotating blade hinge force harmonics and the non-rotating vibratory hub forces could be approximated with good accuracy from measurements at the root of one blade. Comparisons of the hinge force harmonics were made between two rotor systems having a different number of blades.

Robert H. Blackwell, Jr., Sikorsky Aircraft Division, United Aircraft Corporation, assisted in performing the correlation of test data with analysis.

SYMBOLS

Values are given in both the International System of Units (SI) and U. S. Customary Units. The measurements and calculations were made in U. S. Customary Units.

b	number of main rotor blades
c	blade chord, m (in.)
c_m	section pitching moment coefficient, $\frac{m}{\frac{1}{2}\rho c^2[\Omega R(r/R + \mu\sin\psi)]^2}$
c_n	section loading coefficient, $\frac{\ell}{\frac{1}{2}\rho c[\Omega R(r/R + \mu\sin\psi)]^2}$
C_T/σ	rotor thrust coefficient/solidity ratio
C.I.	constant inflow analysis

e	blade offset, m (in.)
F_X	longitudinal rotor hub force, N (lb)
F^*_x	radial blade hinge force, N (lb)
F_{xl}	blade radial force at inboard end of instrumented segment, N (lb)
F_Y	lateral rotor hub force, N (lb)
F^*_y	edgewise blade hinge force, N (lb)
F_Z	vertical rotor hub force, N (lb)
F^*_z	vertical blade hinge force, N (lb)
f/f_c	frequency relative to cutoff
G_i	Gaussian coefficients
I_y	mass moment of inertia of instrumented segment about flapping axis, N-m-sec^2 (lb-in.-sec^2)
I_z	mass moment of inertia of instrumented segment about lag axis, N-m-sec^2 (lb-in.-sec^2)
J	blade torsional mass moment of inertia, N-m-sec^2 (lb-in.-sec^2)
K_i	section aerodynamic pitching moment factors, m^2 (in.^{2})
k_T	blade root torsional spring constant, N-m/rad (in.-lb/rad)
ℓ	section normal loading, N/m (lb/in.)
M_x	root torsional structural moment, N-m (in.-lb)
$M_{x,a}$	aerodynamic pitching moment, N-m (in.-lb)
$M_{x,T}$	model root torsional structural moment, N-m (in.-lb)
M_y	blade flatwise bending moment, N-m (in.-lb)
M_z	blade edgewise bending moment, N-m (in.-lb)
$M_{1.0,90}$	advancing blade tip Mach number ($r/R = 1.0$, $\psi = 90$ deg)
m	section aerodynamic pitching moment, N-m/m (in.-lb/in.)
m_c	blade mass inboard of instrumented segment, kg (lb-sec^2/in.)
m_{IS}	blade instrumented segment mass, kg (lb-sec^2/in.)

n/rev	frequency of n-th harmonic, i.e., n times the main rotor frequency
p	absolute pressure, N/m^2 (psia)
$p_{\infty,h}$	free stream static pressure, N/m^2 (psia)
R	rotor radius, m (in.)
r	blade radial location, m (in.)
T	modal contribution of aerodynamic pitching moment, N-m (in.-lb)
V	forward airspeed, m/sec (kn)
V.I.	variable inflow analysis
X1,X2,..	symbolic blade radial hinge force terms (see table II)
x_B	radial coordinate in blade axis system of center of gravity of instrumented segment, m (in.)
x_{B-1}	radial distance, in blade axis system, from inboard end of instrumented segment to center of gravity of instrumented segment, m (in.)
x_c	radial coordinate, in blade axis system, of center of gravity of mass inboard of instrumented segment, m (in.)
x_R	rotor head displacement in shaft rotating system radial direction, m (in.)
Y1, Y2,..	symbolic blade edgewise hinge force terms (see table II)
y	blade chordwise location measured from leading edge, m (in.)
y_c	edgewise coordinate, in blade axis system, of center of gravity of mass inboard of instrumented segment, m (in.)
y_R	rotor head in-plane displacement in shaft rotating system perpendicular to hub radial direction, m (in.)
Z1,Z2,..	symbolic blade vertical hinge force terms (see table II)
z_c	vertical coordinate, in blade axis system, of center of gravity of mass inboard of instrumented segment, m (in.)
z_R	rotor head vertical displacement in shaft rotating system, m (in.)
β	blade root flapping angle, deg
γ	blade root lag angle, deg

Δp	differential pressure, N/m^2 (psi)
Δx	radial length of blade instrumented segment, m (in.)
ζ	damping ratio
θ	blade root pitch angle, deg
θ_T	blade root torsional elastic twist, deg
μ	advance ratio, $\frac{V}{\Omega R}$
ρ	mass density of air, kg/m^3 ($lb\text{-}sec^2/in.^4$)
ϕ_n	phase angle associated with n-th harmonic, deg
ψ	blade azimuth angle, deg
Ω	rotor angular velocity, rad/sec
ω_T	blade torsional natural frequency, rad/sec

Subscripts:

$( )_c$	cosine component of harmonic
$( )_{MT}$	refers to summation of major terms
$( )_n$	n-th harmonic order
$( )_s$	sine component of harmonic
$( )_1$	at the inboard end of the blade instrumented segment
$( )_3$	at the outboard end of the blade instrumented segment
${}_5( )$	refers to 5-bladed NH-3A rotor system
${}_6( )$	refers to 6-bladed CH-53A rotor system

Miscellaneous:

$(\dot{})$	first derivative with respect to time
$(\ddot{})$	second derivative with respect to time

DATA ACQUISITION AND REDUCTION

The data analyzed in the study reported herein were measured during pre-

vious NH-3A and CH-53A flight test programs. The flight tests were primarily performed to acquire data describing the aerodynamic and dynamic characteristics of each aircraft.

The NH-3A is a compound helicopter capable of not only high forward speeds but also of varying rotor lift and drag. Two auxiliary turbojet engines and a wing including a full-span flap provide the aircraft with these capabilities. The 18.90 m (62 ft) diameter main rotor is a 5-bladed fully articulated system. The -4 deg twisted blades have a modified NACA 0012 airfoil section. Normal gross weight is 8560 kg (18900 lb). A photograph of the NH-3A is included as figure 1.

The CH-53A, a high speed assault transport helicopter, is capable of flight at higher gross weights than is the NH-3A. The aircraft was flown at both 15860 kg (35000 lb) and 19040 kg (42000 lb) gross weights. The 6-bladed fully articulated CH-53A main rotor has a diameter of 21.95 m (72 ft) and the -6 deg twisted blades have a modified NACA 0011 airfoil section. The CH-53A is shown in figure 2.

Instrumentation

An airborne data acquisition system was used to record the aerodynamic and dynamic characteristics of each aircraft. Approximately one hundred channels of data were recorded on a magnetic tape recording system installed in the cabin of the aircraft. This narrow band system provided a continuous frequency modulation multiplexed recording of each measurement. Signal conditioning of the multiplexed output signal was performed before the data were actually recorded on the tape transport. Quasi-static data describing the recorded flight condition were provided on 35 mm film that recorded photopanel measurements. The photopanel measurements included airspeed, altitude, rate of climb, rotor angular velocity, ambient atmospheric conditions, and aircraft attitude. A complete description of the instrumentation and data acquisition methods used is included in reference 4.

A dynamic data sampling signal, used for time reference, was provided in the aircraft by a rotor azimuth pulse generator which divided a main rotor revolution into 5 deg increments. A slotted disc and optical system mounted on the bottom of the main rotor shaft provided this 72/rev signal plus a 1/rev pulse used as the 0 deg azimuth reference. This corresponds to the instrumented main rotor blade aligned over the aircraft tail.

A block diagram of the airborne recording system used on the CH-53A is shown in figure 3. Basically the same system was utilized to record the NH-3A data. The measured blade response data used in the study reported herein include blade pressures; flatwise, edgewise, and torsional bending moments; and pushrod loads. The distribution of the miniature absolute and differential pressure transducers on the instrumented blade is given in figure 4. Absolute pressure transducers were used on the upper and lower surfaces of the blade spar while differential gages were installed through the blade pockets and tip cap. Bending moment measurements were distributed along the blade span to re-

cord the response of the blade.

Data Processing

The primary objective of this program was to perform a detailed analysis of a limited number of rotor revolutions of important flight data. The emphasis was on high-speed and maneuvering flight conditions for both the NH-3A and the CH-53A. The maneuvering conditions considered in this program were comprised of banked right-turn regimes. Left turn data were not available. For the NH-3A, the measured data were acquired only during the actual steady-state period of each banked turn. The available CH-53A right-turn conditions, however, included data measured in the trimmed level flight regime, through a transition period, and finally during the actual steady-state portion of the coordinated turn. Therefore, the NH-3A data cycle studied for the turns consisted only of a rotor revolution during the actual banked turn. For the CH-53A maneuver, three separate cycles were investigated; trimmed level flight, transition, and steady-state coordinated banked turn. Table I describes each of the data cycles investigated in the high-frequency blade response part of this study. Case numbers refer to those used in reference 4 and earlier CH-53A studies.

Processing of the measured data was initiated by the formation of oscillograph traces from the flight test magnetic (analog) tapes. These records were arranged to include the 1/rev and 72/rev signals required for subsequent data reduction. In order to retain possible high-frequency response of the test data, a filtering cut-off frequency of 100 Hz was utilized during the generation of the oscillograph rolls. This had the effect of filtering out unwanted signal noise above 100 Hz while retaining real signal response at frequencies up to approximately 30/rev, depending on the rotor angular velocity. The signal amplitude response using the low pass filters having a cut-off frequency of 100 Hz is shown in figure 5.

Selection of the particular cycles of data to be used in the high-frequency blade response study were chosen by manual scanning of the oscillograph traces. For maneuvers and high-speed conditions the cycles chosen within each regime, described in table I, were selected primarily on the basis of their high-frequency torsional response content. For these cycles the oscillograph roll data for each required measurement were reduced to punch card form.

The 72/rev signal included on the traces was used as a time step interval at which the data were punched into cards. Each parameter was punched as a 73 point time history corresponding to a 0 to 360 deg rotor azimuth period (5 deg azimuth interval). Along with the actual dynamic data for each measurement, calibration factors from the traces were also punched on the cards for later use in conversion of the machine units to engineering units. The dynamic data and calibration factors on the punch cards were input to a computer program for final processing.

A secondary study included in this report was an analysis of main rotor loads. Basic objectives were to determine the major dynamic terms that contribute to harmonics of blade hinge forces and b/rev hub loads and the effect of

the number of main rotor blades on harmonics of the hinge forces. This was accomplished by an analysis of the existing data measured during the flight programs on the NH-3A and CH-53A. Cases were chosen from the available data to cover a wide range of operating conditions.

Data Analysis Methods

Digital computer programs were utilized for final processing of the measured flight-test data. The blade pressure, bending moment, and pushrod load data punched on cards from the oscillographs were converted to engineering units and listed by one program. A second digital program was used during the original flight-test programs to calculate the blade hinge forces and nonrotating b/rev hub loads. From the measured data, the separate dynamic terms contributing to these loads could be calculated by an option in this program.

With laboratory and aircraft calibration factors, along with the oscillograph conversion factors punched on the cards, the machine unit blade response data on punched cards were first converted to engineering unit data by a computer program. This procedure gave the azimuthal history of the measured parameters including response at frequencies up to 100 Hz (filtering cut-off frequency). For each aircraft, 33 measurements were listed in this form. These included 24 blade absolute and differential pressures at 75, 85, and 95 percent radial stations; 3 flatwise bending moments; 3 edgewise bending moments; 2 torsional moments; and the pushrod load. At stations where two absolute pressure transducers were mounted, on the upper and lower blade surfaces, the differential pressure time histories were also calculated. At each of the three blade radial stations the measured chordwise distribution of pressure was then utilized to calculate the blade section loading (airload) and aerodynamic pitching moment time histories. The five chordwise pressure stations were at 4.2, 15.8, 30.0, 60.0, and 91.0 percent of chord. A Gaussian integration scheme was used to calculate the time history of blade airload from the relation

$$\ell_\psi = c \sum_{i=1}^{5} (\Delta p)_{i,\psi} G_i \qquad (1)$$

where G_i are the Gaussian coefficients for the five chordwise stations from G_1 corresponding to 4.2 percent chord to G_5 at 91.0 percent chord. The coefficients are $G_1 = 1/10$, $G_2 = 1/10$, $G_3 = 2/9$, $G_4 = 16/45$, and $G_5 = 2/9$. The aerodynamic pitching moment about the blade feathering axis was also calculated from the pressures utilizing a trapezoidal distribution between the measured pressures. Leading- and trailing-edge differential pressures were assumed to be zero. The relationship for calculation of the pitching moment is

$$m_\psi = \sum_{i=1}^{5} (\Delta p)_{i,\psi} K_i \qquad (2)$$

where K_i are blade geometry factors corresponding to the five chordwise stations

from K_1 at 4.2 percent chord to K_5 at 91.0 percent chord. For each aircraft the factors are

Factor	NH-3A		CH-53A	
	m^2	$in.^2$	m^2	$in.^2$
K_1	3.11×10^{-3}	4.82	6.32×10^{-3}	9.79
K_2	2.31	3.58	4.69	7.27
K_3	-4.88	-7.56	-9.90	-15.34
K_4	-23.16	-35.89	-47.00	-72.85
K_5	-25.21	-39.08	-51.17	-79.32

From the section loading and aerodynamic pitching moments calculated in equations (1) and (2), the azimuthal histories of section loading and pitching moment coefficients were calculated.

The digital computer program used to calculate the dynamic terms contributing to the blade hinge forces and b/rev hub loads is described in detail in reference 4. The Root Response Method is programmed to calculate azimuthal histories of the blade hinge forces from measurements made at the root of the blade. These include flatwise and edgewise bending moments, blade tension, blade root angles, and accelerations at the blade hinge. The resulting equations, given in reference 4 include a large number of dynamic terms in each of the three orthogonal hinge forces: radial, F_x^*; edgewise, F_y^*; and vertical, F_z^*. These terms are harmonically analyzed. Assuming each main rotor blade encounters the same loads azimuthally as the instrumented blade, the non-rotating system b/rev loads are then calculated. This computer program provided the calculation of the separate terms required to determine the major terms contributing to the hinge forces and non-rotating loads. This program also provided comparisons of the effects of the number of blades on these loads for both the NH-3A and CH-53A measured data.

ANALYSIS OF HIGH-FREQUENCY BLADE RESPONSE

The output of the digital computer program used to process the test data read from oscillograph traces provided the basis for a timewise study of high-frequency blade torsional response. It also made possible comparisons of different conditions and different aircraft. Azimuthal time history plots referred

to in subsequent sections of the report are of two forms. Plots of level-flight conditions given in table I indicate an azimuthal range from 0 to 400 deg. For these plots the first 40 deg of the rotor revolution have been repeated to enable better visualization of any high-frequency blade response oscillations occurring near the tail region of the aircraft. Maneuvering conditions are plotted only from 0 to 360 deg since for these regimes, the 0 and 360 deg azimuth values are generally different.

Factors Affecting Blade Torsional Response

The occurrence and magnitude of high-frequency blade torsional oscillations was a primary objective of this study. To determine the effect of the operating condition on this response, various conditions were compared. Of specific interest was the buildup of loads either at high airspeeds or during maneuvering conditions. Analysis of the measured blade response included studies of blade pressures, section loading coefficients, section pitching moment coefficients, blade/tip-vortex wake interactions, blade bending, and aerodynamic pitching moments. The effects of these parameters on blade torsional response are discussed in the following sections.

Effects of airspeed. - The effects of airspeed on the response of the NH-3A blade are shown in figure 6. On the advancing side of the rotor disc the section loading coefficient, c_n; section pitching moment coefficient, c_m; and the root torsional moment, M_x, are basically unaffected by a change in airspeed. On the retreating side, however, moderately higher c_n and c_m amplitudes generally exist at the higher airspeed but the frequency content is the same. The change in M_x is considerably different than that in c_n and c_m due to increased airspeed. While the steady value of the root torsional moment remains approximately the same, there is a large increase in the vibratory content. The frequency of the oscillations is between 6/rev and 7/rev which corresponds to the blade torsional natural frequency of 6.6/rev for the operating conditions shown in figure 6. The measured pushrod loads for these conditions similarly indicate a buildup of the retreating blade oscillations at the same frequencies.

Effects of maneuvers. - To determine the effects of maneuvering flight on blade response, CH-53A cases 41LF (level flight), 41 TR (transition into a banked turn), and 41 TN (steady-state banked turn at a 60 deg angle of bank) were investigated. These effects are shown in figures 7, 8, and 9. An increase in the steady value of c_n can be noted in the typical data, shown at $r/R = 0.85$ in figure 7, as the aircraft progresses from level flight, through a transition period, and finally into the 2g coordinated turn. This corresponds to increased rotor thrust required to maintain attitude. Also shown is an increase in high-frequency content in the first and fourth quadrants of rotor azimuth for the turn. This is due to an increased effect of the instrumented blade passing closer to the trailing vortices shed from preceding blades. Larger magnitude oscillations occur in the fourth quadrant compared to those in the first.

Typical of the spanwise distributions for the same CH-53A maneuvering conditions, are the section pitching moment coefficients at $r/R = 0.85$ given in figure 8. Compared to level flight, the steady values of c_m are not appreciably affected by the maneuvering conditions, but a definite increase in the higher

harmonic content is evident. The advancing side of the rotor disc experiences several oscillations of very high frequency, above 30/rev, which also are probably due to blade vortex crossings in the wake. In the vicinity of 270 deg azimuth there is a growth of one small amplitude oscillation during level flight, into a short duration high amplitude spike during transition, and finally into two separate high magnitude fluctuations in the turn cycle. Along with the generation of the two spikes near ψ = 270 deg, a third large amplitude fluctuation appeared in the region over the aircraft tail during the turn. Although instrumentation attitude limitations prevented knowledge of the exact rotor orientation with respect to the free stream during turns, it is believed that the large amplitude c_m variations are due to vortex crossing effects. Examination of the measured blade pressures at r/R = 0.85 indicates that large excursions in the differential pressure at the 4.2 percent chord station were the cause of the corresponding c_m fluctuations. These are discussed in a subsequent section of this report.

The c_m data shown in figures 6 and 8 have indicated a steady leading edge up condition existing for both the NH-3A and CH-53A conditions. Steady c_m values calculated from measured pressures vary between 0.02 and 0.04. Existing standard NACA 0011 and 0012 steady and unsteady airfoil data, references 5 and 6, indicate that these positive steady values are unattainable over the angle of attack and Mach-number environment experienced in the flight conditions. The basic NH-3A blade has a modified 0012 airfoil and a modified 0011 airfoil is used on standard CH-53A blades. However, both of the test instrumented blades had chordwise epoxy fairing bands covering the area around the surface mounted pressure transducers and a spanwise fairing over the instrumentation wiring to the root of the blades. Details of the application and extent of these fairings are given in reference 4. It is possible, therefore, that these fairings, which had the effect of making the airfoil section unsymmetrical, may be the source of resulting leading edge up pitching moments on the blade.

The existence of the positive pitching moments is also indicated in the measured blade root torsional moments shown in figure 9. Increased harmonic content is also evident in the torsional moment as the steady-state turn cycle is attained. The high amplitude retreating blade torsional moment oscillations during the turn do not indicate a direct correlation with the c_m fluctuations shown in figure 8 due to variations of the c_m distribution along the blade. The root torsional moment measurement records the integrated effect of loadings along the entire blade length.

Effects of blade/tip-vortex wake interactions. - For 4-bladed H-34 maneuvering conditions, reference 3 indicated that a direct correlation existed between high-frequency retreating blade oscillations and the passage of each blade by the tip vortices generated by preceding blades. In the present study, the available cases were investigated to determine whether this interaction existed for the 5-bladed NH-3A or the 6-bladed CH-53A. It should be noted that the number of blades and the advance ratio can affect the frequency and strength of the blade loads induced by the blade/vortex interactions. Also the sensivity of a given blade design to such periodic excitation will, of course, depend on the blade natural frequencies.

The non-distorted helical pattern of the blade tip vortex trajectories is shown in figure 10 for NH-3A case 72. Shown is a view from above and perpendicular to the rotor tip path plane. Indicated in the figure are the plan view intersections of the 95 percent blade station with the wake pattern formed from the tip vortex of each blade. Three of these crossings occur in the fourth rotor quadrant and six in the first quadrant. These intersections represent possible blade/wake interactions, but the proximity of the blade and the tip vortices, along with the circulation strength, depend on the rotor orientation with respect to the free stream and the wake inflow velocities.

The azimuthal histories of blade differential pressures at 75, 85, and 95 percent radial stations are shown in figures 11, 12, and 13 for NH-3A case 72. Included within the plots are the azimuthal locations of possible blade/wake interactions determined from the helical wake pattern shown in figure 10. Indicated are the intersections of the tip vortices with the blade radial station corresponding to the plotted blade pressures. These locations also indicate the directional sense of the tip vortex tangential velocity as the instrumented blade approaches. Figures 11, 12, and 13 do not indicate, for NH-3A case 72, any strong correlation between the possible first quadrant vortex crossings and the pressure response. In general the pressure variations across the chord appear to behave similarly except at the 30.0 percent, and to a lesser extent at the 15.8 percent, chord station on the advancing blade at 85 and 95 percent radial stations. These fluctuations, in the general shape of a square wave, appear to be due to a critical Mach-number effect which will be discussed in the succeeding report section. They are not believed to be the result of any blade/wake intersections. On the retreating side of the disc there is evidence of probable vortex crossing effects, the strongest occurring at approximately 280 deg azimuth where relatively rapid pressure fluctuations correspond to a possible crossing at the same time. However, other lower frequency pressure oscillations occur where vortex crossings do not appear to exist, such as those that initiate at the 85 and 95 percent blade stations over the nose of the aircraft. Vortex crossings are unlikely in this region since, as can be seen in figure 10, the blades are approaching undisturbed air.

Based on the pressures shown in figures 11, 12, and 13, the NH-3A right turn at a 60 deg angle of bank does not appear to exhibit a strong correlation between the possible blade/vortex crossings and the measured pressure response. However, this maneuver condition did display a limited effect while the steady state level flight conditions that were analyzed did not exhibit any noticeable effect of the blade/vortex crossings.

In figure 14, the c_n and c_m time histories, calculated from the measured pressures at $r/R = 0.95$, shown in figure 13, are plotted along with the torsional moment measured at the root of the blade. Included in the c_m plot are the possible vortex crossings with the 95 percent blade radial station determined from the plan view of the non-distorted tip vortex trajectories. No appreciable oscillations occur in c_n or c_m on the advancing blade other than one near $\psi = 40$ deg which is attributable to the critical Mach-number effect discussed in the following section. On the retreating side, however, several oscillations occur in both c_n and c_m, two of which agree fairly well in phase with vortex crossings at 287 and 317 deg azimuth. Comparison of the measured

root torsional moment in figure 14 with the azimuthal locations of possible blade/vortex crossings shows that the torsional moment oscillations initiate at 180 deg azimuth, prior to any possible crossings. In fact the largest torsional moment oscillation occurs prior to the first helix crossing with the 95 percent span of the blade. The c_m distributions at 75 and 85 percent blade span (not shown) similarly do not indicate blade/vortex crossings at those stations to be a direct cause of the root moment oscillations.

Analysis of other NH-3A maneuver cases resulted in the same general conclusions as described for case 72. A limited degree of correlation existed between possible blade/vortex intersections and the pressure and c_m response. None of the cases examined, however, indicated a direct correlation between the blade/wake interactions and the NH-3A retreating blade oscillations measured in both the root torsional moment and the pushrod load.

The effect of the blade/wake intersections was also examined for CH-53A conditions. The measured pressure distributions at 75, 85, and 95 percent blade radial stations for CH-53A case 41TN, a 60 degree angle of bank right turn, are shown in figures 15, 16, and 17. The corresponding blade and non-distorted wake vortex crossings are also indicated. A very definite high-frequency response occurs in the advancing blade pressures, especially at 75 and 85 percent span stations. The r/R = 0.75 station indicates approximately 8 advancing blade oscillations, appearing in all chordwise stations, occurring at the same time as the vortex crossings and at the same frequency, approximately 30/rev. In addition several retreating blade oscillations occur roughly in the region of possible crossings.

Maneuver case 41TN, however is atypical among the data for the CH-53A in so far as the effect of blade/wake interactions on blade pressures is concerned. Examination of the pressure time histories for other CH-53A cases, including the level flight and transition cycles prior to the case 41TN turn, indicates little or no fluctuations in the region of possible crossings. Therefore, although the exact rotor tip path plane orientation in the free stream is unknown for the turn, it does appear that the instrumented blade encountered strong vortex effects as the blade passed close to, or through, the trailed vortices. The rotor orientation and coning angle of the other cases was apparently such that the trailed vortices did not pass close to the blade. Also, since the turn condition is generating higher rotor thrust than the level flight conditions examined, the relative strength of the vortices should be greater.

The results of the pressure fluctuations on c_n and c_m at 75 percent blade span for CH-53A case 41TN are shown in figure 18 along with the measured root torsional moment. The occurrence of the advancing blade pressure oscillations at all five chordwise stations results in similar excitation of c_n and c_m. The root torsional moment in this region also exhibits some high-frequency response at about 25/rev, slightly lower than the approximately 30/rev pressure oscillation frequency at both 75 and 85 percent span. The frequency difference may be due to differently phased pressure oscillations over the remaining blade area. On the retreating side of the blade, fairly good agreement exists between the higher frequency pressure, c_n, and c_m fluctuations at 75 percent span. The c_n distribution also has two relatively large amplitude oscillations near ψ= 245 and ψ = 330 deg. Examination of the pressures in these regions, shown in figure

15, indicates a phase difference between the five pressures across the chord. This is similar to the findings of reference 3 during a maneuver condition and is probably indicative of local dynamic stall effects. The phasing differences result in the large c_m oscillations. The measured root torsional moment for the CH-53A case 41TN turn exhibits frequency response in the 20/rev to 30/rev range whereas the NH-3A case 72 turn shown in figure 14 does not. This is attributable to the effect of the blade/wake interactions which are not evident in the NH-3A case. The large amplitude root torsional moment oscillations on the case 41TN retreating blade are somewhat different from the c_m oscillations at 75 percent span due to different azimuthal histories of c_m at other radial stations. The c_m at r/R = 0.85 is shown in figure 8.

In summary, blade/wake interaction effects appeared to occur strongly in only one case investigated, a CH-53A banked turn. For both the NH-3A and the CH-53A, maneuver conditions appeared to be affected more by these effects than did the level flight regimes. The level flight CH-53A and NH-3A cases exhibited little or no effect, apparently due to either an absence of close rotor blade proximity to the wake or low vortex strength. The CH-53A turn did, however, experience relatively strong first and fourth rotor quadrant effects on measured blade pressures, c_n, c_m, and root torsional moment. However, these effects do not appear to be the direct cause of either NH-3A or CH-53A high amplitude retreating blade control load oscillations.

Effects of advancing blade critical Mach number. - Examination of the measured blade pressure data revealed a change in the azimuthal history that occurred in several cases in the region of the advancing blade. Reference 7 describes a similar change in H-34 pressure data which appears as an approximate square wave caused by two step changes in the differential pressure. This effect is demonstrated by the NH-3A case 72 pressure shown in figures 11, 12, and 13. For this case the occurrence of the step changes is most pronounced in the measured pressure at r/R = 0.85 and y/c = 0.300 as shown in figure 12. Evidence of the effect is generally seen only in the 30.0 and 15.8 percent chord station pressures for all NH-3A and CH-53A cases. Figure 12 shows the sequence of pressure changes for the y/c = 0.300 station to be a step increase at ψ = 50 deg followed by a step decrease to the original pressure level at ψ = 115 deg. These square waves always appear roughly symmetric about an azimuth point between 80 and 100 deg. This corresponds to the blade environment of highest local Mach number.

Figure 19 shows this effect on the measured differential and absolute pressures for NH-3A case 72. The greatest effect at 30.0 percent chord is seen to occur in the 85 percent span station while a lesser magnitude effect is seen at r/R = 0.95. No effect is apparent at 75 percent. The last three plots of figure 19 present the corresponding measured absolute pressures on the upper and lower blade surfaces at the three spanwise stations. The absolute pressures shown have a zero reference when the aircraft was in a static ground condition. Due to flight at altitude, the free-stream static pressure changed and the absolute transducer readings included this delta static pressure change. The free-stream static pressure, $p_{\infty,h}$, is indicated in the plots. As indicated, the square wave effect in the differential pressure is due to a corresponding square wave occurring in the upper surface absolute pressure. The largest step changes

in absolute pressure occur at r/R = 0.85 corresponding to the large effect seen in the differential pressure. The Karman-Tsien relation, reference 5, was used to predict the absolute pressure required on the upper surface such that the local Mach number reaches unity. This critical pressure is dependent on the free-stream Mach number. In general this indicated that the absolute pressures reached in the area of the first step change correspond to pressure at or above the critical pressure. At 75 percent span, where no step changes in pressure occur, the Karman-Tsien relation predicts the critical pressures to be above the pre-sures on the blade.

It is believed that the generation of the step changes in pressure are due to a shock occurring over the upper blade surface when the critical Mach number is reached locally. The first step change in the negative absolute pressure sense could be due to the pressure buildup forward of the actual shock followed later in azimuth by a step change in the opposite pressure sense. The actual shock may be strongest aft of the 30.0 percent chord station. Due to the limited number of pressure measurements across the chord, the next station was at 60.0 percent, and the transducer at this station did not experience the step change effect. Analysis indicates that the effect does occur in the region of high free-stream Mach number where the local Mach number is capable of reaching unity.

Similar results were found for CH-53A conditions. The pressure distributions for a high speed level flight condition, case 44, are shown in figure 20. The critical Mach-number effect is apparent in the 30.0 percent chord pressure at 85 and 95 percent radial stations but not at 75 percent. Similar to the NH-3A case 72, the CH-53A case 44 square wave azimuthal duration is slightly greater and begins earlier at r/R = 0.95 than at r/R = 0.85. This is probably due to a higher free-stream Mach number existing toward the blade tip in this region.

Other NH-3A and CH-53A conditions at lower maximum free-stream Mach numbers do not exhibit the step changes in pressure at blade locations that do encounter these changes shown in figures 19 and 20. This also indicates the dependence on critical Mach number for this effect to occur. The pressures reached in these lower Mach-number conditions do not reach those corresponding to a critical Mach-number encounter.

Effects of blade bending. - Reference 6 postulated the possibility of a significant effect of flatwise and edgewise blade bending on root torsional moments. The use of the product of the flatwise and edgewise bending moments measured at a point on the blade, as an indicator gave fairly good phase correlation of the product and the measured torsional moment retreating blade oscillations. The product was used as an indicator of load-deflection terms caused by the product of blade lift times edgewise blade displacement due to bending, and by the product of drag load times flatwise bending displacement. No attempt was made, however, to determine the magnitude of the flatwise/edgewise coupling terms. In the present study a semi-empirical method, again utilizing the measured flatwise and edgewise moments, was developed to determine the magnitude, as well as the phase, of the flatwise/edgewise coupling.

The semi-empirical method developed utilizes a normal mode approach, sim-

ilar to that described in reference 8, to model the blade bending. The blade was modeled at 15 spanwise segments and was assumed to respond only in its first normal mode in the flatwise, edgewise, and torsional degrees of freedom. To segregate the flatwise/edgewise coupling influence from other torsional excitations, the only loads considered to act are the flatwise and edgewise shears and moments and the torsional moments at each end of the blade segments. Therefore, the torsional moment at the inboard end of any segment can be determined from the shears and moments at the outboard end and the relative flatwise and edgewise bending between the ends of the segment. Analytical flatwise and edgewise shears, moments, and displacements can be represented in terms of the blade modal response. The measured flatwise and edgewise bending moments on the blade, at $r/R = 0.65$ for the NH-3A and $r/R = 0.68$ for the CH-53A, were used to describe this modal response. From the known boundary conditions at the blade tip, the torsion at the inboard end of any segment can be determined from the outboard loadings. Therefore, it is possible to derive an equation for the root torsional moment in terms of blade physical properties, normal mode shapes, and the product of flatwise and edgewise moments measured at one radial station. This semiempirical method was applied to NH-3A and CH-53A cases exhibiting large measured retreating blade torsional oscillations.

Applying this method has shown that, although the phase correlation is fairly good, the amplitude of the flatwise/edgewise coupling effect on blade torsion is low in the region of the measured oscillations. The comparisons for cases exhibiting large measured oscillations are shown in figures 21 and 22. The cases shown are high speed NH-3A and CH-53A conditions. For NH-3A case 43 the maximum coupling oscillation amplitude is only about 20 percent of the corresponding measured torsional oscillation and is less in the regions of the other oscillations. The maximum coupling oscillation amplitude for CH-53A case 44 does locally reach approximately 50 percent of the measured value. Other coupling oscillations are of lower magnitude however. Additional NH-3A and CH-53A conditions exhibit a similar degree of correlation between measured torsional oscillations and those due to flatwise/edgewise coupling effects. It is concluded, therefore, that the coupling of flatwise and edgewise loadings as a source of torsional oscillations is small and is not the major cause of measured retreating blade torsional oscillations for either of the articulated low twist NH-3A (-4 deg) or CH-53A (-6 deg) blades. In fact, due to the fairly good phase correlation, it may be possible for torsion to be a contributor to the flatwise and edgewise response of these blades due to coupling.

Effects of aerodynamic pitching moments. - Discussion in the previous sections has ruled out two possible sources as the major cause of retreating blade torsional oscillations. The available measured data have shown that no one-to-one correspondence appears to exist between possible blade/vortex crossings and torsional oscillations. Also the coupling of flatwise and edgewise response is not a primary source of the large measured torsional fluctuations. Further analysis of the data, however, has shown that the measured oscillations appear to be the result of a forced torsional vibration of the blade due to the total aerodynamic pitching moment acting on it. This can be demonstrated by applying the pitching moment, calculated from the measured blade pressures, to a simple single-degree-of-freedom spring/mass torsional model of the blade. As an approximation of the aerodynamic pitching moment, the section pitching mo-

ments calculated from the pressures at 75, 85, and 95 percent span stations were used to calculate a total moment for the entire blade. A numerical spanwise integration was used assuming a linear change in moment from zero at r/R = 0.30 to the value calculated from the pressures at r/R = 0.75. An azimuthal time history of the aerodynamic pitching moment was found from this integration.

A single-degree-of-freedom system with damping was assumed to model the blade in torsion. The basic second-order linear differential equation with constant coeeficients that controls the oscillatory torsional motion at the blade root, θ_T, is

$$\ddot{\theta}_T + 2\zeta\omega_T\dot{\theta}_T + \omega_T^2\theta_T = \frac{T}{J} \tag{3}$$

where ζ is the nondimensional damping ratio, ω_T the torsional natural frequency of the blade, T the modal contribution of the aerodynamic pitching moment $M_{X,a}$ along the blade, and J the torsional modal mass moment of inertia. Only the first torsional mode was included in defining ω_T, T, and J. A computer program was used to numerically solve equation (3) for the root elastic twist θ_T. Having θ_T, the model oscillatory root torsional moment $M_{X,T}$ was calculated from

$$M_{X,T} = k_T\,\theta_T \tag{4}$$

where k_T is the root torsional spring constant.

The response of the simple torsional model to the applied aerodynamic pitching moment was determined for several NH-3A and CH-53A cases. Examples of the resulting torsional moment compared to the measured root moment are shown in figures 23 and 24 for NH-3A case 71 and CH-53A case 44 respectively. The curve shown at the top of each figure represents the azimuthal history of the aerodynamic pitching moment calculated from the measured blade pressures. Both cases indicate the same general trend. A relatively high leading-edge-up moment exists in the first quadrant of azimuth, followed by a decrease to approximately zero moment on the retreating side and, finally, an increase to the first quadrant values. On the advancing side the aerodynamic moment alone matches the root structural moment fairly well. The large amplitude torsional oscillations experienced by the retreating side structural moment are not exhibited by the aerodynamic moment. However, application of the aerodynamic load to the model oscillator does result in retreating blade fluctuations of the torsional root response. By including 10% of critical damping ($\zeta = 0.10$), it was possible to predict fairly well both the magnitude and frequency of the measured oscillation. A slight phase lag of the calculated response compared with the measured response occurs in both the NH-3A case 71 and the CH-53A case 44. This may be due to the constant damping factor used in the oscillator model. Actual in-flight aerodynamic damping is generally not constant but varies with blade azimuth.

The mechanism causing the retreating blade torsional moments is believed to be initiated by the advancing blade aerodynamic pitching moment. The sudden decrease in large leading-edge-up advancing blade moment appears to initiate oscillations at the blade torsional natural frequency for the remainder of the

rotor cycle. These occur due to simple blade spring and inertia effects. The NH-3A first torsional natural frequency is 6.6/rev while the CH-53A's is 6.0/rev. Variations of the aerodynamic moment later in the cycle either tend to increase the amplitude of the oscillations or to assist in damping them out. Although the calculation of the aerodynamic pitching moment was approximate and a simplified single-degree-of-freedom blade model was used, the prediction of oscillations due to the application of only the aerodynamic moment is encouraging.

Correlation with Analytically Derived Results

The purpose of the correlation study was both to evaluate the present analytical capability for predicting helicopter blade torsional response and to understand better the nature of the torsional excitation for maneuvering and high-speed flight conditions. The effects of unsteady aerodynamics and non-uniform rotor inflow upon the correlation of blade section aerodynamic coefficients and blade structural torsional moment were evaluated. The analytical solutions were examined to determine the sources of the calculated torsional excitation.

Description of programs and procedures.- Analytical description of rotor blade response requires proper modeling of both dynamic and aerodynamic effects. The Normal Modes Aeroelastic Blade Analysis was used to calculate blade elastic response. As described in reference 8 this analysis represents blade flatwise, edgewise, and torsional elastic deformation by a summation of normal mode responses. For a given rotor inflow and a set of control positions this program carries out a timewise integration of the blade equations of motion to solve for the modal response. Blade elastic motions and aerodynamic forces and moments are fully coupled. At each radial and azimuthal position, blade section loading and pitching moment coefficients are obtained from appropriate steady or unsteady data tables. To model unsteady aerodynamic effects the procedures and data given in reference 6 were used. Briefly this method is based on airfoil data obtained from a 0012 airfoil section undergoing sinusoidal angle-of-attack changes. Section lift and pitching moment coefficients were measured and tabulated as functions of instantaneous blade angle of attack and its first two time derivatives. Unsteady aerodynamic lift and moment coefficients were obtained in the computer program by entering the unsteady data tabulations with calculated angle-of-attack parameters. Because only unsteady 0012 data are available, they were used to approximate the unsteady 0011 section characteristics of the CH-53A. Steady drag data were used throughout the study. Variable rotor inflow was determined using the Prescribed Wake Analysis which is described in reference 9. For a given flight condition this program calculates the induced velocity distribution over the rotor disc due to the rotor wake. For this study the wake was approximated by the classical skewed helicoid defined when the trailing vortex filaments generated by the blade are carried downstream. When the positions and strengths of the vortex filaments are determined the velocity induced at each blade position is calculated using the Biot-Savart law. In this way close blade-vortex passages result in large and rapid fluctuations in induced velocity. The program is strictly a steady-flight analysis. Its use for maneuvers implies a quasi-steady treatment of the time varying aircraft condition.

In the aeroelastic analysis, blade flexibility was modeled using rigid

body flapping and lagging degrees of freedom and six elastic modes: three flatwise, two edgewise, and one torsional. For the level-flight conditions, use of measured cyclic and collective pitch and rotor shaft angle gave analytical rotor lift and propulsive force very near test values. In maneuvering flight, where rotor shaft angle was not accurately known, an iteration was performed in which shaft angle was varied to achieve approximately the correct rotor lift. Since both unsteady aerodynamics and variable rotor inflow were thought to be necessary for modeling high-frequency rotor torsional response, the separate effects of unsteady aerodynamics and variable inflow were examined. Accordingly the aeroelastic program was run with steady aerodynamics and variable inflow, unsteady aerodynamics and variable inflow, and with unsteady aerodynamics and constant inflow corresponding to the average momentum induced velocity.

In order to establish representative trends for the effects of aerodynamic and inflow modeling and to assess the degree of correlation, six cases were studied in detail. Of the conditions shown in table I, NH-3A cases 43 and 72 and CH-53A cases 41LF, 41TR, 41TN, and 44 were analyzed and the resulting section loading and pitching moment coefficients, total aerodynamic blade pitching moments, and root torsional moments were plotted and compared with test data. It was felt that the results of NH-3A case 72 and CH-53A cases 41LF, 41TN, and 44 were representative and the results presented in the following section will be taken entirely from these cases.

Discussion of results.- The results of the correlation study indicate that rotor blade aerodynamic/dynamic behavior can be reasonably well predicted using the present analytical methods. Certain problem areas are pointed out however. Insight into the mechanism of torsional motion is also provided.

For NH-3A case 72, which is a 60 deg angle of bank turn at $\mu = 0.35$ and $C_T/\sigma = 0.085$, a full set of correlation results is given in figures 25 through 28. The abbreviations V.I. and C.I. used in figures 25 through 42 refer respectively to the use of a variable inflow and a constant inflow analysis. In figure 25, which shows the root torsional moment correlation, three results are evident. First the test data show a steady positive displacement from the analytical results of approximately 400 N-m (3540 in.-lb). Second the use of variable inflow in place of the uniform momentum velocity greatly improves the correlation of the high-frequency response. Finally the use of unsteady aerodynamics led to slightly higher retreating blade torsional oscillations although test values were not achieved. Examination of figure 26 which shows the correlation of total analytical aerodynamic pitching moment and pitching moment calculated from test pressures indicates that the test aerodynamic moment is more positive than the analytical predictions. Also the higher frequency makeup of the time history is best matched when variable rotor inflow is used. The buildup of torsional moment for the variable inflow cases appears to be the result of local blade stall which begins inboard at $r/R = 0.50$ at $\psi = 180$ deg and propagates out along the blade through the third quadrant of rotor azimuth. Figure 27 shows the comparison of the outboard c_m coefficients reduced from test data and those calculated in the Normal Modes Analysis. As described previously the noseup pitching moment coefficients which are evident in the test data are believed to be the result of asymmetry in the airfoil contour introduced by pressure transducer fairing. The point of rapid pitching moment coefficient buildup is fairly well matched by

the analytical results, although the c_m variation in stall is not well described. Figure 28 shows the time histories of blade section loading coefficients at r/R = 0.75, 0.85, and 0.95. The best correlation with test data is achieved using unsteady aerodynamics and variable rotor inflow.

CH-53A case 41 was studied during the level-flight, transition, and steady-state turn phases. These data were taken at $\mu = 0.24$ and C_T/σ ranging from 0.063 for level flight to 0.099 for the turn. Results of the level flight and steady-state turn calculations are shown in figures 29 through 32 and 33 through 36 respectively. The two root torsion moment plots, figures 29 and 33, show that the rise in oscillatory control moment is predicted by the analysis. As observed for the NH-3A case the measured moments are generally more noseup. In the steady-state turn the rotor angle of attack relative to the free stream was not known and a shaft angle of attack of 0 deg was used to make the analytical lift agree with the measured value. One result of the small shaft angle was that the rotor wake passed through the cone prescribed by the blades, causing large induced velocity spikes at inboard blade sections and precipitating local stall and large nosedown aerodynamic pitching moments. Figures 30 and 34 show the differences between the aerodynamic pitching moment calculated analytically and that determined by the approximate integration of section pitching moment data. The integrated test aerodynamic moment for this case using only outboard pitching moment data does not agree well with the analytical calculation. Samples of the section pitching moment coefficient correlation for the level-flight and turn conditions are shown in figures 31 and 35. As previously shown for the NH-3A the test pitching moment data show a steady noseup value which is not predicted by the analysis with standard airfoil data. Typical section loading coefficient results shown in figures 32 and 36 depict the increase in the vibratory component of blade lift which accompanies higher blade loading and deeper penetration into stall. For case 41TN, the variable inflow program has apparently overpredicted the level of velocity fluctuation felt by the advancing blade. Inaccurate modeling of either the strength or position of the trailed vortices is the apparent source of the discrepancy.

The final correlation results to be presented are for CH-53A case 44 which was a level-flight condition flown at $\mu = 0.38$ and $C_T/\sigma = 0.057$. Figure 37 shows that none of the analytical results predict the high level of test oscillatory root torsional moment. For this case it was shown in figure 24 that the blade root torsional signature could be fairly well described as the forced response to the applied aerodynamic pitching moment. The analytical pitching moment coefficients shown in figures 38 and 39 do not match the test values. The solutions obtained using unsteady aerodynamics and variable inflow generally give the best agreement but do not match the test advancing blade positive pitching moment coefficients. Fairly good agreement between test and analytical normal force coefficients is shown in figures 40 and 41.

As a further investigation of the torsional response for CH-53A case 44, an attempt was made to force the analytical aerodynamic moment to agree with that calculated from test pressures. In this way, calculated blade dynamic response could be compared directly with measured response for the same input moment. Accordingly the standard 0011 c_m data were modified by shifting the below-stall pitching moment coefficients to 0.02. This value was chosen as an average of the c_m values in the test data. The changes in aerodynamic pitching moment and

root torsional moment caused by this modification are shown in figure 42. Although the desired nose-up change in advancing blade aerodynamic moment was only partly accomplished, an improvement in both the amplitude and azimuthal variation of the resulting torsional moment is achieved. This supports what was found above with the simple single-degree-of-freedom torsional model. Torsional moments applied to the advancing blade serve as initial conditions for retreating blade response. Without proper modeling of advancing blade aerodynamics the retreating blade torsional oscillation cannot be obtained.

A final attempt to understand the nature of the blade torsional response was made by examining the terms which contribute to analytical torsional response. In the Normal Modes Analysis coupled equations for blade flatwise, edgewise, and torsional modal acceleration are solved simultaneously at each rotor azimuth. For the CH-53A case 44, run with the modified pitching moment data, the time histories of the major terms contributing to non-dimensional torsional modal response are shown in figure 43. The three primary effects which determine the response of the first elastic torsional mode are (1) the aerodynamic contribution which is made up of pure pitching moment and moments created around the blade elastic axis by lift and drag acting at the blade quarter chord, (2) the blade torsional inertia, and (3) dynamic moments about the blade elastic axis caused by flapping and centrifugal acceleration acting at the blade section centers of gravity. The high-frequency torsional modal response in the fourth quadrant is primarily the result of the applied aerodynamic moment and the blade torsional inertia. In agreement with the results shown above for the simple torsional oscillator model, this shows that the blade torsional moment, which is proportional to the modal response, is basically a forced response to the applied aerodynamic moment.

ANALYSIS OF ROTOR VIBRATORY FORCE DATA

A secondary area of study included in this program involved an analysis of the in-flight vibratory loads encountered by the main rotor on both the NH-3A and the CH-53A. These loads were calculated from measurements recorded during earlier flight-test programs over a wide range of operating conditions. The study reported herein included a determination of the primary dynamic terms resulting in the harmonics of blade hinge forces and the b/rev hub loads. Also the effects of the number of main rotor blades on harmonics of the hinge forces were sought.

Major Blade Hinge Force Dynamic Terms

The purpose of this study was to attempt to define, in a relatively few number of terms, a method to calculate the harmonics of main rotor articulated blade hinge forces from blade geometry and test measurements. Knowledge of the harmonic content of the hinge forces enables the determination of the vibratory loads fed by the rotor into the fuselage. Reference 4 describes the successful use of the Root Response Method to determine the hinge forces on the NH-3A over a wide range of flight conditions. This method was also used successfully with the CH-53A flight data. To determine the loads, measurements near the root end

of one blade are recorded during flight. From these data a computer program calculates the azimuthal history and corresponding Fourier series coefficients of the three rotating system hinge forces: radial, F_X^*; edgewise, F_Y^*; and vertical, F_Z^*. Since measurements are made in the local blade axis system, transformation of the equations of motion between the local blade and rotor head axis systems is required. The axis systems involved are shown in figure 44. The resulting hinge force equations in the rotor head system include between 80 and 150 dynamic terms. Definition of the terms are included in reference 4. It is desirable to simplify these expressions to include only the major terms.

During the present study, analysis of the available NH-3A and CH-53A flight data has resulted in a simplified expression for each of the three hinge forces. A maximum of only six terms was found necessary to describe any of the forces on either aircraft. The number of terms required to give an approximation of any harmonic from the first through the seventh, generally within 15 percent in amplitude and 10 deg in phase, varies between one and six. Table II indicates the terms required to achieve this accuracy for NH-3A and CH-53A rotor systems. The first seven harmonics are included since they comprise all harmonics required to determine the b/rev hub loads in the fixed system of either aircraft. Generally the same terms, with the exception of the X3, Y5, Y7, and Z6 hub motion terms, are important for the same harmonic on both aircraft. The hub motion terms are important for different harmonics due to the difference in the number of main rotor blades, i.e., five on the NH-3A and six on the CH-53A. As table II indicates, by measuring the flatwise and edgewise bending at each end of a short root end instrumented segment, the blade tension near the root, the root blade angular motions (hunting, flapping, and feathering), and the root head translation motions, the harmonics of the hinge forces can be determined.

Tables III and IV indicate the application of these approximations to typical NH-3A and CH-53A conditions. Compared are the summations of the major terms, indicated in table II, and the exact calculation comprised of all terms. Harmonic error of the approximation is generally within 15 percent of the exact amplitude and 10 deg of the correct phase. Also apparent in each direction is the general decrease in harmonic amplitude with increased harmonic order.

An example of how only a few of the many terms contributing to the calculation of the hinge force can approximate the exact calculation is shown in figure 45. Shown are the major terms contributing to the fifth harmonic of the edgewise hinge force for a high-speed CH-53A condition. The five terms required to approximate the harmonic, indicated in table II, are plotted in vector form along with their vector sum, $F_{Y,5,MT}^*$, and the exact calculation, $F_{Y,5}^*$. In this instance the approximation is within 7 percent of amplitude and 5 deg of the exact phase. Each of the five terms is of significant amplitude. The source of the Y1 term is the product of measured blade tension and root lag motion. The edgewise shear force causing edgewise blade bending across the root instrumented segment results in the largest magnitude term, Y2. The Y6 and Y8 terms exist due to lag motion inertia of the blade cuff mass inboard of the instrumented segment. The source of the Y7 term is the vibratory motion of the rotor head. Other harmonics indicate similar correlation between the exact and approximate solutions.

It has been shown that, for an articulated rotor system, the vibratory loads acting on the rotor head in the rotating system can be determined fairly accurately using only a few dynamic terms. Azimuthal histories of measurements near the root of one blade can be recorded and the terms indicated in table II calculated in time history form. Standard harmonic analysis of these time histories then provides the required Fourier coefficients of each term.

Major Rotor Hub Force Dynamic Terms

Knowledge of the blade hinge forces encountered in flight enables one to calculate the fixed system forces which the rotor system feeds into the fuselage and which consequently excite the airframe. The fixed system vibratory loads occur, when each blade is assumed to have the same azimuthal hinge forces as does the instrumented blade, at a frequency that is an integer multiple of the number of blades times the rotor speed. A 5-bladed rotor system for example, can theoretically excite the fuselage with loads at 5/rev, 10/rev, 15/rev, etc. For articulated rotors, generally only the b/rev loads have significant amplitudes compared to the 2b/rev, 3b/rev, etc. loads. Therefore, knowing the major dynamic terms contributing to the rotating system hinge force harmonics, an analysis was undertaken to determine which of these were the primary contributors to the fixed system b/rev hub loads. Specifically the major dynamic blade terms contributing to the b/rev hub forces were defined for both the NH-3A and the CH-53A rotor systems.

The b/rev hub forces, $F_{X,b}$, $F_{Y,b}$, and $F_{Z,b}$ can be represented as Fourier cosine and sine components of the b-th harmonic in terms of the hinge force harmonic coefficients as follows

$$F_{X,bc} = \frac{b}{2}\left(F^*_{x,b-1,c} + F^*_{x,b+1,c} + F^*_{y,b-1,s} - F^*_{y,b+1,s}\right) \tag{5}$$

$$F_{X,bs} = \frac{b}{2}\left(F^*_{x,b-1,s} + F^*_{x,b+1,s} - F^*_{y,b-1,c} + F^*_{y,b+1,c}\right) \tag{6}$$

$$F_{Y,bc} = \frac{b}{2}\left(-F^*_{x,b-1,s} + F^*_{x,b+1,s} + F^*_{y,b-1,c} + F^*_{y,b+1,c}\right) \tag{7}$$

$$F_{Y,bs} = \frac{b}{2}\left(F^*_{x,b-1,c} - F^*_{x,b+1,c} + F^*_{y,b-1,s} + F^*_{y,b+1,s}\right) \tag{8}$$

$$F_{Z,bc} = bF^*_{z,b,c} \tag{9}$$

$$F_{Z,bs} = bF^*_{z,b,s} \tag{10}$$

where the hinge force cosine and sine harmonic coefficients are defined from the corresponding amplitude and phase. For example

$$F^*_{z,b,c} = F^*_{z,b} \sin\phi_{z,b} \tag{11}$$

$$F^*_{z,b,s} = F^*_{z,b} \cos\phi_{z,b} \tag{12}$$

The same NH-3A and CH-53A flight conditions that were used to determine the major hinge force dynamic terms were also analyzed to determine which of these terms are also the primary terms causing the fixed system b/rev hub forces. As equations 5 through 10 indicate, only the (b±1)-th in-plane hinge forces (F_x^* and F_y^*) and the b-th vertical hinge force (F_z^*) excite the fixed system at the b/rev frequency. It was found that generally all of the terms required to achieve a good approximation of the hinge force harmonics are also needed to give a reasonable estimation of the b/rev hub forces.

Figures 46 through 48 and 49 through 51 indicate, respectively for NH-3A and CH-53A conditions at $\mu = 0.36$, the major dynamic terms contributing to the hub forces. Also included is the degree of agreement with the exact calculation. The upper chart in each figure indicates the major terms contributing to the b/rev cosine component of the fixed system force. The lower chart shows those for the sine component. The NH-3A 5/rev in-plane hub forces result from 4 and 6/rev rotating system in-plane hinge forces while the 5/rev vertical hub force comes from 5/rev vertical hinge forces. Similarly, 5 and 7/rev in-plane and 6/rev vertical hinge forces transform into the 6/rev CH-53A fixed system loads. Comparison of the major NH-3A and CH-53A terms shows in many cases that there are usually several large magnitude terms causing the fixed system vibratory loads. Also the same terms do not always exhibit the largest magnitudes and, therefore, all terms shown in figures 46 through 51 must be included to form a reasonably good approximation of the exact calculation. For the NH-3A example shown the approximations indicated give excellent agreement with the exact computation. The CH-53A case indicates an acceptable correlation, but not as good as the NH-3A example for some forces. This represents the minimum degree of correlation between the exact and approximate computations for the CH-53A conditions analyzed. The vertical loads in figure 51 indicate the poorest degree of correlation. However, comparison with the corresponding NH-3A loads in figure 48 and other CH-53A conditions indicates that the magnitude of these loads is low.

Effects of the Number of Main Rotor Blades on Harmonics of Blade Hinge Forces

The availability of blade hinge force data for both the 5-bladed NH-3A and the 6-bladed CH-53A over a wide range of operating conditions made possible a study of the effects of the number of blades on these loads. Available harmonics of the hinge forces extended from level-flight conditions at $\mu = 0.09$ to $\mu = 0.36$ for both aircraft. The flight conditions used for the NH-3A correspond to a nominal gross weight of 8560 kg (18900 lb) and a neutral aircraft center of gravity. The NH-3A was in a compound configuration (auxiliary jets and wing installed) but the conditions to be discussed were flown with the jets at idle. A nominal gross weight of 15860 kg (35000 lb) and neutral aircraft center of gravity comprised the CH-53A configuration. Comparisons of the first seven harmonics of the NH-3A and CH-53A hinge forces are shown in figures 52, 53, and 54 at advance ratios of 0.1, 0.2, and 0.3. Each force harmonic has been nondimensionalized by the steady (mean) value of vertical hinge force.

Figures 52, 53, and 54 show that generally higher amplitude harmonics exist for the CH-53A with the primary exception being the first harmonic verti-

cal force. This is due to differences in rotor trim for the conditions considered. Similar trends occur at the three advance ratios shown. The two in-plane hinge forces, $F^*_{x,n}$ and $F^*_{y,n}$, generally have relatively low amplitude second harmonics, higher middle order harmonics, and low amplitude high order harmonics (sixth and seventh). The harmonic amplitude of the vertical hinge force generally decreases as harmonic order increases. The large amplitude fourth harmonic edgewise hinge force on the CH-53A, shown in figure 53, is due to an edgewise blade resonance near the corresponding 4/rev frequency.

It is believed that figures 52, 53, and 54 can be used to approximate the magnitude of hinge force harmonics generated by an articulated rotor system if they are known for another hinged rotor system having one more or one less blade. This should be applicable to blades of similar construction and geometry as the NH-3A or CH-53A blades. Applicability of these curves to blades having considerably different construction, geometry, or number of blades per rotor requires further investigation.

CONCLUSIONS

1. As anticipated, larger high-frequency control loads were found to occur on the retreating blade as rotor load factor or airspeed increased.

2. From the test data analyzed, only a limited blade/tip vortex interaction effect appears in the measured blade pressures and resulting section loading and pitching moment coefficients. The CH-53A blade/vortex interactions appeared to have a stronger effect than those on the NH-3A. The most noticeable effects were experienced by each aircraft in maneuvering, rather than level flight, conditions. Even here, however, these interactions did not appear to dominate the torsional moment oscillatory amplitudes.

3. Blade/tip vortex interactions do not exhibit a direct azimuthal correlation with retreating blade torsional oscillations.

4. Evidence of blade upper surface shock, due to a critical Mach-number encounter, was found in the measured pressure data, corroborating similar observations by NASA on the H-34 blade.

5. Coupling of flatwise and edgewise blade response is not a major cause of the measured retreating blade torsional oscillations for the low twist blades tested and analyzed.

6. The high-frequency blade control loads primarily result from the forced dynamic response of the blades produced by the time varying aerodynamic pitching moments. Although fluctuations in the pitching moment caused by stall flutter effects may serve to amplify or attenuate retreating blade response, the relatively rapid changes in pitching moments on the advancing blades appear to excite blade torsional oscillations that persist to the retreating side of the disc. (Stall flutter is probably a major contributor to high-frequency control load oscillations when operating well

above the knee of the control load curve, but it was found that for the less stalled conditions analyzed in this study, the principal cause of high-frequency control loads appears to be a forced dynamic response of the blade due to the aerodynamic moment.)

7. The instrumented blades exhibited significant positive pitching moments in flight test despite the fact that the airfoil section was nominally symmetrical. These moments may have been the result of instrumentation fairings used or possibly may have arisen from a more fundamental source.

8. Fair correlation of measured blade airloadings with those predicted using a normal mode, rigid hub, blade aeroelastic analysis was achieved. The inclusion of unsteady aerodynamics and variable inflow effects results in the best agreement. To improve the correlation it appears mandatory to include in the analysis the positive airfoil pitching moment coefficients observed in the test data.

9. The equations presented in reference 4 for computing hub vibratory forces from measurements of blade root dynamic response can be considerably simplified. Many of the dynamic correction terms due to motion of the hub, blade cuff, and instrumented blade segment can be neglected.

10. For the two rotors analyzed, the harmonics of root shear, nondimensionalized by steady axial (vertical) blade shear, differed significantly, indicating the need for (1) further work to define all controlling parameters and (2) caution in applying these results to other rotor designs.

RECOMMENDATIONS

1. Additional work should be conducted to investigate the source of the positive pitching moments observed on the flight test blades. At the very least, two dimensional tests of a simulated blade section should be conducted to determine if the instrumentation fairings were a significant contributor.

2. Improved procedures for modeling the airloads produced on a blade passing close to a series of vortices should be developed based on a lifting surface representation of the blade.

3. A study should be conducted to correlate vibratory root shears predicted by analysis with those measured.

Sikorsky Aircraft Division,
United Aircraft Corporation,
Stratford, Connecticut, November 21, 1972

REFERENCES

1. Harris, Franklin D.; and Pruyn, Richard R.: Blade Stall-Half Fact, Half Fiction. J. Am. Helicopter Soc., vol. 13, no. 2, Apr. 1968, pp. 27-48.

2. Fisher, Richard K., Jr.; and McCroskey, W.J.: Detailed Aerodynamic Measurements on a Model Rotor in the Blade Stall Regime. Preprint 521, Am. Helicopter Soc., May 1971.

3. Ward, John F.: Helicopter Rotor Periodic Differential Pressures and Structural Response Measured in Transient and Steady-State Maneuvers. Preprint 423, Am. Helicopter Soc., June 1970.

4. Fenaughty, Ronald; and Beno, Edward: NH-3A Vibratory Airloads and Vibratory Rotor Loads. SER 611493 (NASC Contract NOw 64-0528-f, C/N 5368-65), Sikorsky Aircraft Div., United Aircraft Corp., Jan. 1970.

5. Abbott, Ira H.; and von Doenhoff, Albert E.: Theory of Wing Sections. Dover Publications, Inc., 1959.

6. Arcidiacono, P.J.; Carta, F.O.; Casellini, L.M.; and Elman, H.L.: Investigation of Helicopter Control Loads Induced by Stall Flutter. USAAVLABS Technical Report 70-2 (Contract DAAJ02-68-C-0048), Sikorsky Aircraft Div., United Aircraft Corp., Mar. 1970.

7. Ward, John F.; and Young, Warren H., Jr.: A Summary of Current Research in Rotor Unsteady Aerodynamics With Emphasis on Work at Langley Research Center. Presented to AGARD Conference on Aerodynamics of Rotary Wings (Marseilles, France), Sept. 13-15, 1972.

8. Arcidiacono, Peter J.: Prediction of Rotor Instability at High Forward Speeds, Vol. I, Steady Flight Differential Equations of Motion for a Flexible Helicopter Blade with Chordwise Mass Unbalance. USAAVLABS Technical Report 68-18A (Contract DA 44-177-AMC-332(T)), Sikorsky Aircraft Div., United Aircraft Corp., Feb. 1969.

9. Landgrebe, A.J.: An Analytical Method for Predicting Rotor Wake Geometry. J. Am. Helicopter Soc., vol. 14, no. 4, Oct. 1969, pp. 20-32.

TABLE I. - TEST CONDITIONS FOR HIGH-FREQUENCY BLADE RESPONSE STUDY

Case Identification	Aircraft	Regime	V		μ	ΩR		$M_{1.0,90}$	C_T/σ
			m/sec	kn		m/sec	ft/sec		
12	NH-3A	Level flight, with wings	71.5	139.0	0.36	202.	662.	0.81	0.056
43	NH-3A	Level flight, with wings	95.6	186.0	0.47	202.	662.	0.88	0.058
71	NH-3A	Right turn, 45° angle of bank, without wings	67.0	130.5	0.33	206.	675.	0.81	0.080
72	NH-3A	Right turn, 60° angle of bank, without wings	71.0	138.1	0.35	206.	675.	0.82	0.085
41LF	CH-53A	Level flight	51.8	100.8	0.24	216.	710.	0.80	0.063
41TR	CH-53A	Transition into right turn	51.8	100.8	0.24	216.	710.	0.80	0.078
41TN	CH-53A	Right turn, 60° angle of bank	51.8	100.8	0.24	216.	710.	0.80	0.099
44	CH-53A	Level flight	81.5	158.8	0.38	216.	710.	0.89	0.057

TABLE II. - DYNAMIC TERMS REQUIRED FOR APPROXIMATION OF NH-3A AND CH-53A HARMONICS OF HINGE FORCES

Harmonic of Hinge Force	Terms Required for Approximation of Total Harmonic of Hinge Force [a]																	
	X1	X2	X3	X4	Y1	Y2	Y3	Y4	Y5	Y6	Y7	Y8	Z1	Z2	Z3	Z4	Z5	Z6
$F^*_{x,1}$	N,C[b]																	
$F^*_{x,2}$	N,C	N,C																
$F^*_{x,3}$	N,C	N,C																
$F^*_{x,4}$	N,C	C	N															
$F^*_{x,5}$	N,C		C															
$F^*_{x,6}$	N,C	C	N															
$F^*_{x,7}$	N,C	C	C	N														
$F^*_{y,1}$					N,C	N,C												
$F^*_{y,2}$					N,C	N,C	C			C								
$F^*_{y,3}$					N,C	N,C				N,C								
$F^*_{y,4}$					N,C	N,C				N,C	N							
$F^*_{y,5}$					N,C	N,C	N			N,C	C	C						
$F^*_{y,6}$					N,C	N,C			N	N,C	N							
$F^*_{y,7}$					N,C	N,C	N	N		N,C	C	C						
$F^*_{z,1}$													N,C					

TABLE II. - DYNAMIC TERMS REQUIRED FOR APPROXIMATION OF NH-3A AND CH-53A HARMONICS OF HINGE FORCES - Continued

Harmonic of Hinge Force	Terms Required for Approximation of Total Harmonic of Hinge Force [a]																	
	X1	X2	X3	X4	Y1	Y2	Y3	Y4	Y5	Y6	Y7	Y8	Z1	Z2	Z3	Z4	Z5	Z6
$F^*_{z,2}$													N,C				N,C	
$F^*_{z,3}$													N,C			N	N,C	
$F^*_{z,4}$													N,C	N,C	N,C	N	N,C	
$F^*_{z,5}$													N,C	N,C	N	N	N,C	N
$F^*_{z,6}$													N,C		N,C	N	N,C	C
$F^*_{z,7}$													N,C		N,C	N	N,C	

[a]Definition of symbolic terms is as follows

Symbolic Term	Complete Definition
X1	$-F_{xl}\cos\beta\cos\gamma$
X2	$2\dot{\gamma}\Omega m_c \cos^2\beta\cos\gamma\left[x_c\cos\beta + \sin\beta(y_c\sin\theta + z_c\cos\theta)\right]$
X3	$-m_c\cos^2\beta\cos^2\gamma\,(\ddot{x}_R - 2\dot{y}_R\Omega - x_R\Omega^2)$
X4	$\ddot{\beta}m_c x_c \cos^2\theta\sin\beta\cos\gamma$
Y1	$-F_{xl}\cos\beta\sin\gamma$
Y2	$-\frac{1}{\Delta x}(M_{zl} - M_{z3})\cos\theta\cos\gamma$

TABLE II. - DYNAMIC TERMS REQUIRED FOR APPROXIMATION OF NH-3A AND CH-53A HARMONICS OF HINGE FORCES - Concluded

Symbolic Term	Complete Definition
Y3	$-\frac{1}{\Delta x}(M_{y1} - M_{y3})\ \sin\theta\cos\gamma$
Y4	$-\frac{\ddot{\gamma}}{\Delta x}\left[x_B m_{IS}(\Delta x - x_{B-1}) - I_z\right]\cos^2\theta\ \cos\gamma\ \cos\beta$
Y5	$-\frac{m_{IS}}{\Delta x}(\Delta x - x_{B-1} - x_B)(\cos\theta\cos\gamma + \sin\theta\sin\beta\sin\gamma)(\cos\theta\cos\gamma)(\ddot{y}_R + 2\dot{x}_R\Omega - y_R\Omega^2)$
Y6	$-\ddot{\gamma}m_c(x_c\cos\theta\cos\beta + z_c\sin\beta)\ \cos\theta\cos\gamma$
Y7	$-m_c(\cos\theta\cos\gamma + \sin\theta\sin\beta\sin\gamma)(\cos\theta\cos\gamma)(\ddot{y}_R + 2\dot{x}_R\Omega - y_R\Omega^2)$
Y8	$-\ddot{\gamma}m_c(x_c\cos\beta\sin\theta + y_c\sin\beta)\ \sin\theta\cos\gamma$
Z1	$F_{x1}\sin\beta$
Z2	$-\frac{1}{\Delta x}(M_{z1} - M_{z3})\ \cos\beta\sin\theta$
Z3	$\frac{1}{\Delta x}(M_{y1} - M_{y3})\ \cos\beta\cos\theta$
Z4	$\frac{\ddot{\beta}}{\Delta x}\cos\theta\left[x_B\ m_{IS}(\Delta x - x_{B-1}) - I_y\right]\ \cos\beta\cos\theta$
Z5	$\ddot{\beta}m_c x_c\ \cos^2\theta\cos\beta$
Z6	$-m_c\ddot{z}_R\cos^2\beta\cos^2\theta$

[b] $_{N,C}$ signifies term required for both the NH-3A and the CH-53A rotors

N signifies term required only for the NH-3A rotor

C signifies term required only for the CH-53A rotor

TABLE III. - SAMPLE COMPARISON OF APPROXIMATE AND EXACT CALCULATION OF NH-3A HARMONICS OF BLADE HINGE FORCES

Compound mode, $V = 72.0$ m/sec (140.0 kn), $\mu = 0.36$, $C_T/\sigma = 0.043$

Harmonic of Hinge Force	Summation of Major Dynamic Terms (Approximate Solution)			Summation of all Dynamic Terms (Exact Solution)			Harmonic of Hinge Force Absolute Error Due to Approximation	
	Amplitude		Phase	Amplitude		Phase	Amplitude	Phase
	N	lb	deg	N	lb	deg	%	deg
$F^*_{x,1}$	2480	559	231	2520	568	228	2	3
$F^*_{x,2}$	431	97	267	534	120	275	19	8
$F^*_{x,3}$	516	116	140	516	116	135	0	5
$F^*_{x,4}$	1000	226	349	1050	237	354	5	5
$F^*_{x,5}$	271	61	166	298	67	163	9	3
$F^*_{x,6}$	725	163	308	725	163	307	0	1
$F^*_{x,7}$	85	19	115	95	21	114	10	1
$F^*_{y,1}$	1940	436	58	1930	433	62	1	4
$F^*_{y,2}$	747	168	13	770	173	13	3	0
$F^*_{y,3}$	587	132	348	578	130	350	2	2
$F^*_{y,4}$	551	124	271	525	118	271	5	0
$F^*_{y,5}$	56	13	1	50	11	11	20	10
$F^*_{y,6}$	142	32	21	162	37	27	14	6
$F^*_{y,7}$	34	8	355	36	8	359	5	4
$F^*_{z,1}$	23400	5270	103	24400	5470	102	4	1
$F^*_{z,2}$	1460	328	253	1420	320	249	3	4
$F^*_{z,3}$	1990	448	211	2080	467	214	4	3
$F^*_{z,4}$	83	19	7	102	23	359	20	8
$F^*_{z,5}$	322	72	209	300	67	210	7	1
$F^*_{z,6}$	316	71	327	313	70	326	1	1
$F^*_{z,7}$	34	8	154	34	8	150	0	4

TABLE IV. - SAMPLE COMPARISON OF APPROXIMATE AND EXACT CALCULATION OF CH-53A HARMONICS OF BLADE HINGE FORCES

$V = 78.4$ m/sec (152.4 kn), $\mu = 0.36$, $C_T/\sigma = 0.055$

Harmonic of Hinge Force	Summation of Major Dynamic Terms (Approximate Solution			Summation of All Dynamic Terms (Exact Solution)			Harmonic of Hinge Force Absolute Error Due to Approximation	
	Amplitude		Phase	Amplitude		Phase	Amplitude	Phase
	N	lb	deg	N	lb	deg	%	deg
$F^*_{x,1}$	6510	1470	182	7160	1610	182	9	0
$F^*_{x,2}$	582	131	129	595	134	128	2	1
$F^*_{x,3}$	1510	340	356	1740	391	353	13	3
$F^*_{x,4}$	1900	427	340	2090	470	332	9	8
$F^*_{x,5}$	831	187	248	685	154	235	21	13
$F^*_{x,6}$	818	184	354	916	206	1	11	7
$F^*_{x,7}$	268	60	324	266	60	318	1	6
$F^*_{y,1}$	4400	990	67	4850	1090	70	9	3
$F^*_{y,2}$	480	108	153	511	115	154	6	1
$F^*_{y,3}$	2010	452	282	2350	528	278	14	4
$F^*_{y,4}$	3120	700	256	3460	779	256	10	0
$F^*_{y,5}$	408	92	59	440	99	54	7	5
$F^*_{y,6}$	595	134	32	734	165	25	19	7
$F^*_{y,7}$	249	56	79	295	66	74	16	5
$F^*_{z,1}$	16600	3720	92	17200	3870	88	4	4
$F^*_{z,2}$	6750	1520	253	6540	1470	251	3	2
$F^*_{z,3}$	7250	1630	155	7470	1680	159	3	4
$F^*_{z,4}$	911	205	353	782	176	344	16	9
$F^*_{z,5}$	1160	260	250	1300	293	253	11	3
$F^*_{z,6}$	130	29	173	101	23	206	29	33
$F^*_{z,7}$	149	34	26	176	40	9	15	17

Figure 1.- NH-3A Test Aircraft.

Figure 2.- CH-53A Test Aircraft.

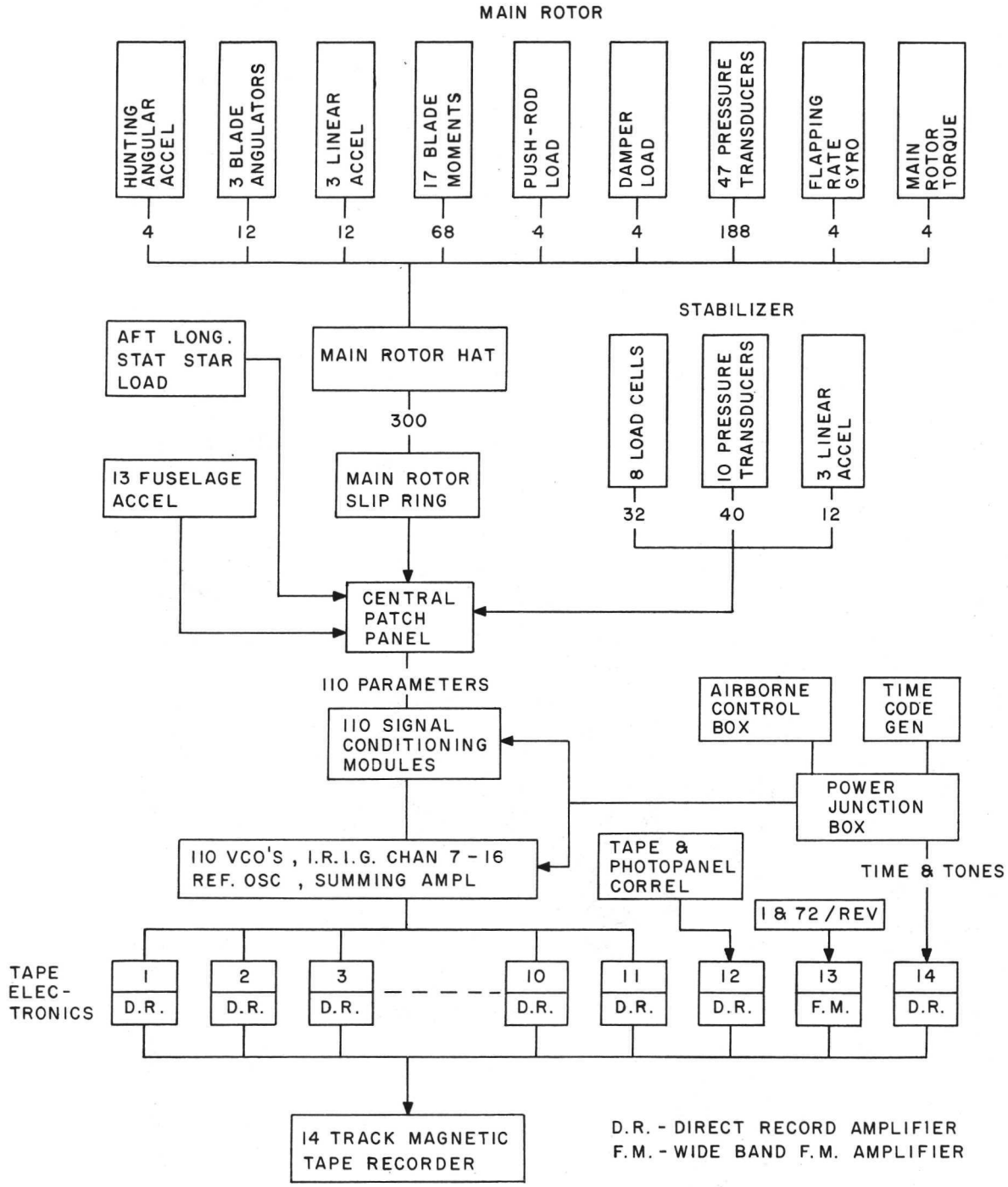

Figure 3.- Block Diagram of Airborne Recording System.

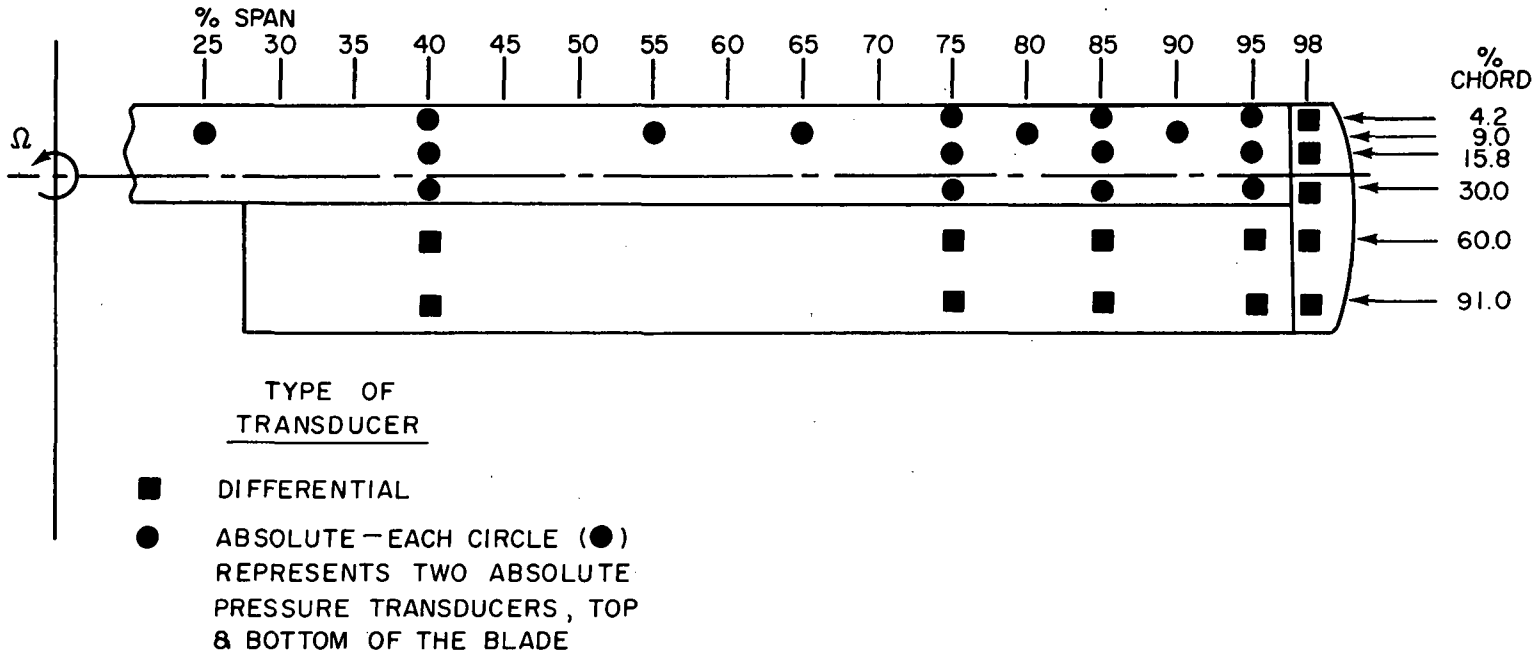

Figure 4.- Blade Pressure Transducer Locations.

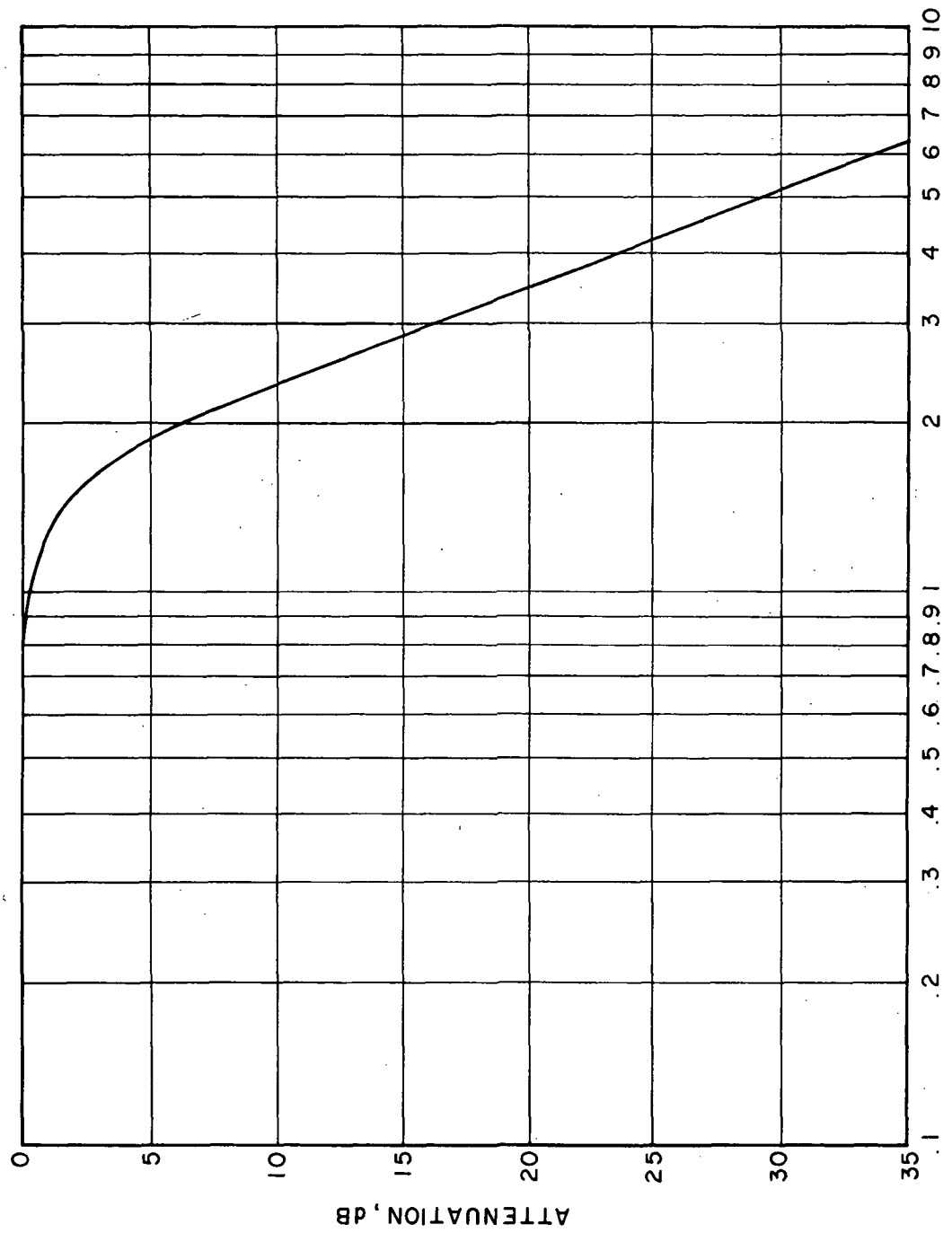

Figure 5.- Characteristics of Constant Amplitude Low Pass Filters Used in Data Reduction.

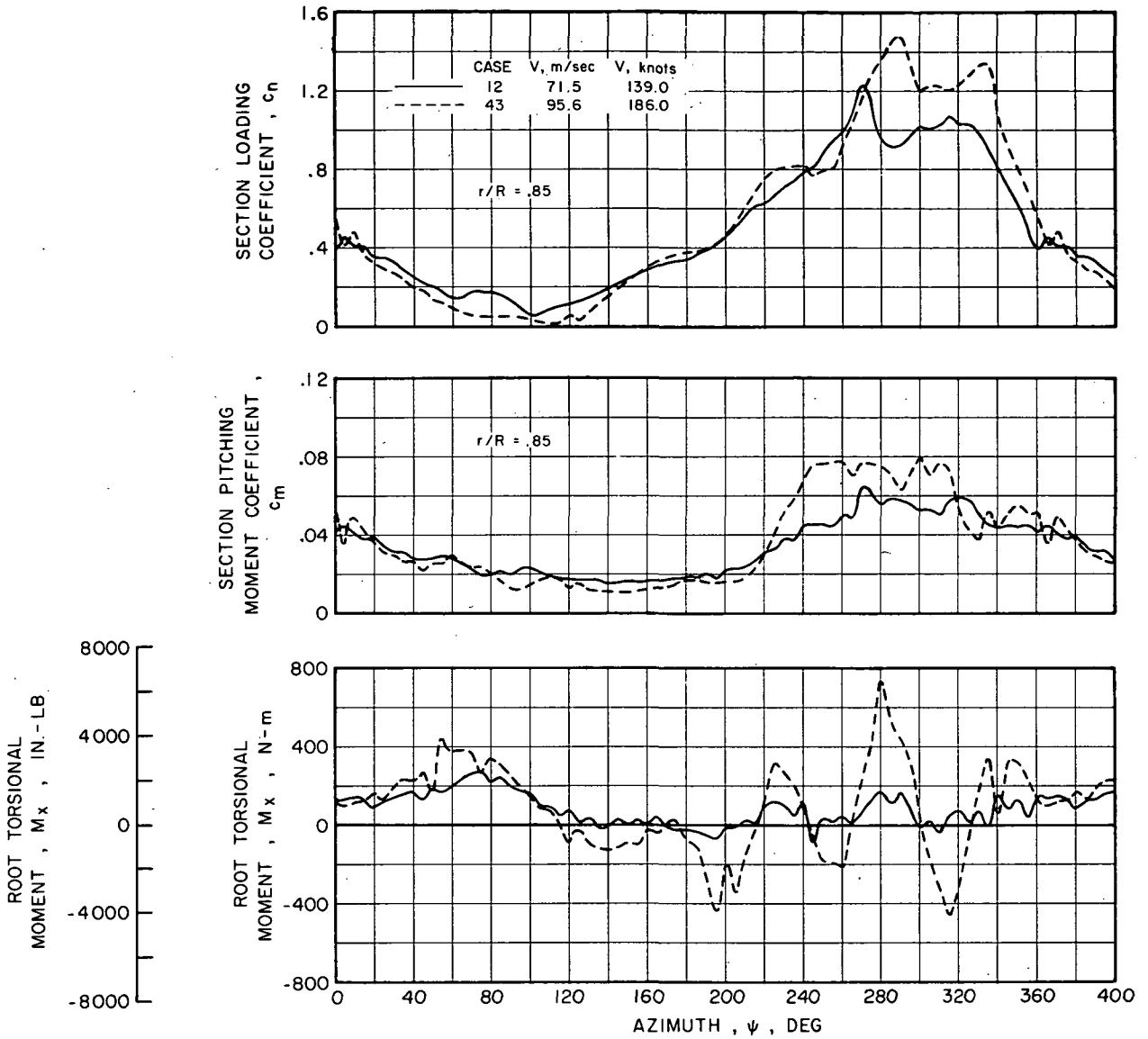

Figure 6.- Effects of Airspeed on Main Rotor Blade Response for the NH-3A.

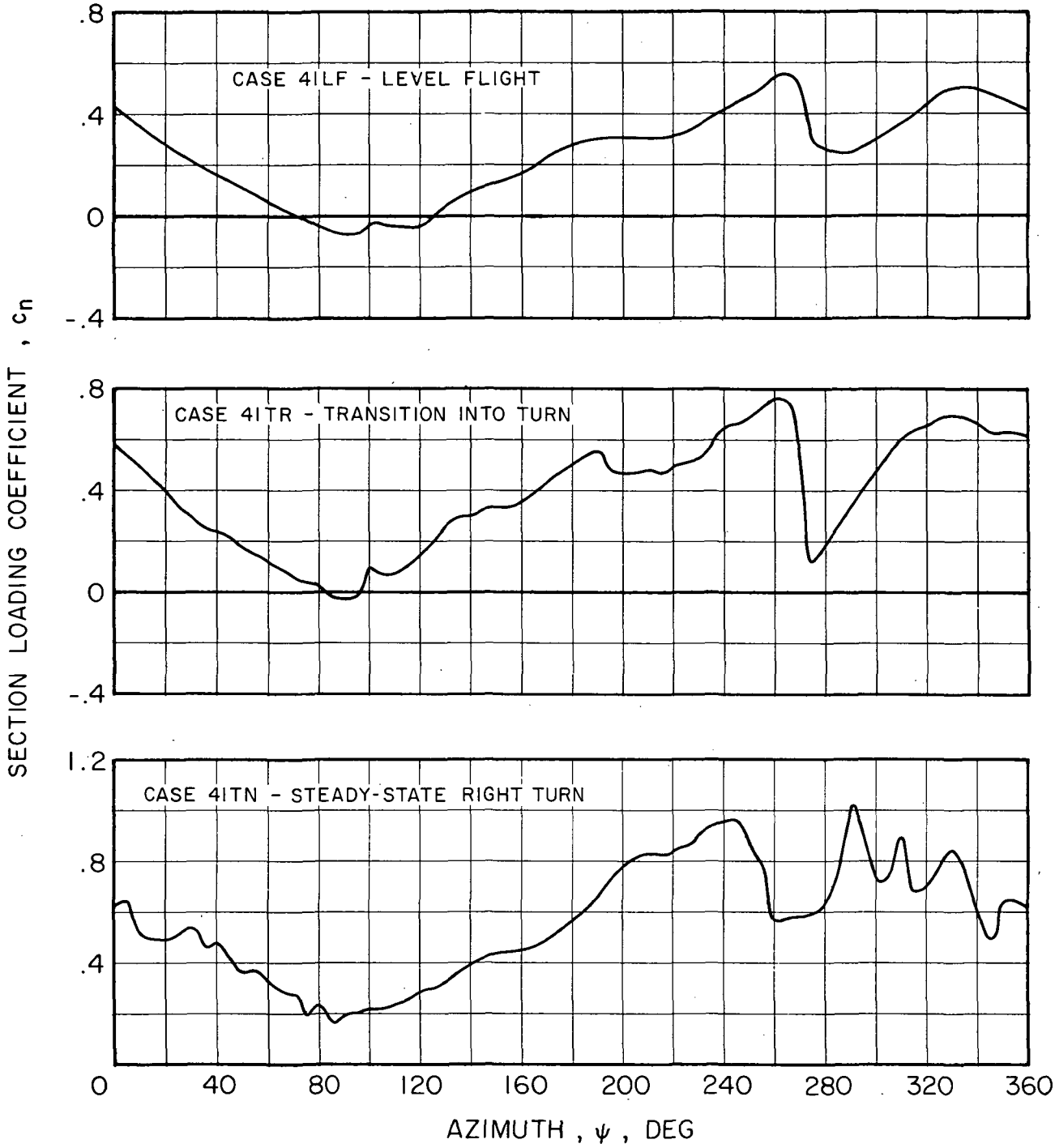

Figure 7.- Maneuver Effects on CH-53A Main Rotor Blade Section Loading Coefficient at r/R = 0.85.

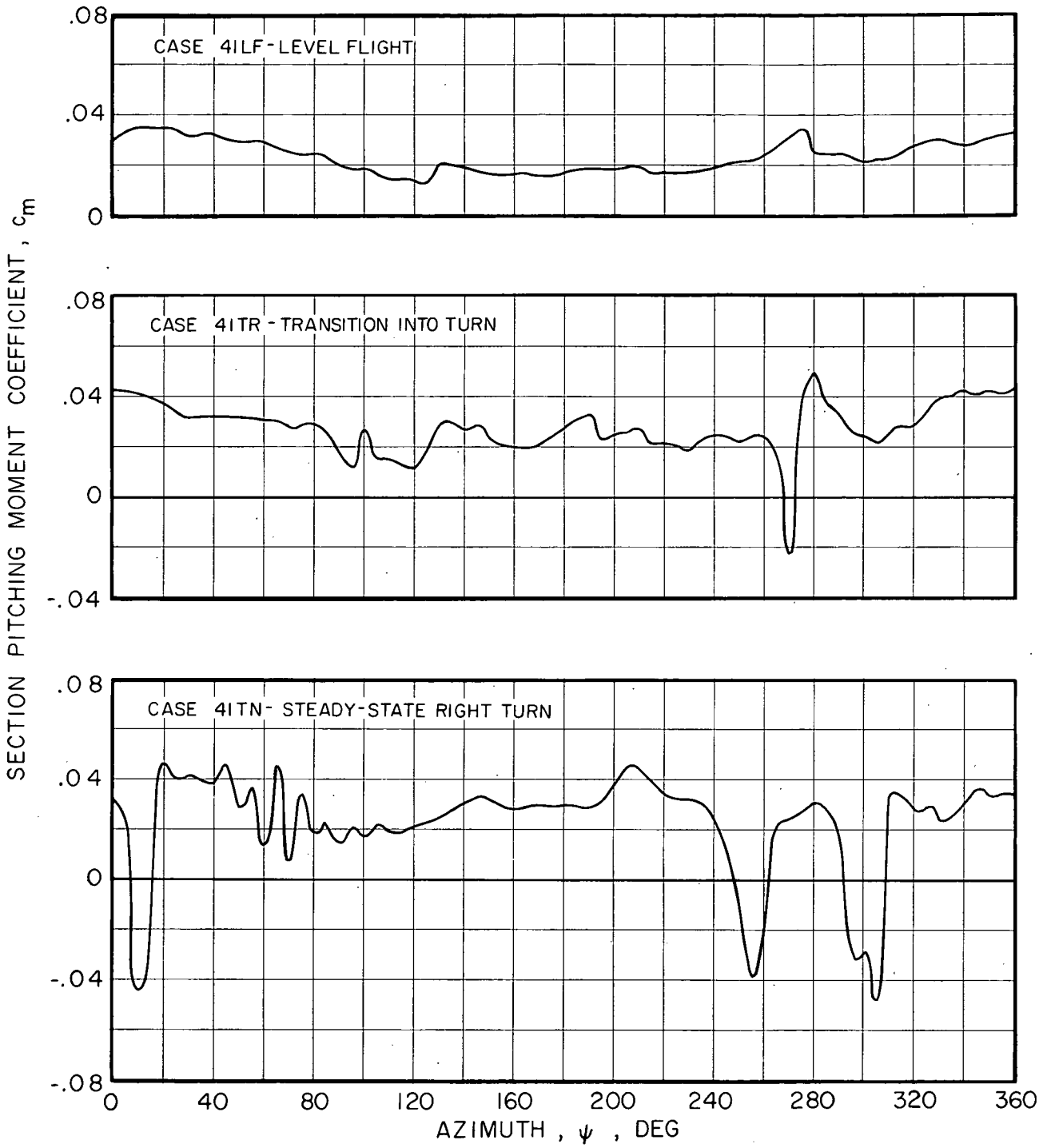

Figure 8.- Maneuver Effects on CH-53A Main Rotor Blade Section Pitching Moment Coefficient at r/R = 0.85.

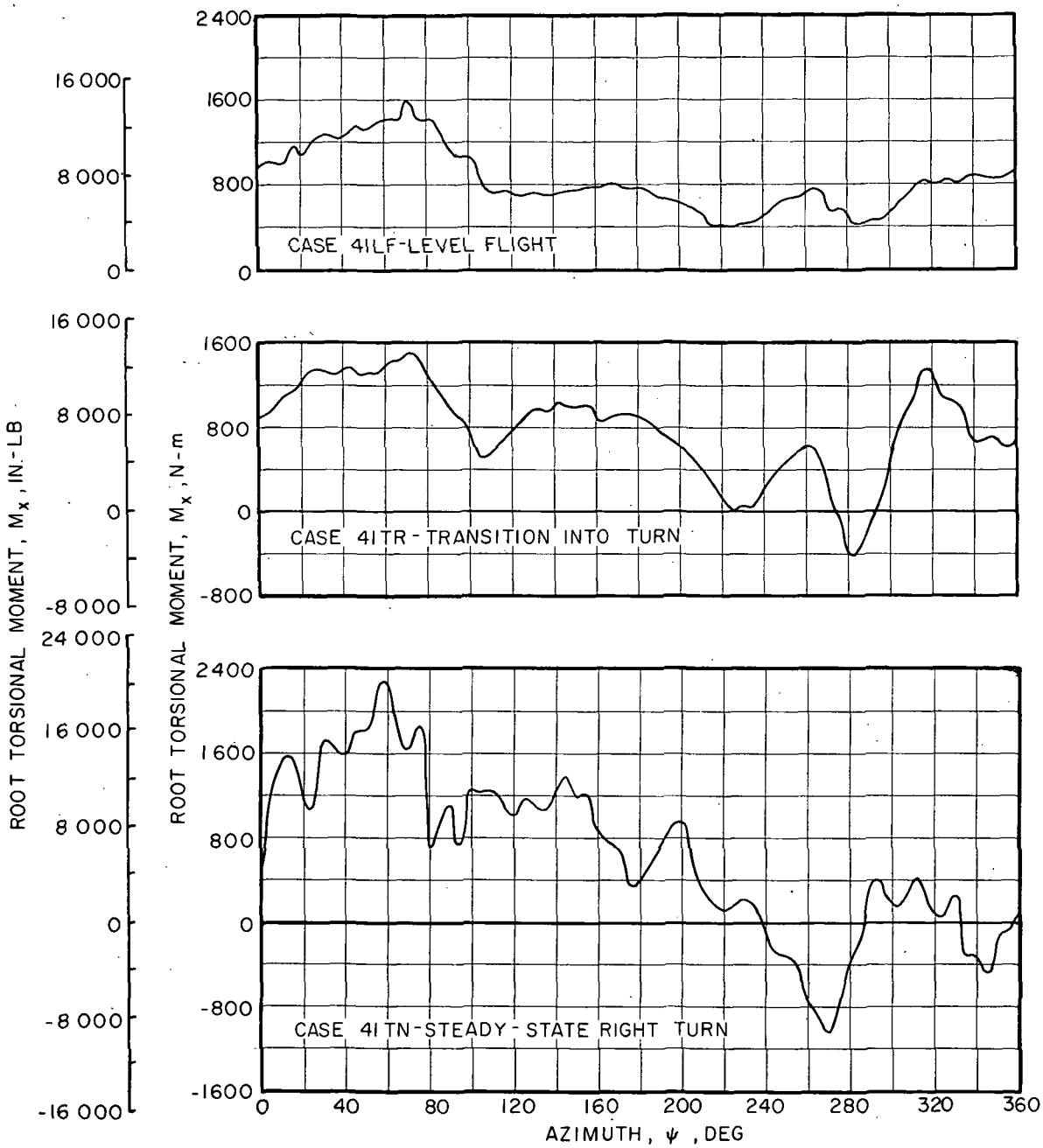

Figure 9.- Maneuver Effects on CH-53A Root Torsional Moment.

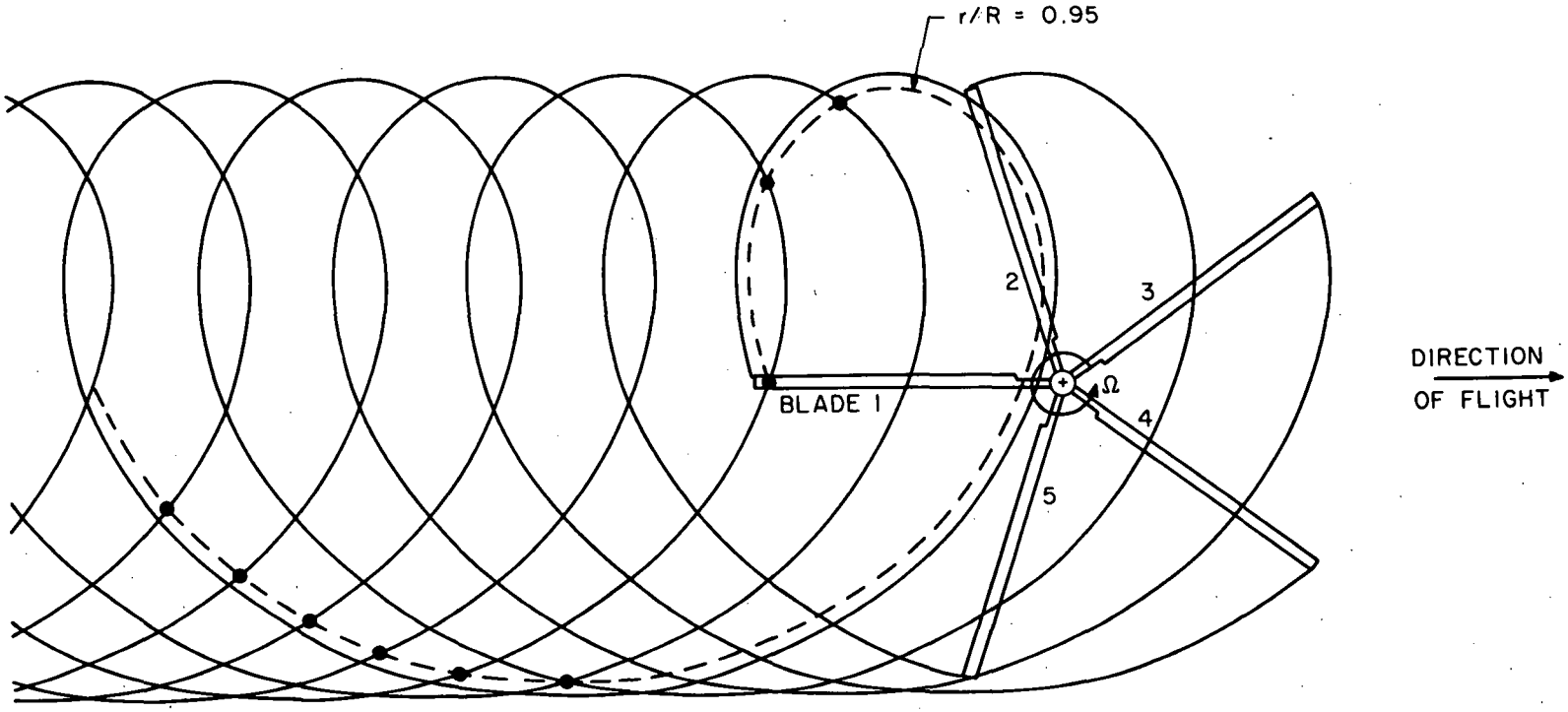

Figure 10. - Plan View of Non-distorted Wake Helical Pattern for NH-3A Case 72, Right Turn, 60 deg Angle of Bank, $\mu = 0.35$.

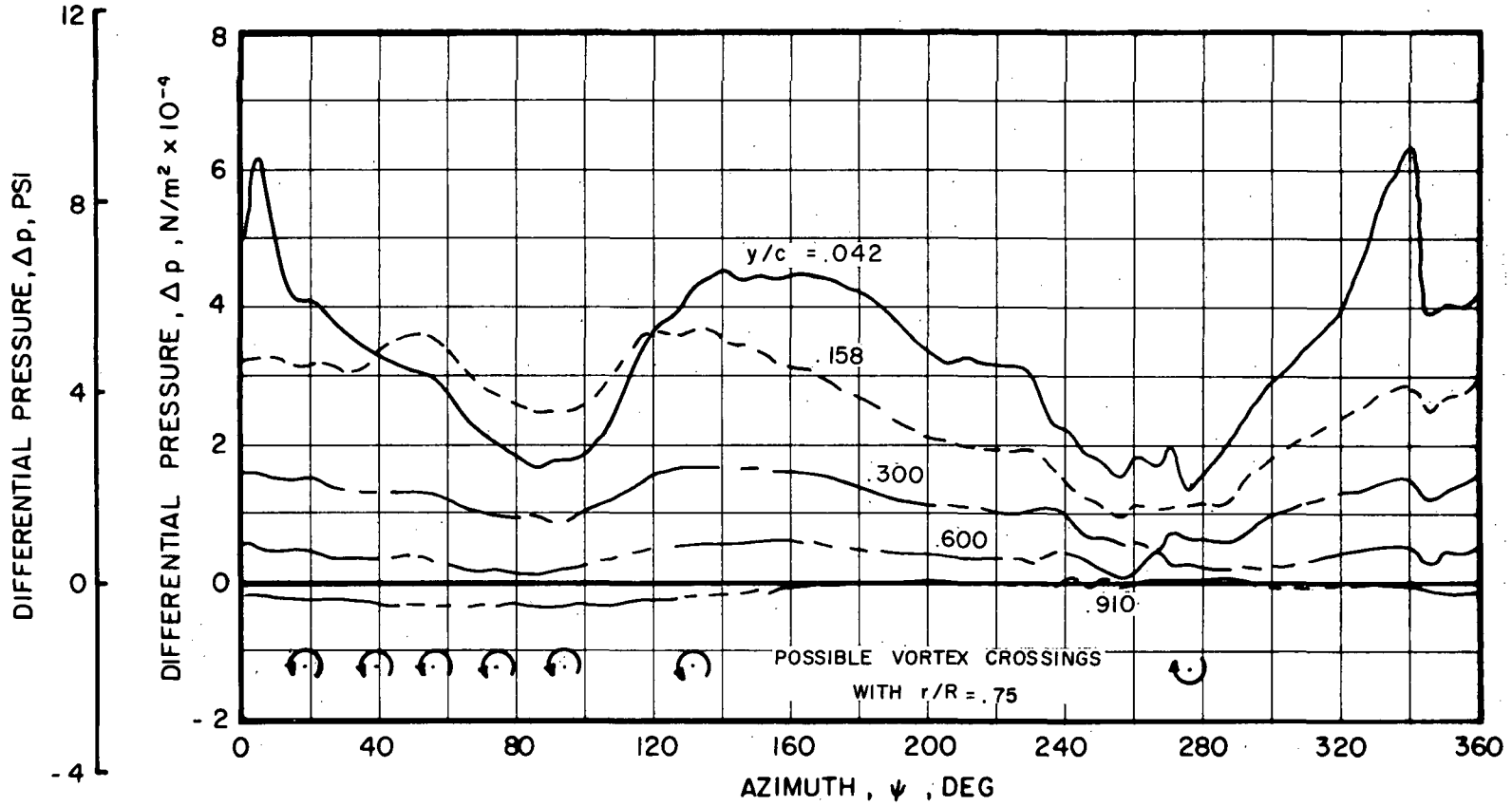

Figure 11.- Azimuthal Histories of Blade Differential Pressure at r/R = 0.75 for NH-3A Case 72.

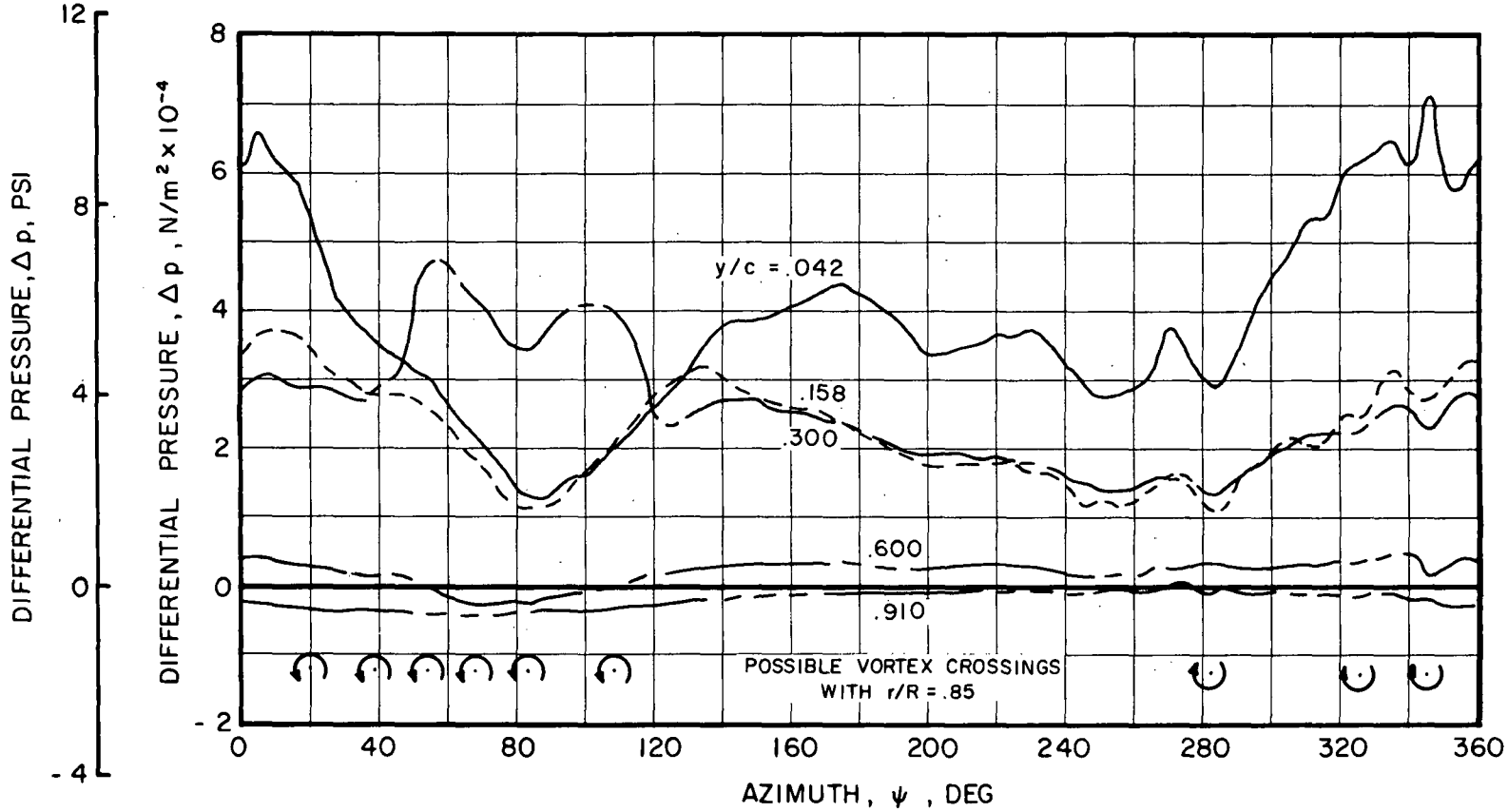

Figure 12.- Azimuthal Histories of Blade Differential Pressure at r/R = 0.85 for NH-3A Case 72.

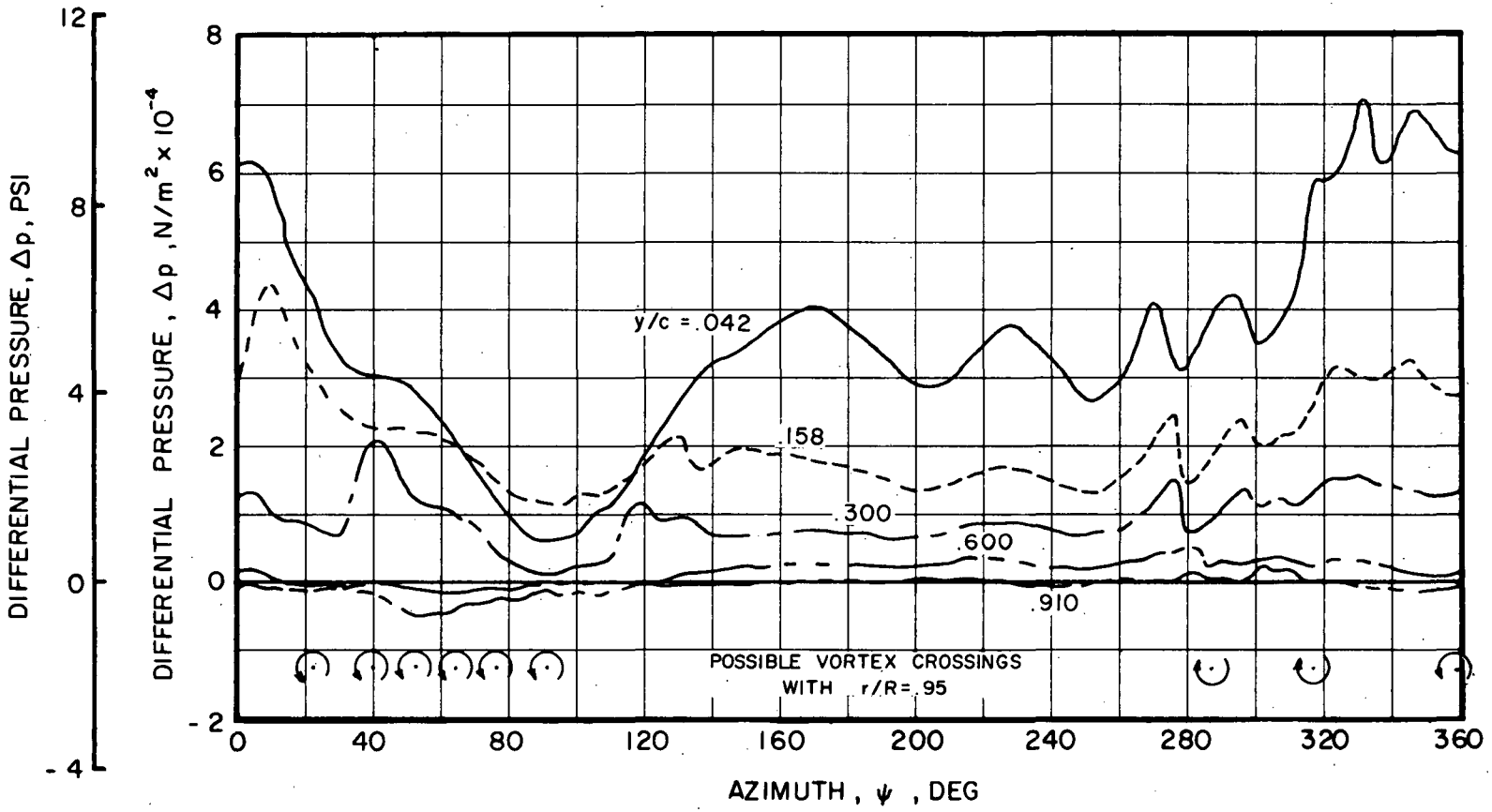

Figure 13.- Azimuthal Histories of Blade Differential Pressure at r/R = 0.95 for NH-3A Case 72.

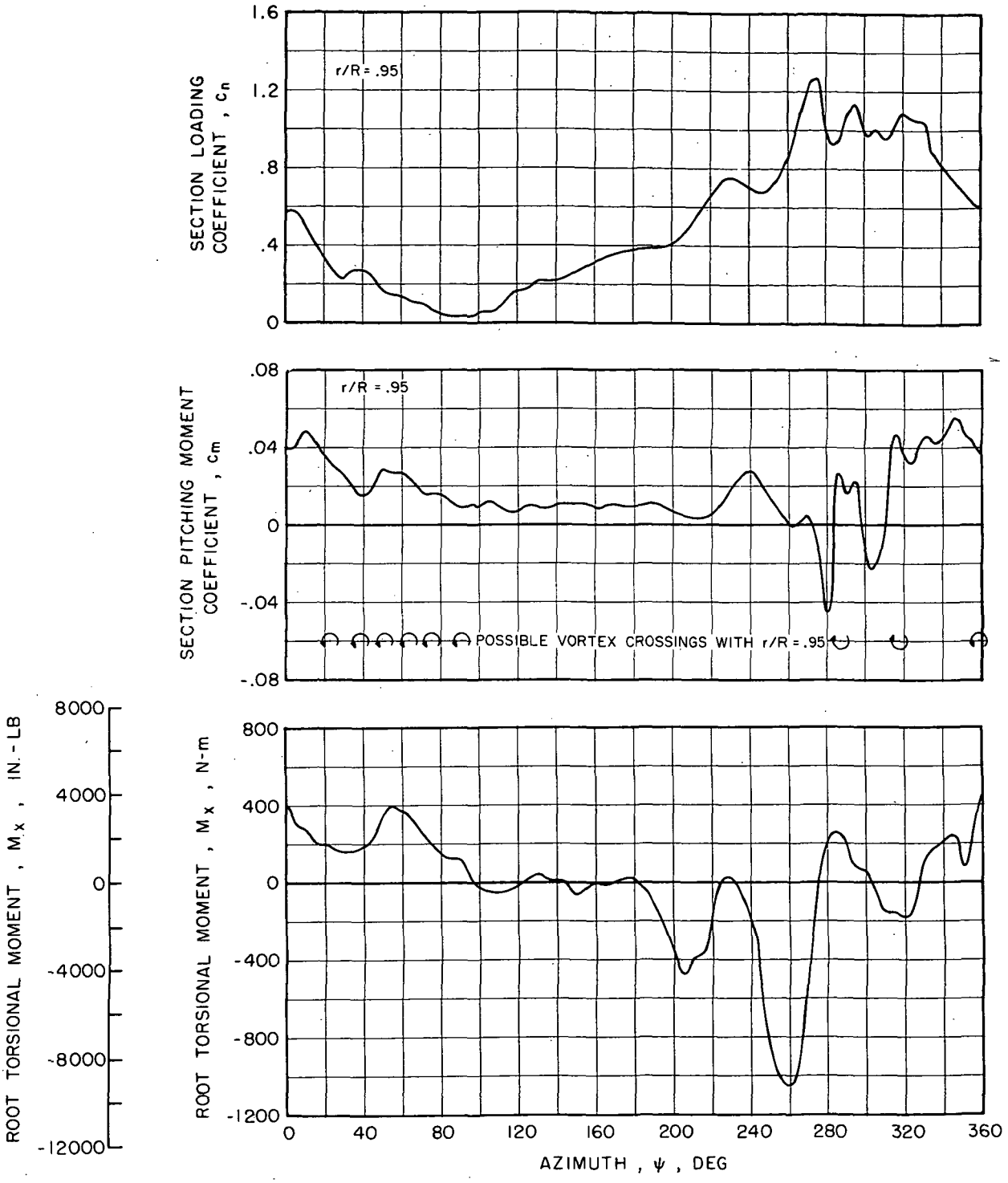

Figure 14.- Azimuthal Histories of Section Loading Coefficient, Section Pitching Moment Coefficient, and Root Torsional Moment for NH-3A Case 72.

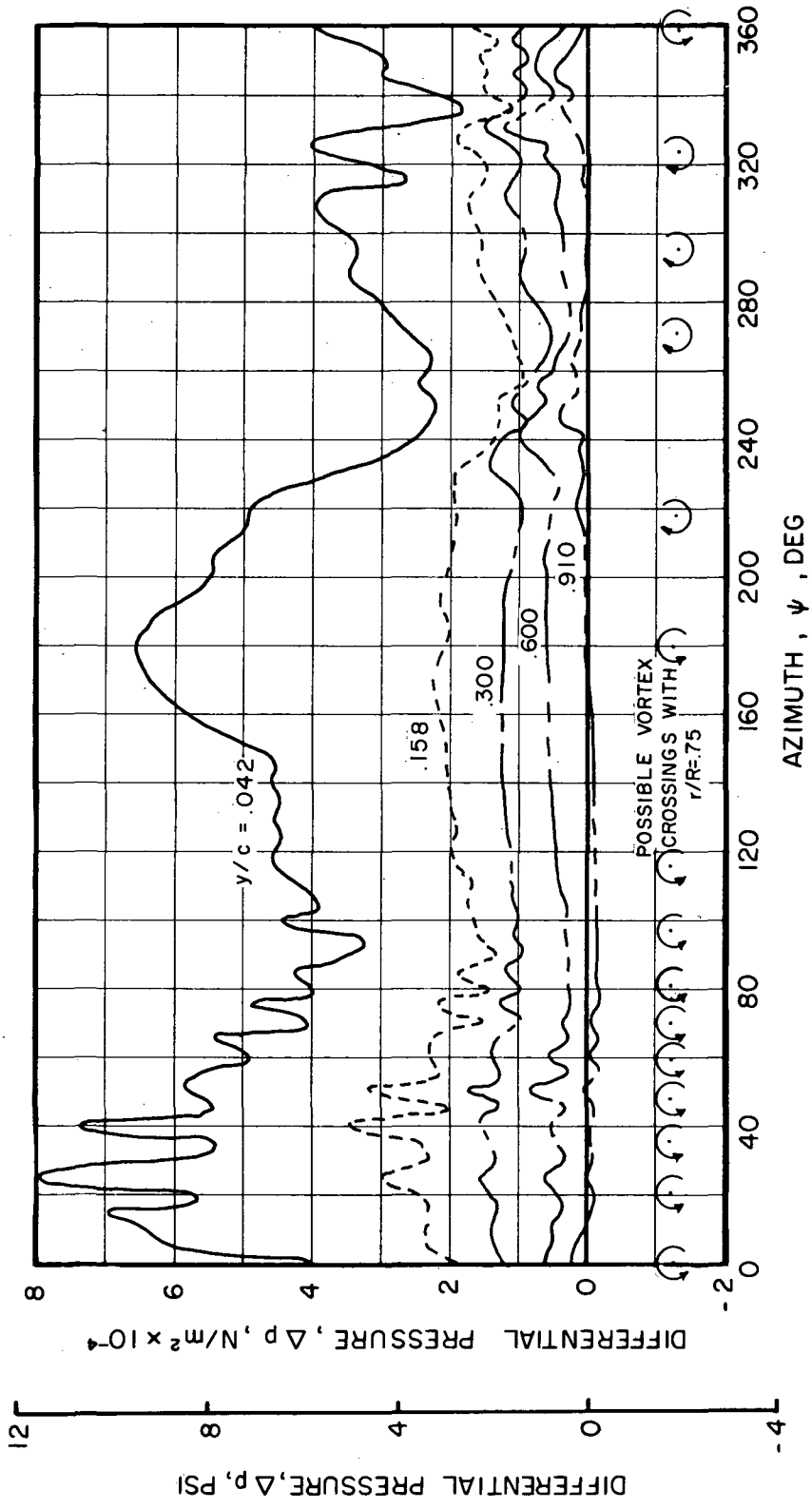

Figure 15.- Azimuthal Histories of Blade Differential Pressure at r/R = 0.75 for CH-53A Case 41TN.

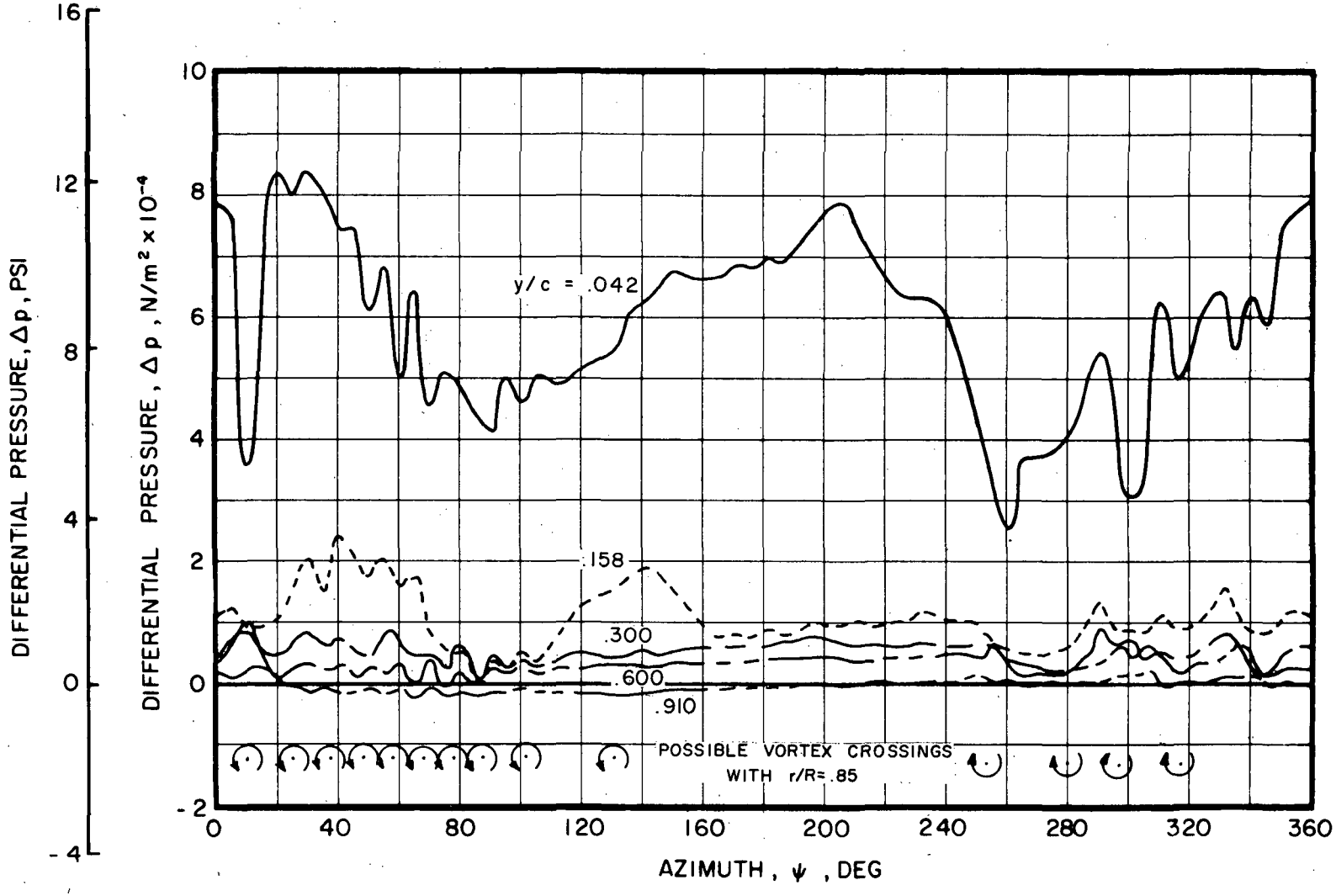

Figure 16.- Azimuthal Histories of Blade Differential Pressure at r/R = 0.85 for CH-53A Case 41TN.

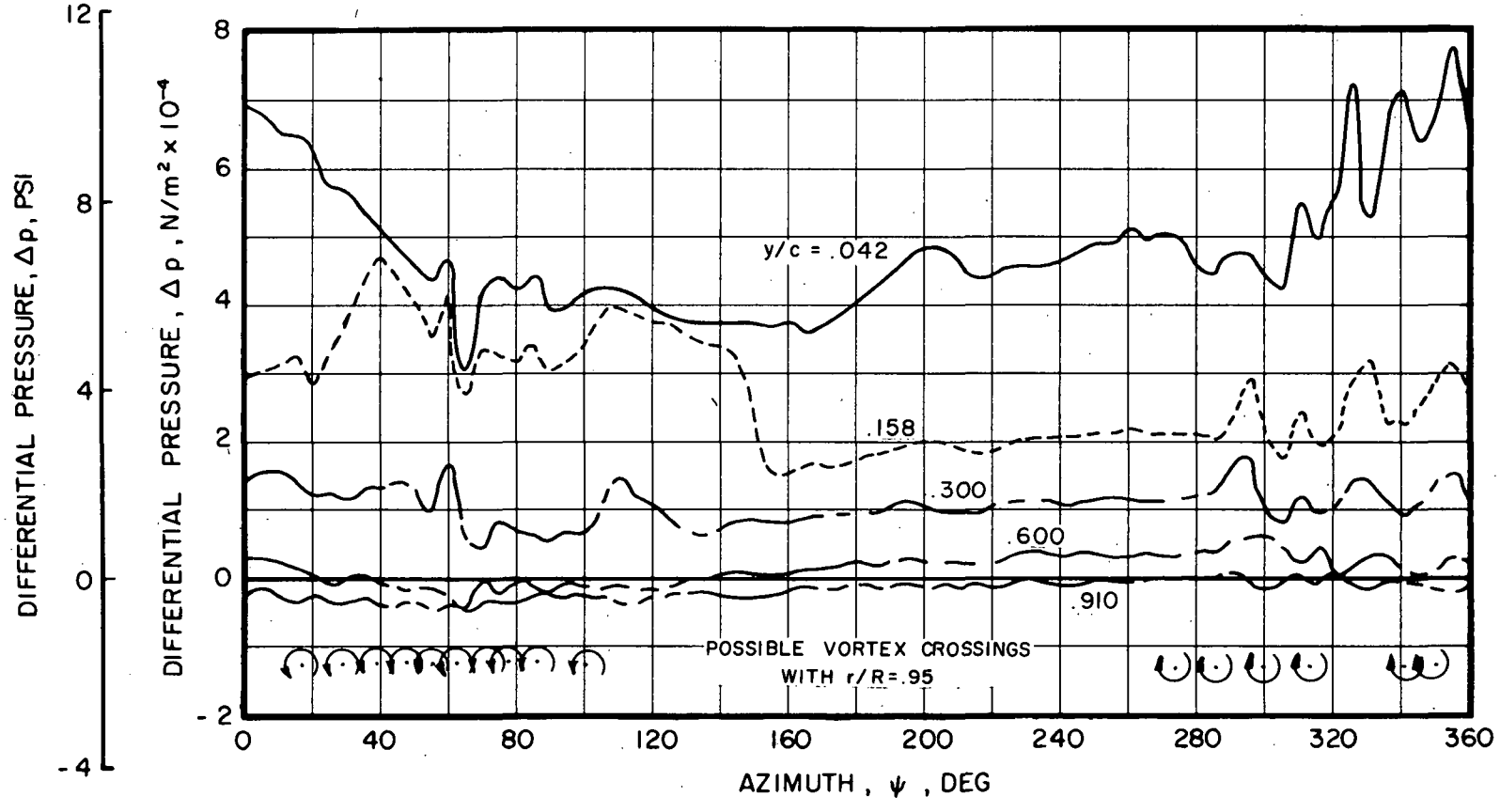

Figure 17.-- Azimuthal Histories of Blade Differential Pressure at r/R = 0.95 for CH-53A Case 41TN.

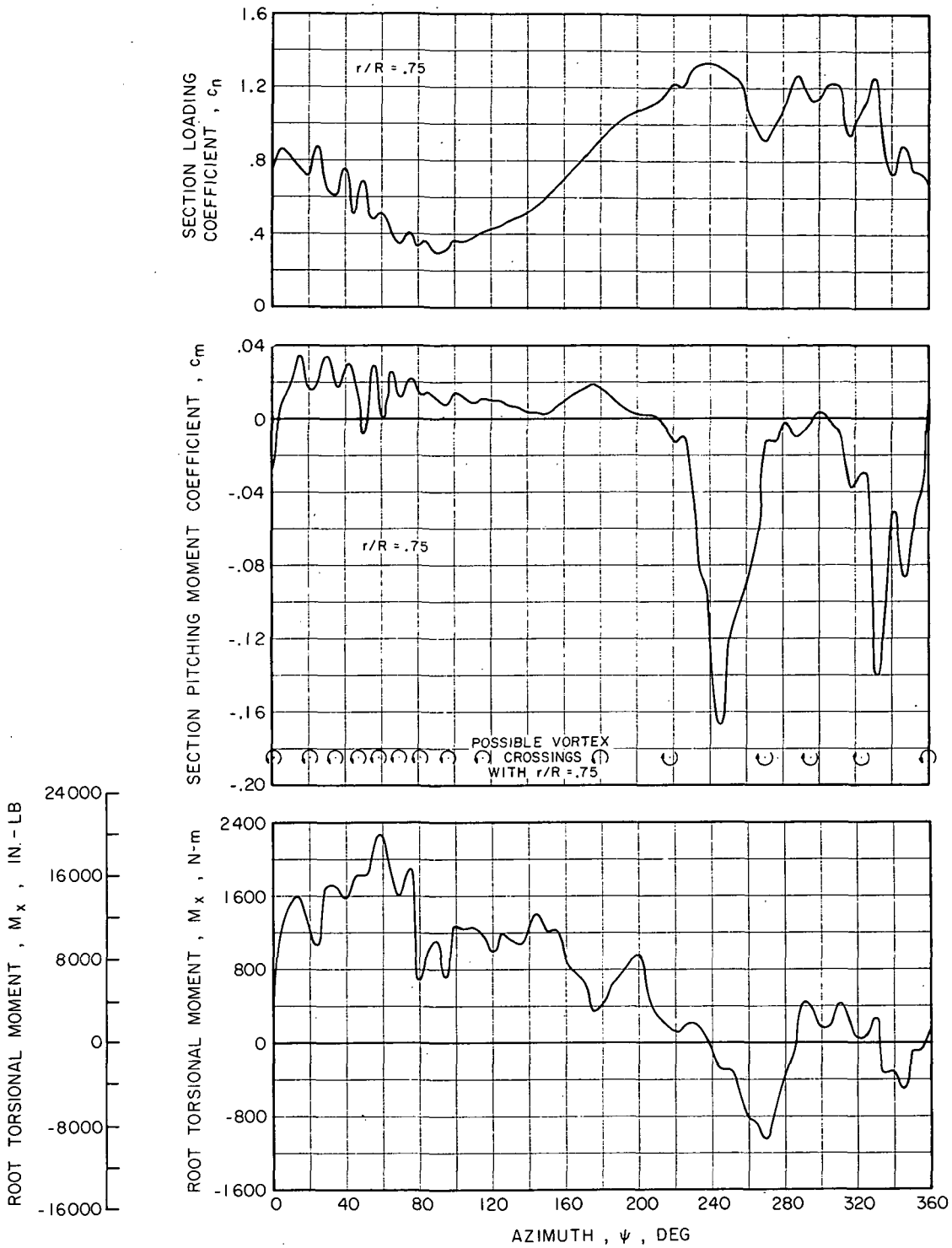

Figure 18.- Azimuthal Histories of Section Loading Coefficient, Section Pitching Moment Coefficient, and Root Torsional Moment for CH-53A Case 41TN.

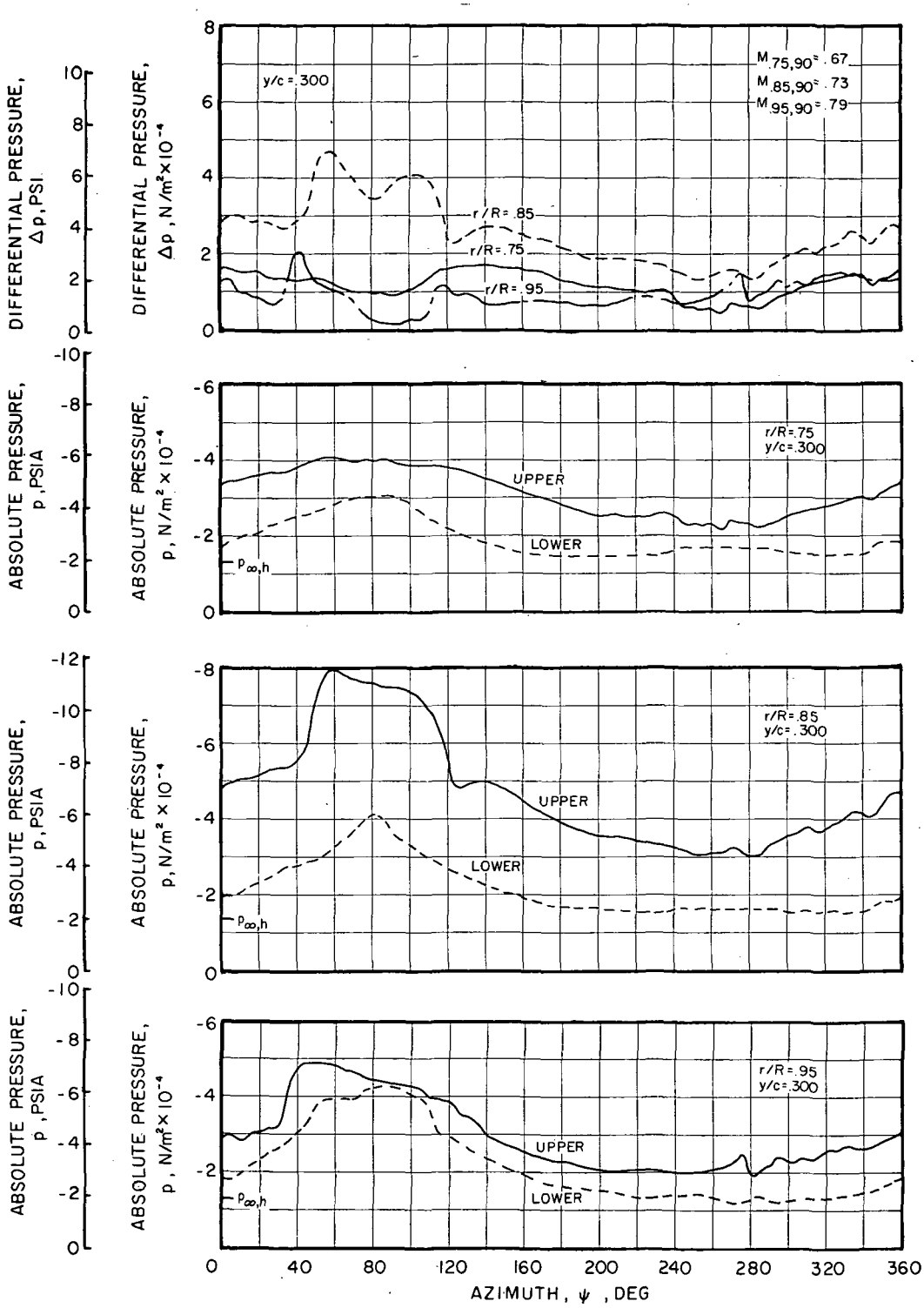

Figure 19.- Critical Mach-Number Effect on Blade Pressure Azimuthal Histories for NH-3A Case 72.

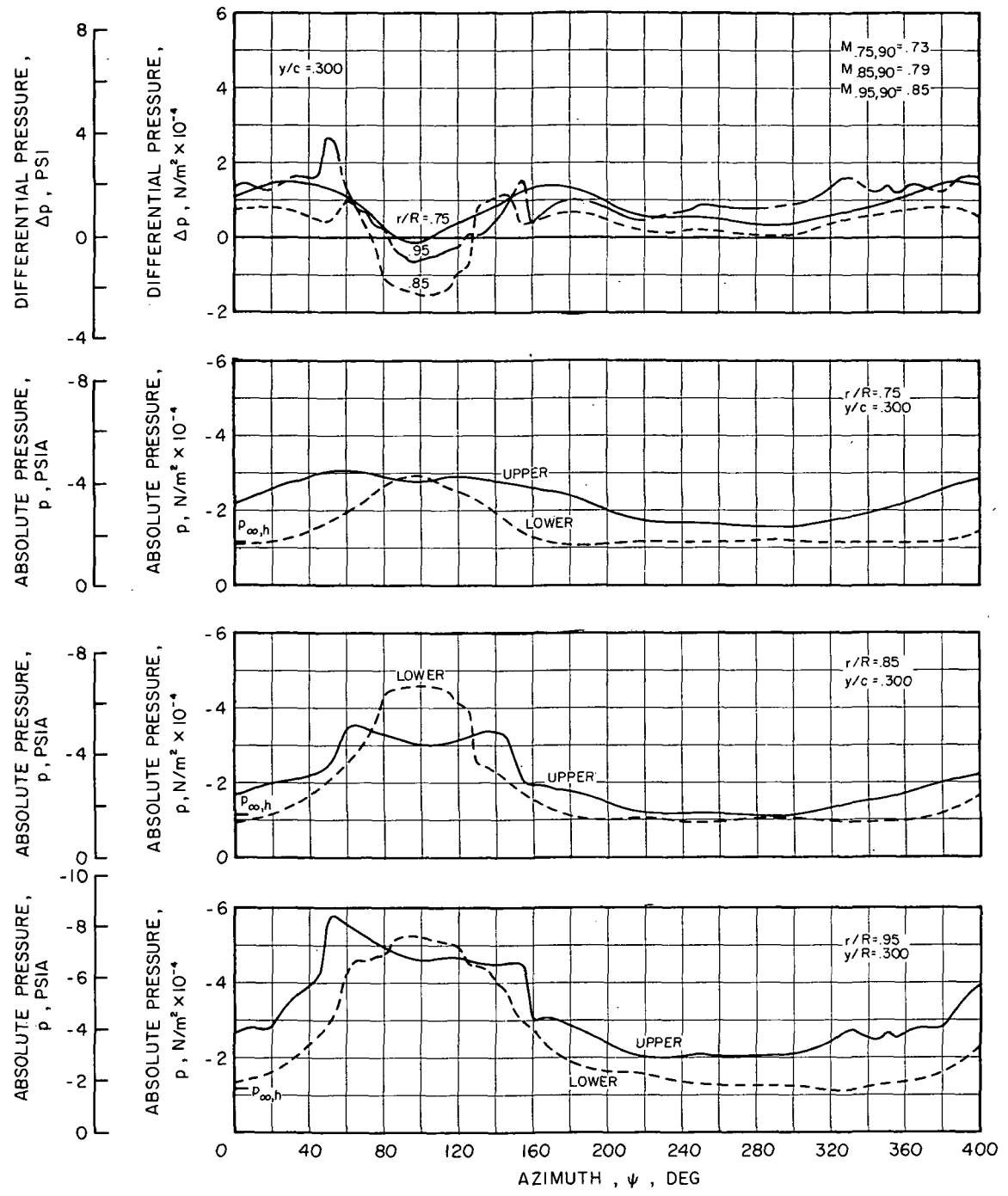

Figure 20.- Critical Mach-Number Effect on Blade Pressure Azimuthal Histories for CH-53A Case 44.

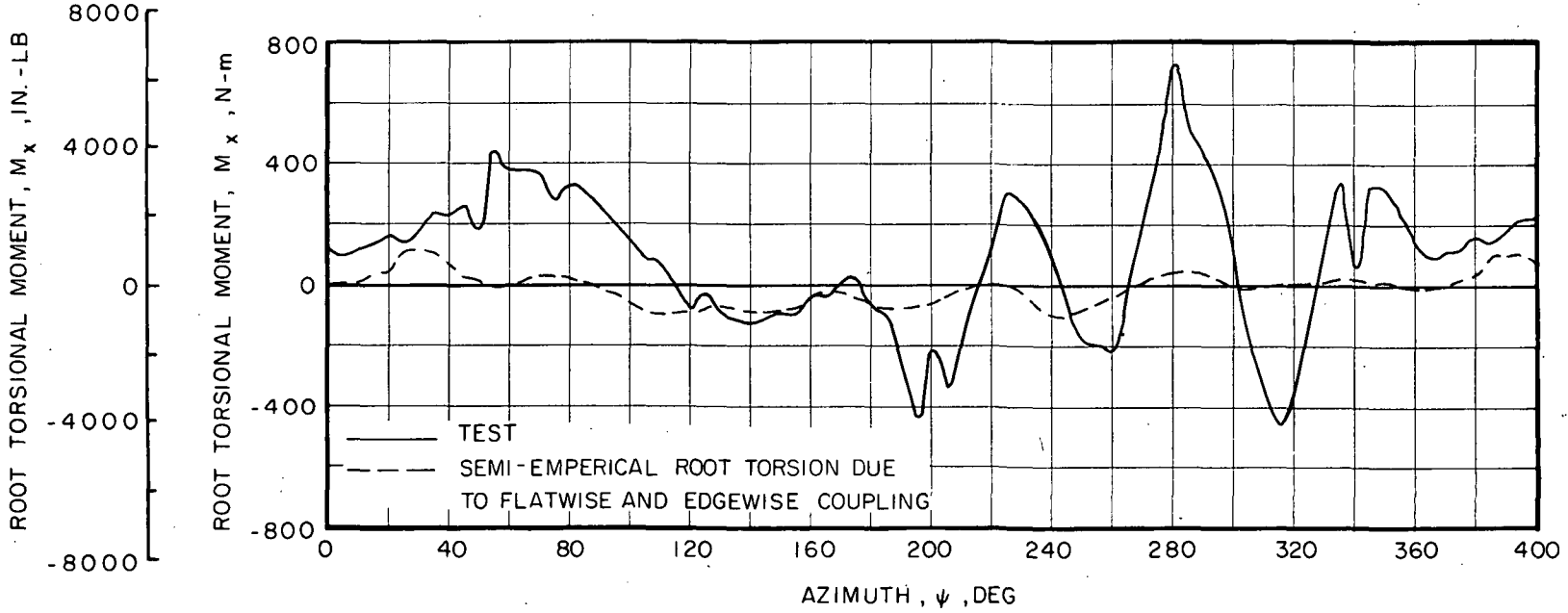

Figure 21.- Contribution of Blade Flatwise and Edgewise Coupling to Root Torsion for NH-3A Case 43.

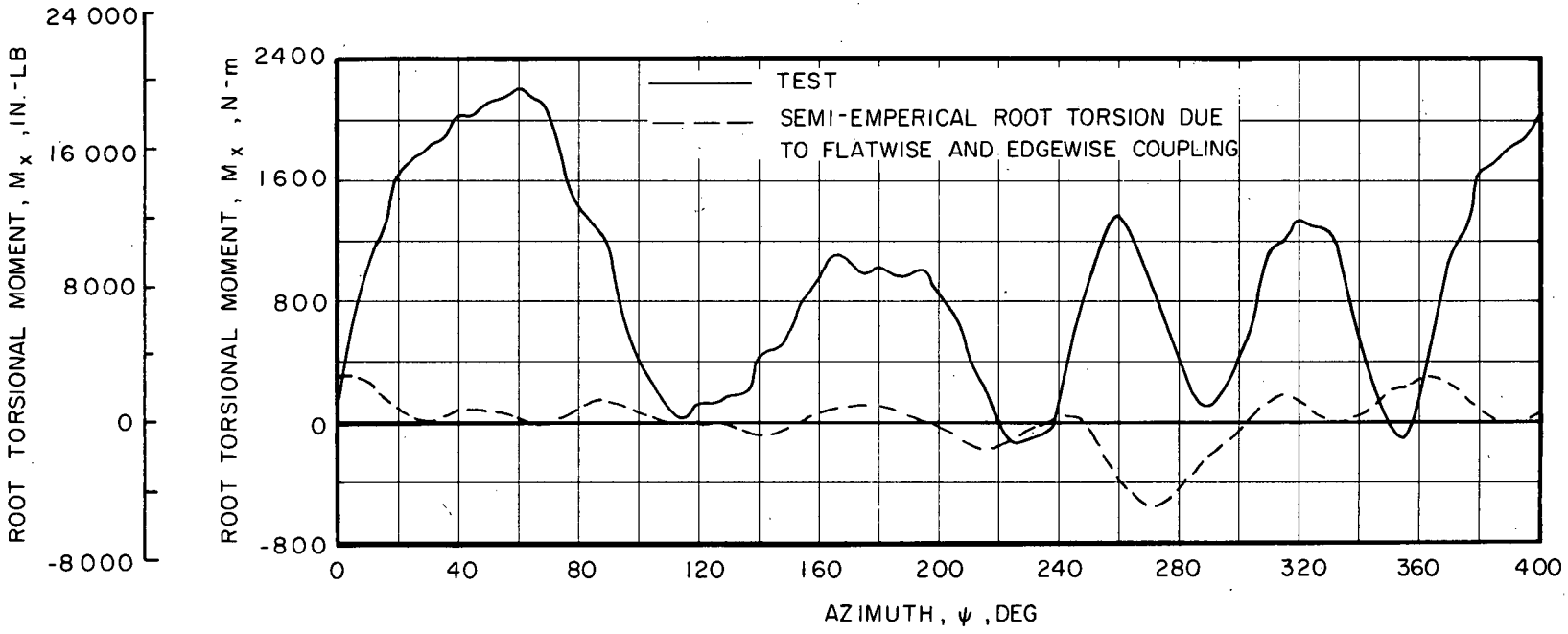

Figure 22.- Contribution of Blade Flatwise and Edgewise Coupling to Root Torsion for CH-53A Case 44.

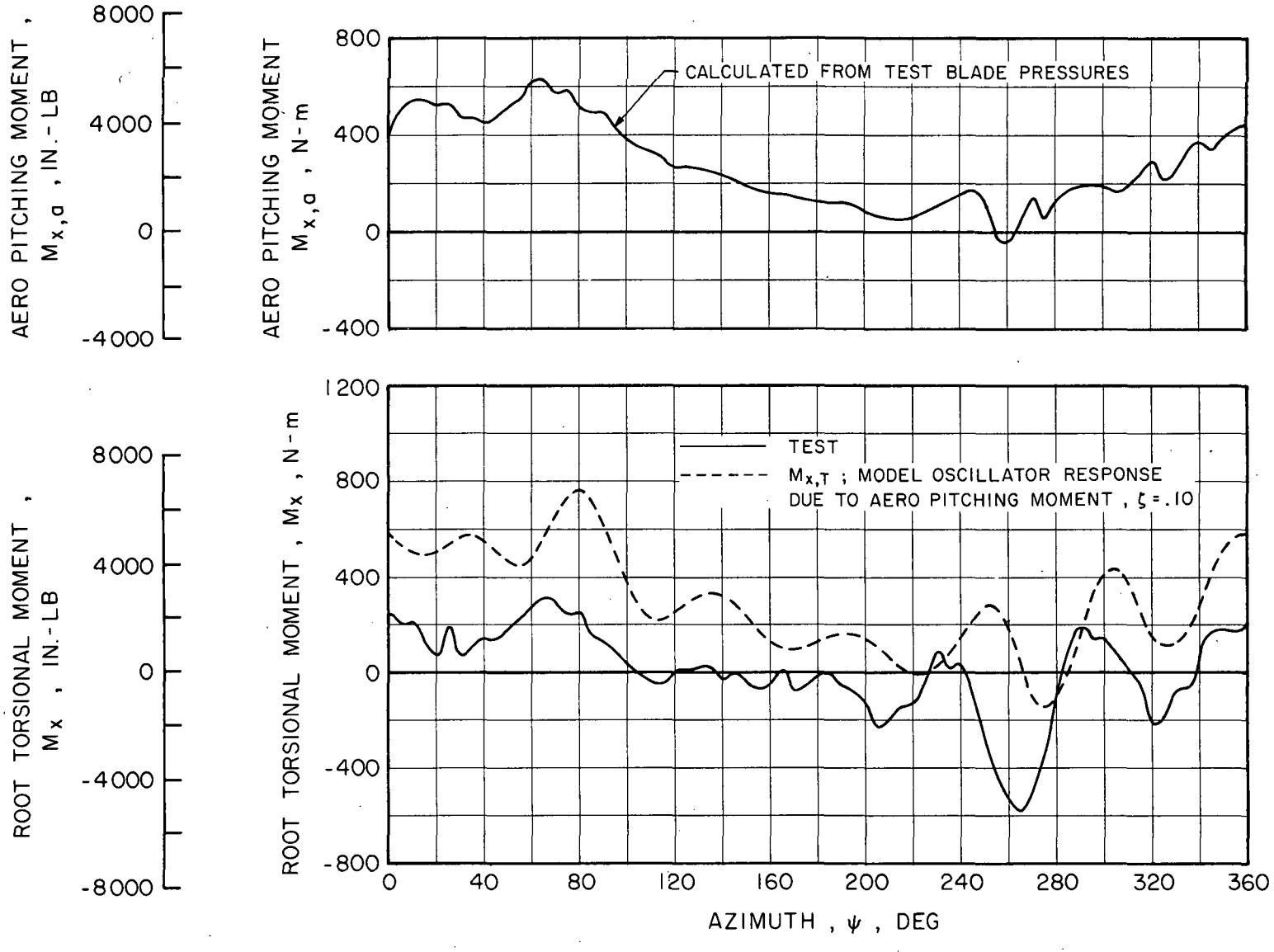

Figure 23.- Comparison Between Measured Blade Torsional Response and Torsional Oscillator Model Response to Aerodynamic Pitching Moment for NH-3A Case 71.

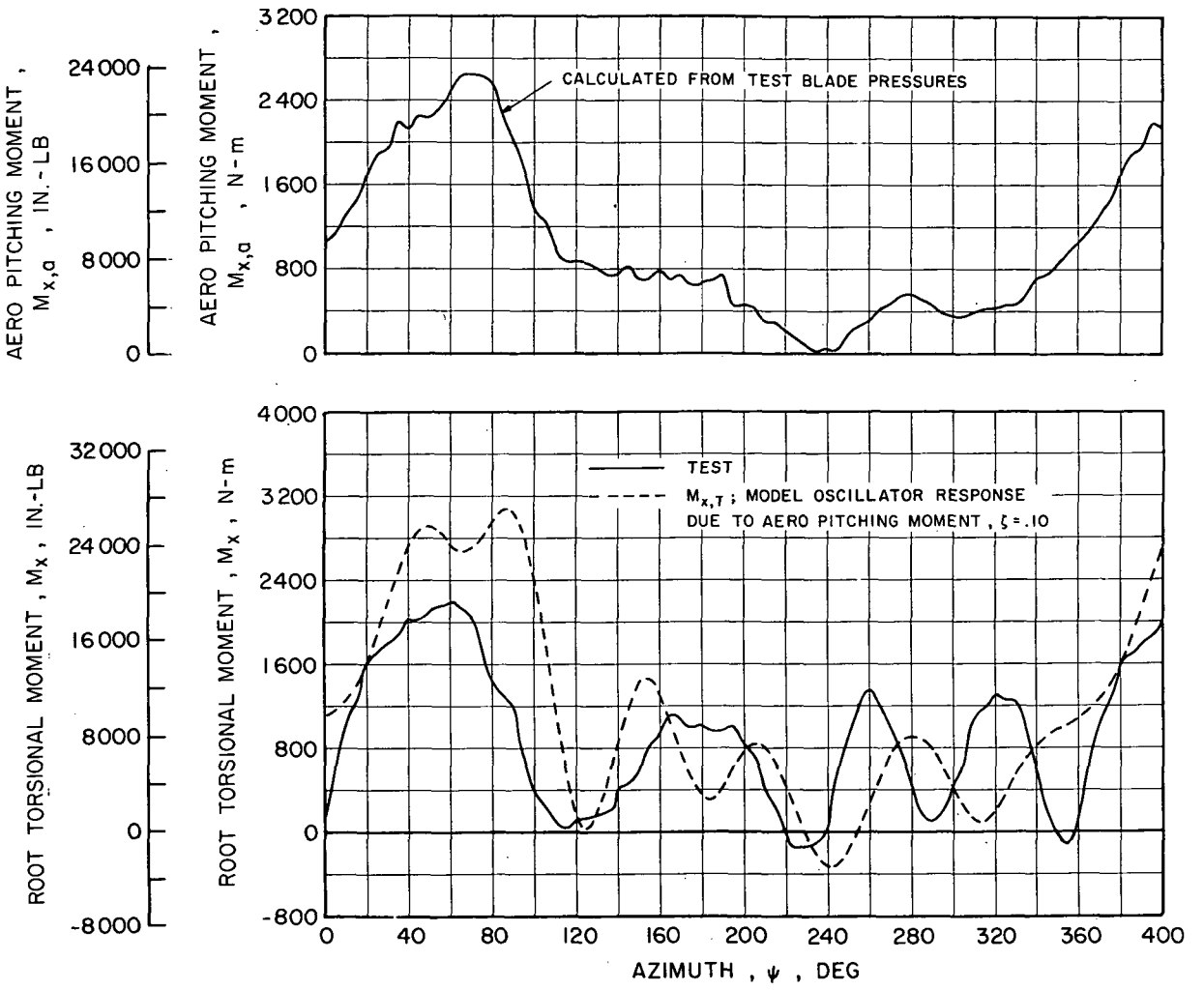

Figure 24.- Comparison Between Measured Blade Torsional Response and Torsional Oscillator Model Response to Aerodynamic Pitching Moment for CH-53A Case 44.

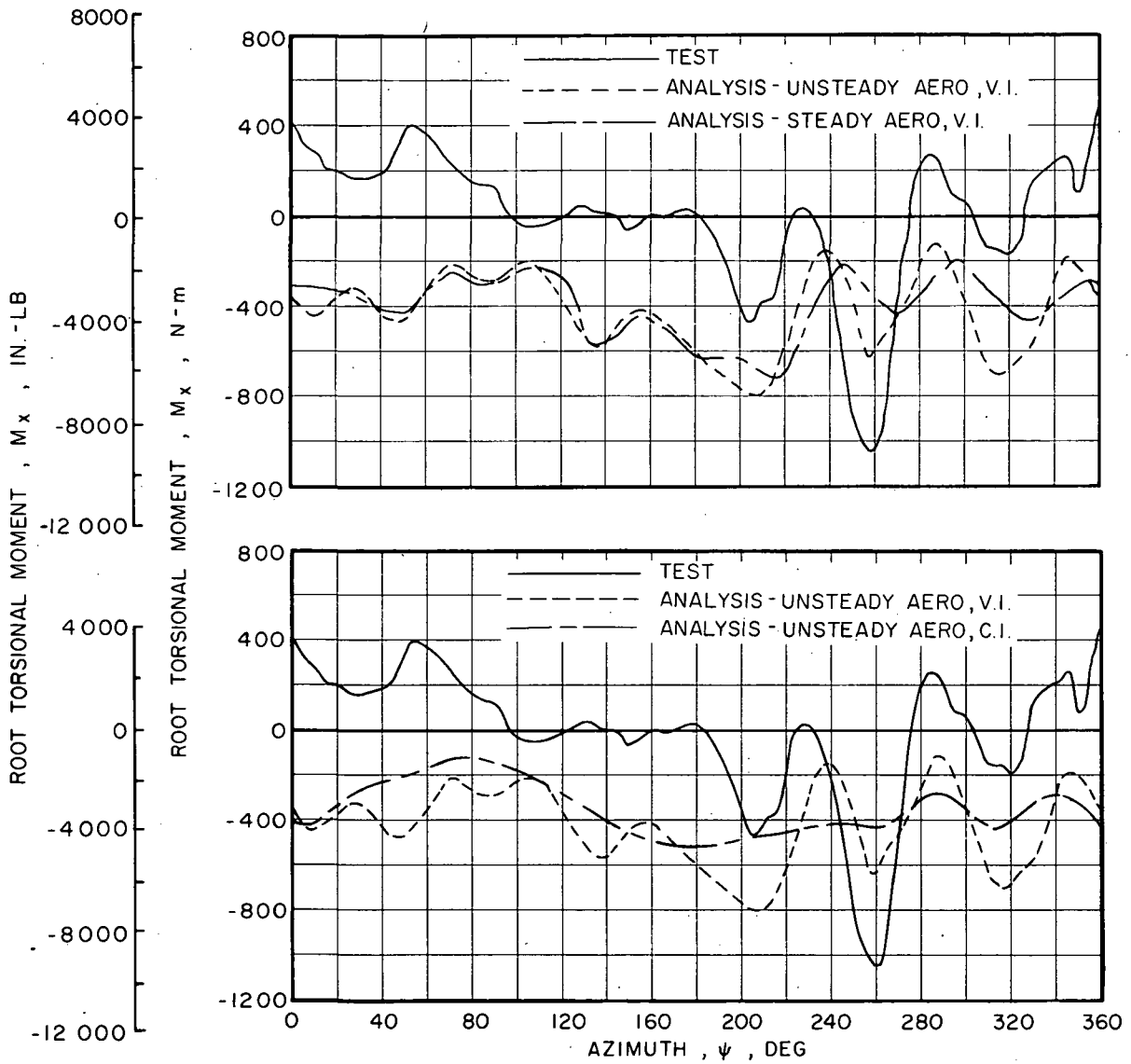

Figure 25.- Correlation of Root Torsional Moment for NH-3A Case 72.

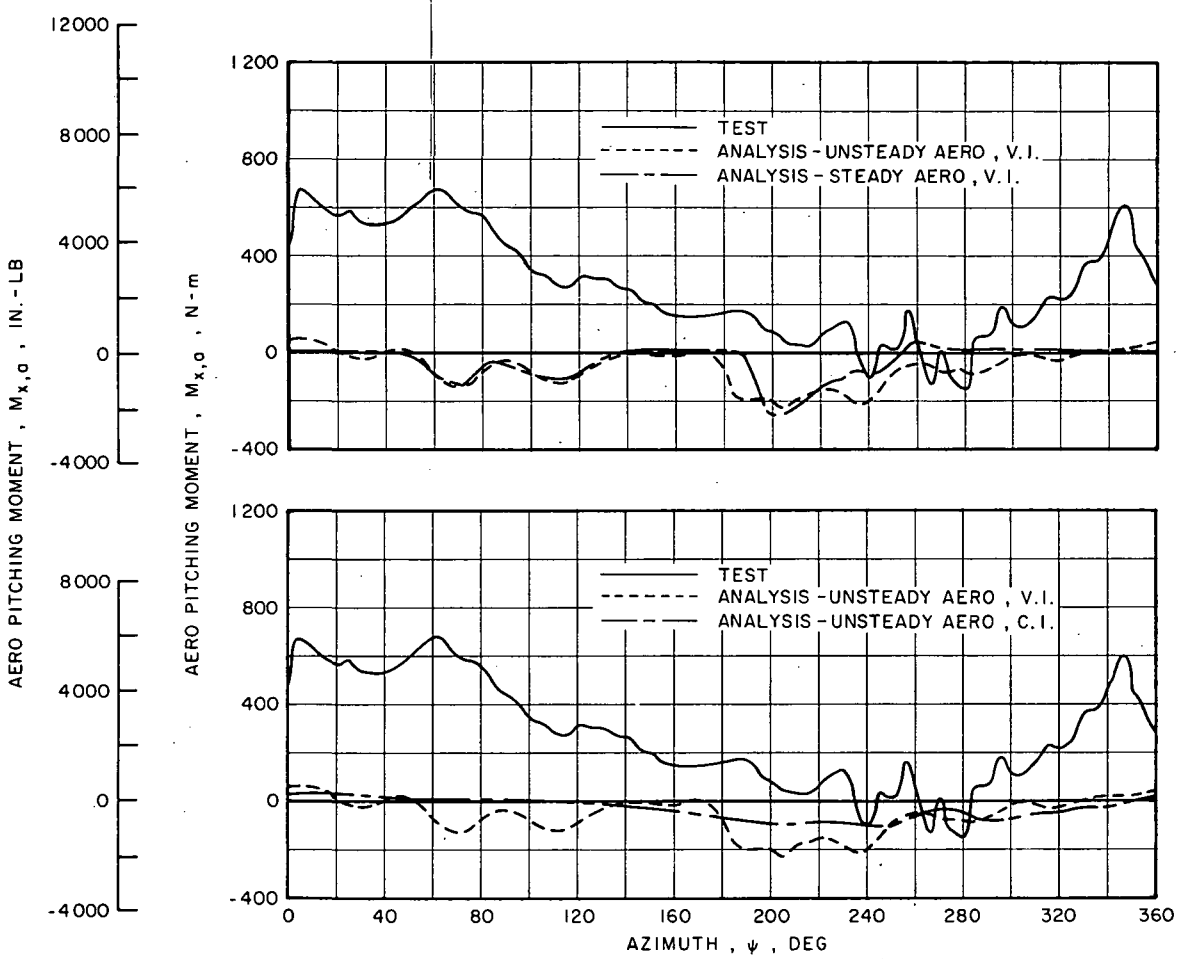

Figure 26.- Correlation of Aerodynamic Pitching Moment for NH-3A Case 72.

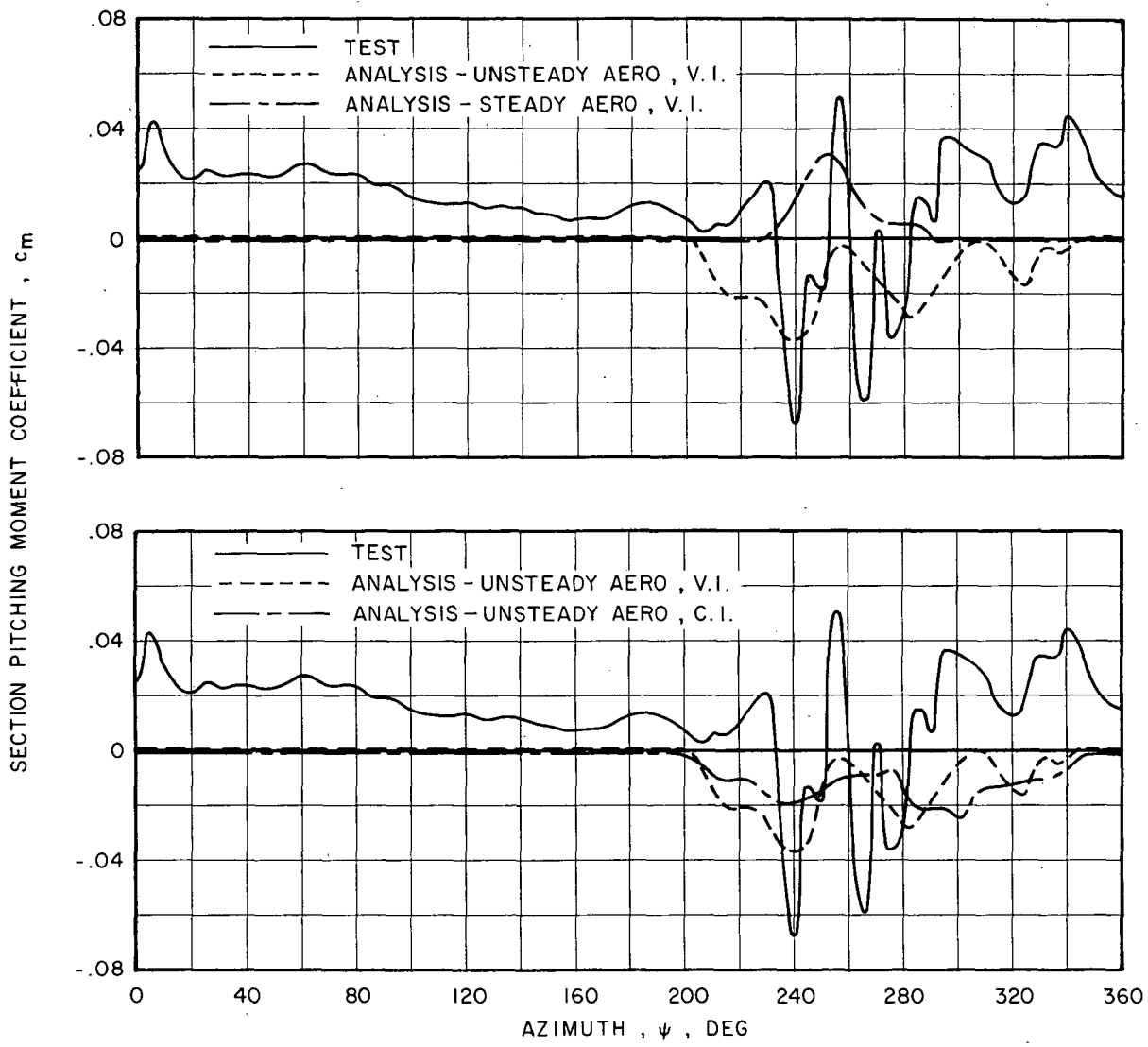

(a) r/R = 0.75

Figure 27.- Correlation of Section Pitching Moment Coefficient for NH-3A Case 72.

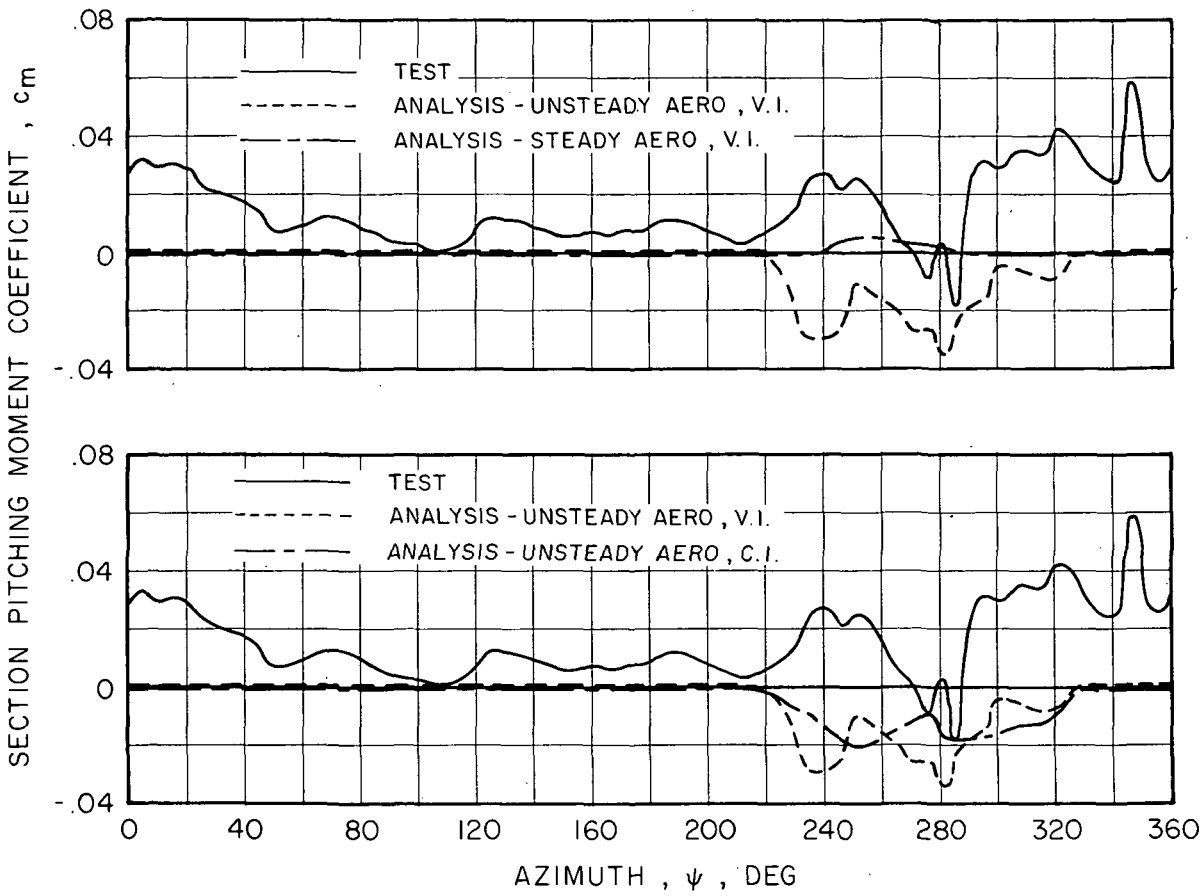

(b) $r/R = 0.85$

Figure 27.- Continued.

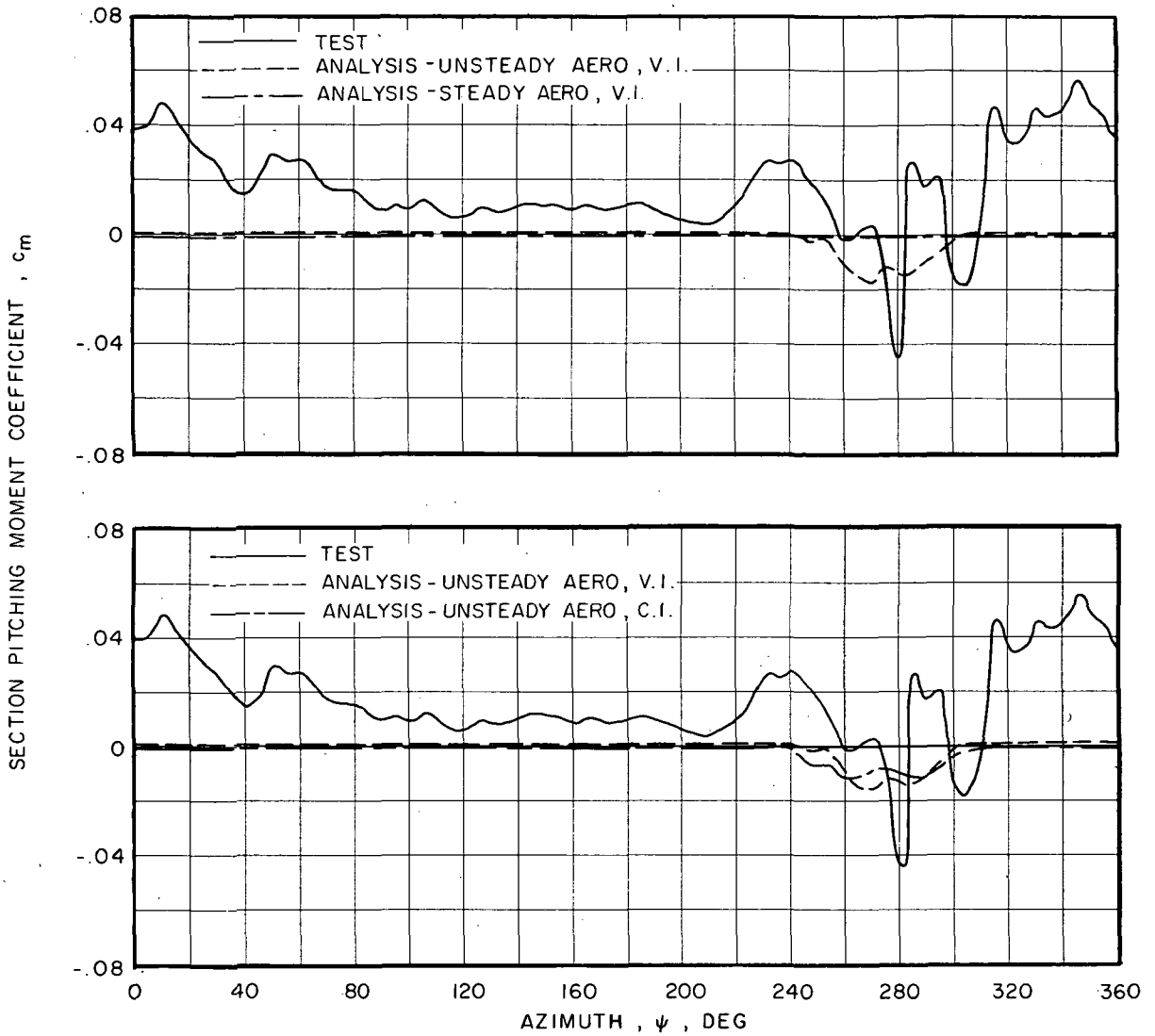

(c) r/R = 0.95

Figure 27.- Concluded.

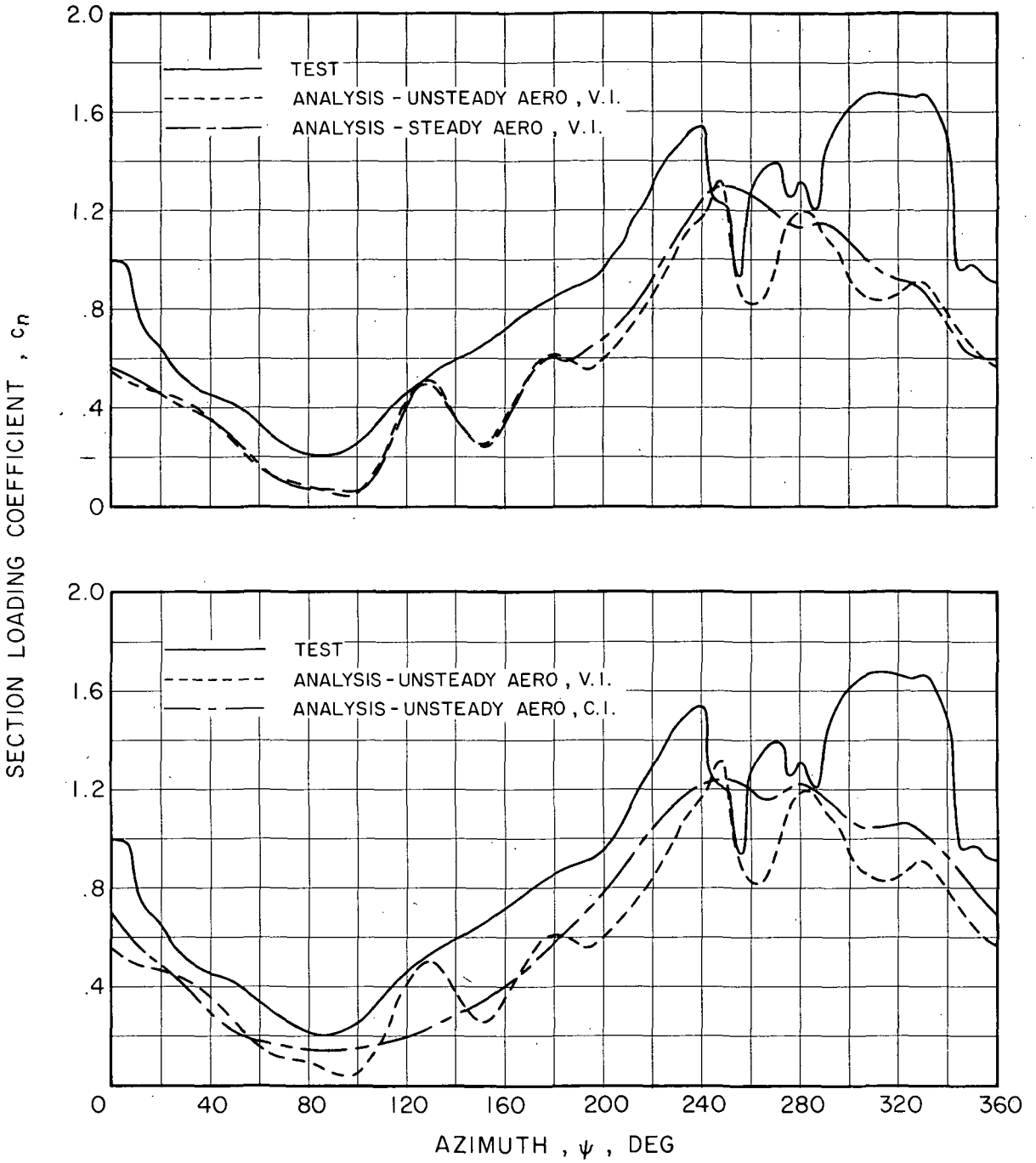

(a) r/R = 0.75

Figure 28.- Correlation of Section Loading Coefficient for NH-3A Case 72.

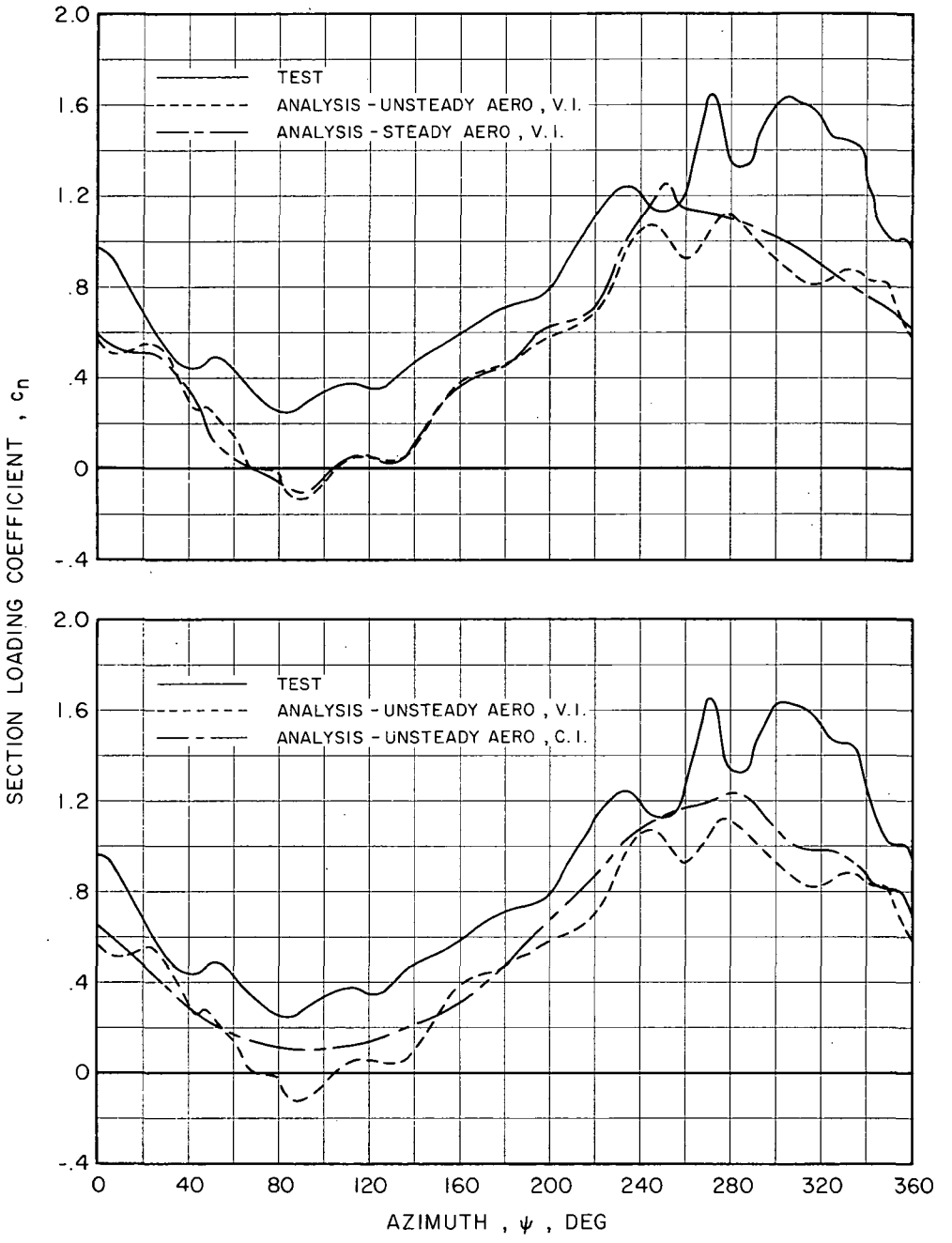

(b) r/R = 0.85

Figure 28.- Continued.

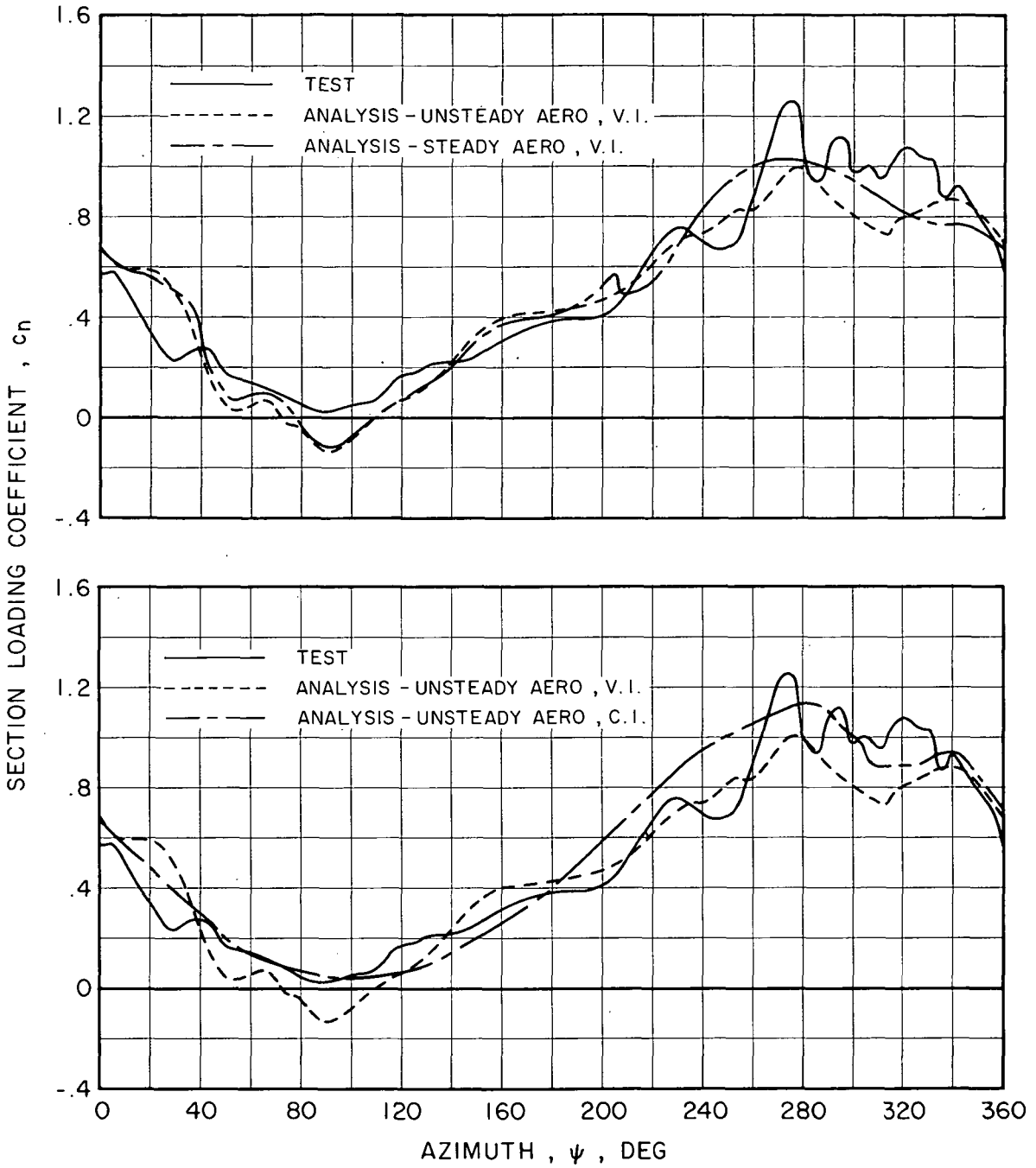

(c) r/R = 0.95

Figure 28.- Concluded.

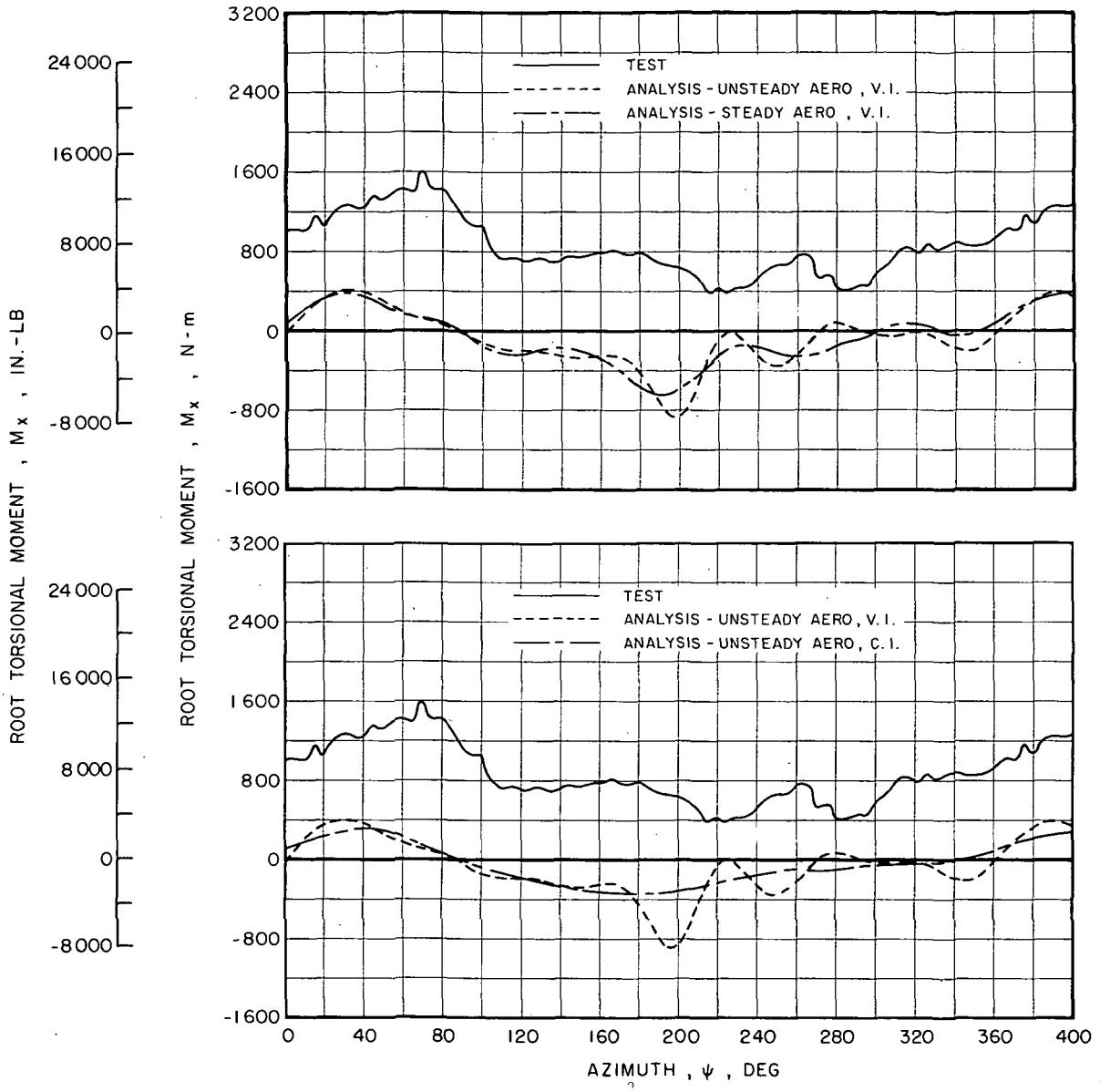

Figure 29.- Correlation of Root Torsional Moment for CH-53A Case 41LF.

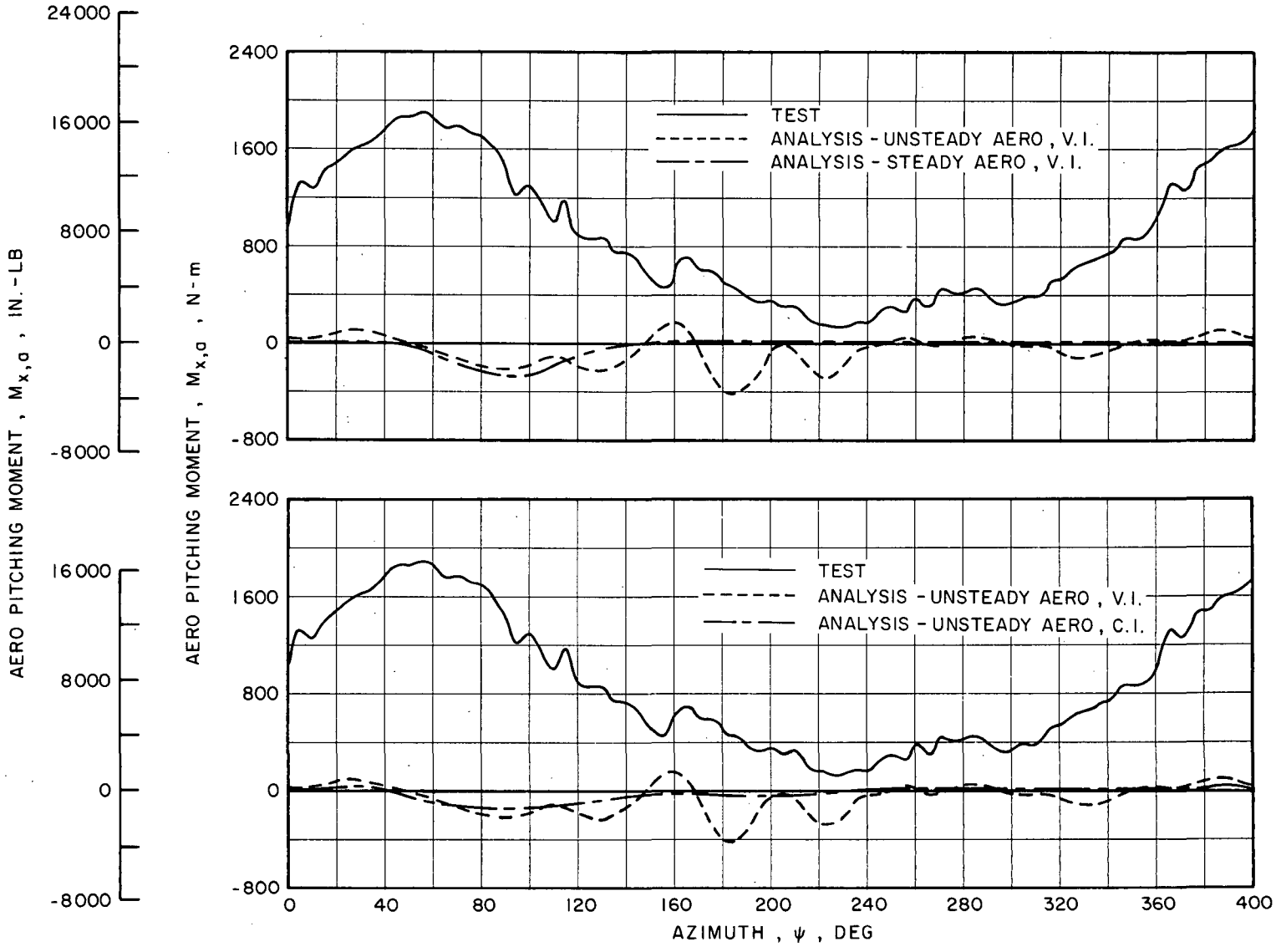

Figure 30.- Correlation of Aerodynamic Pitching Moment for CH-53A Case 41LF.

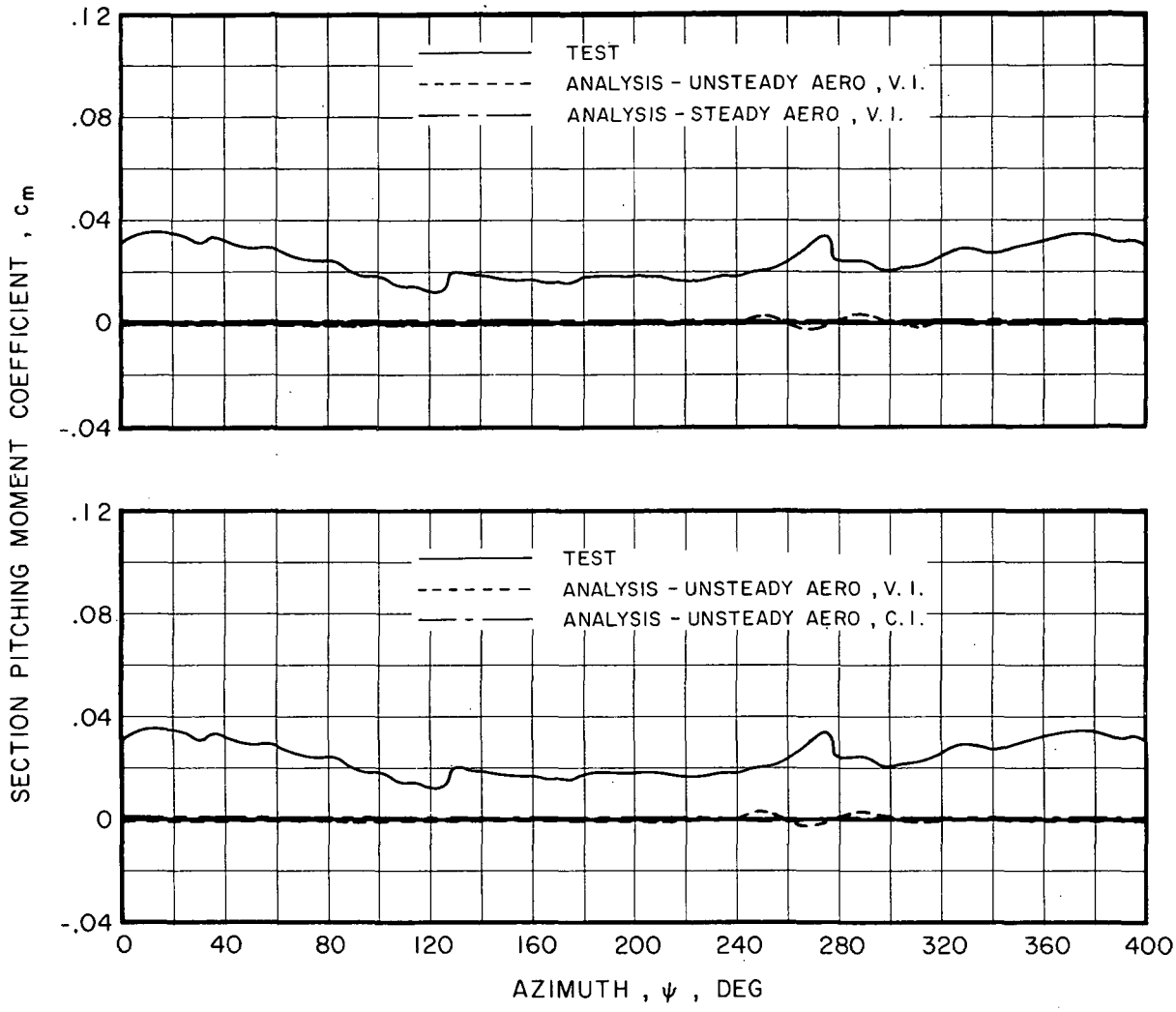

Figure 31.- Correlation of Section Pitching Moment Coefficient at r/R = 0.85 for CH-53A Case 41LF.

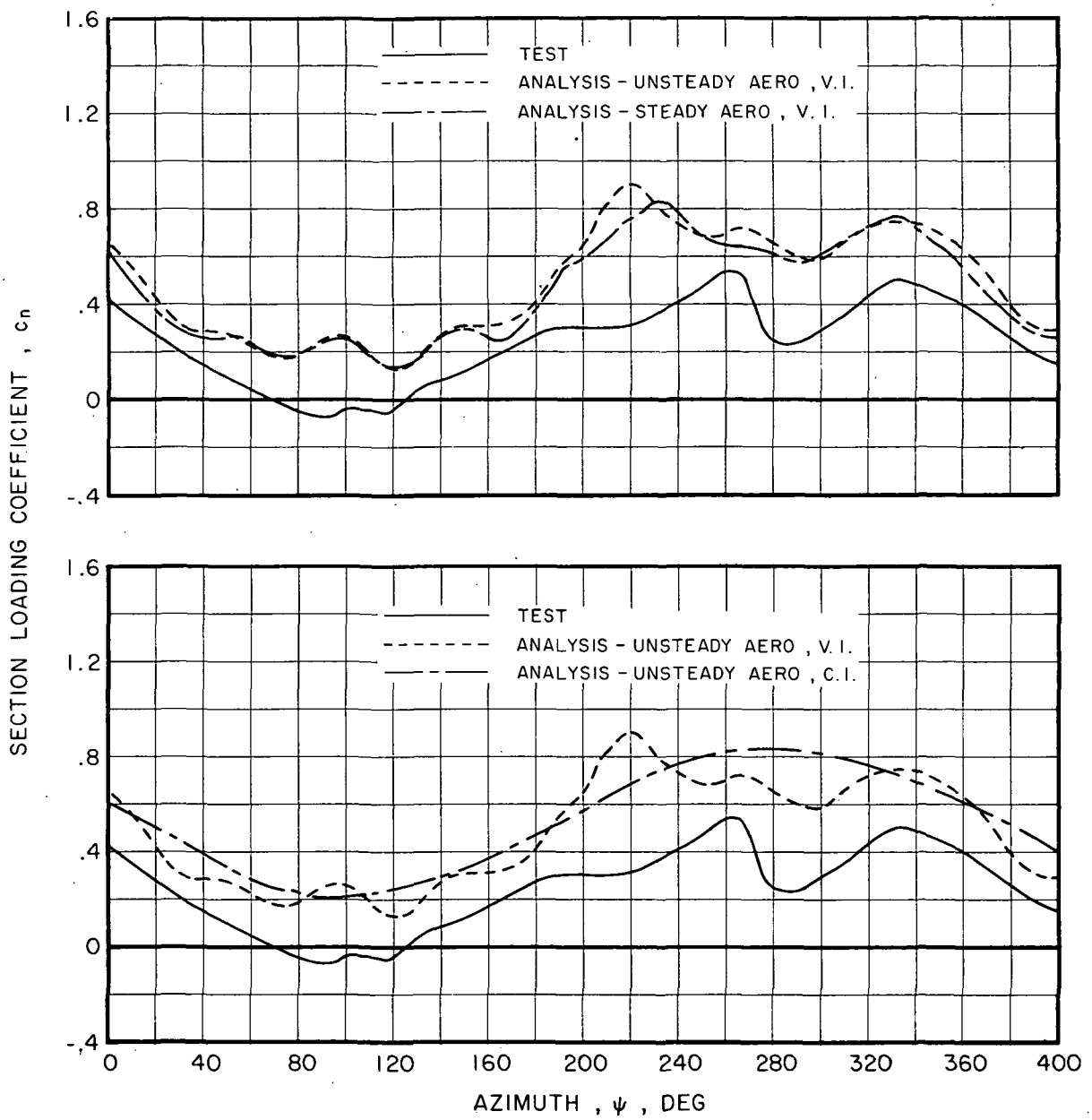

Figure 32.- Correlation of Section Loading Coefficient at r/R = 0.85 for CH-53A Case 41LF.

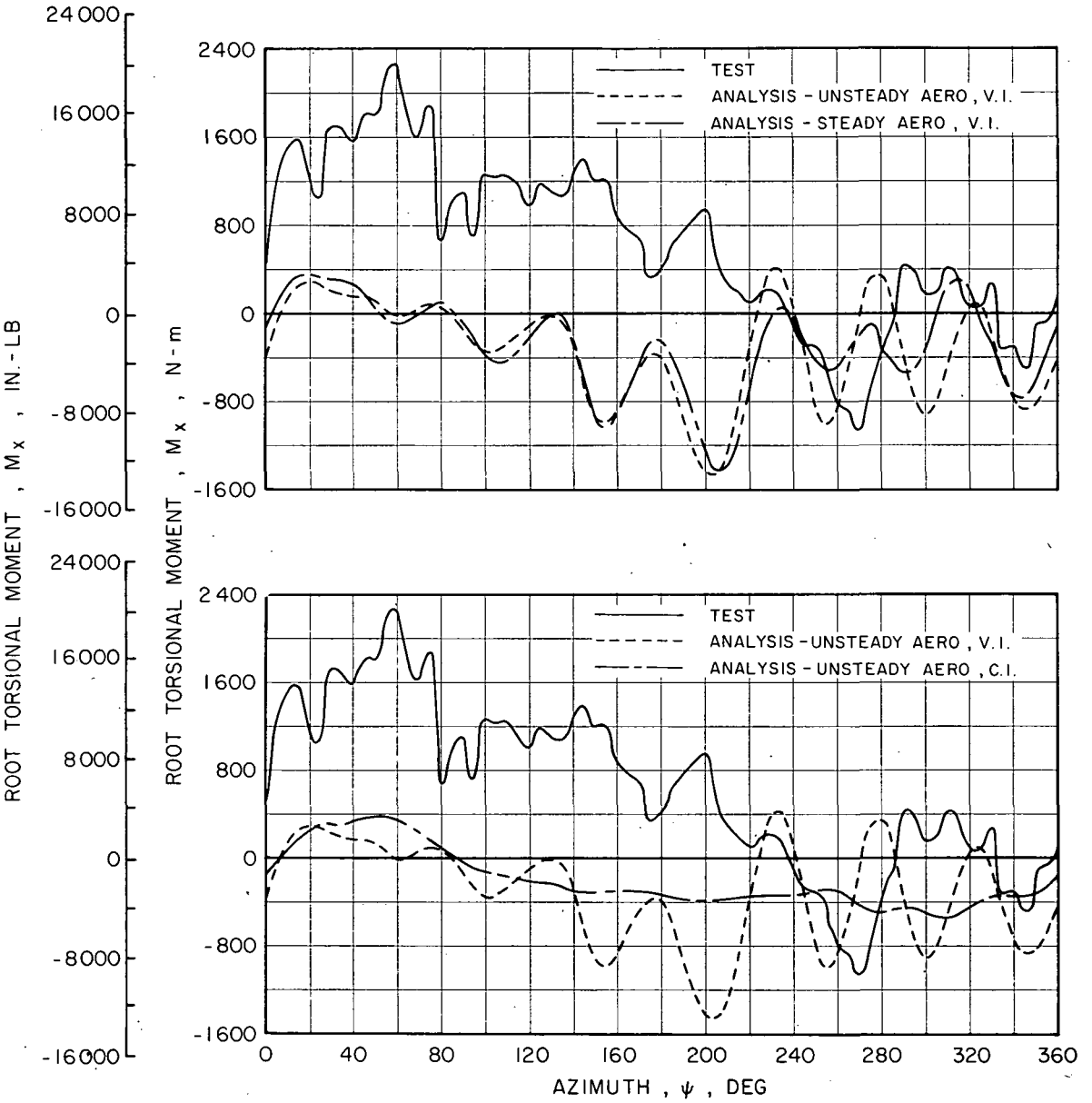

Figure 33.- Correlation of Root Torsional Moment for CH-53A Case 41TN.

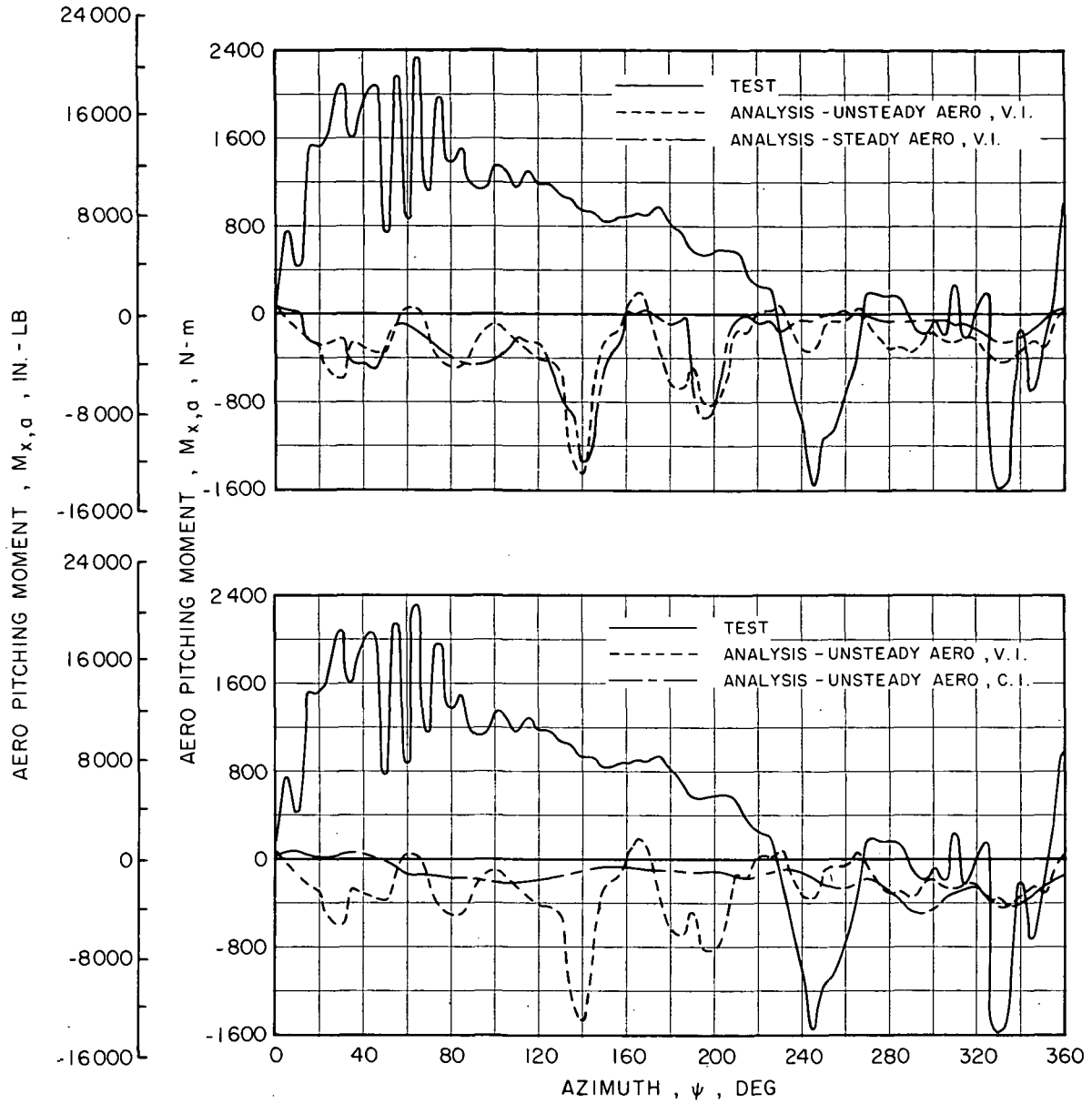

Figure 34.- Correlation of Aerodynamic Pitching Moment for CH-53A Case 41TN.

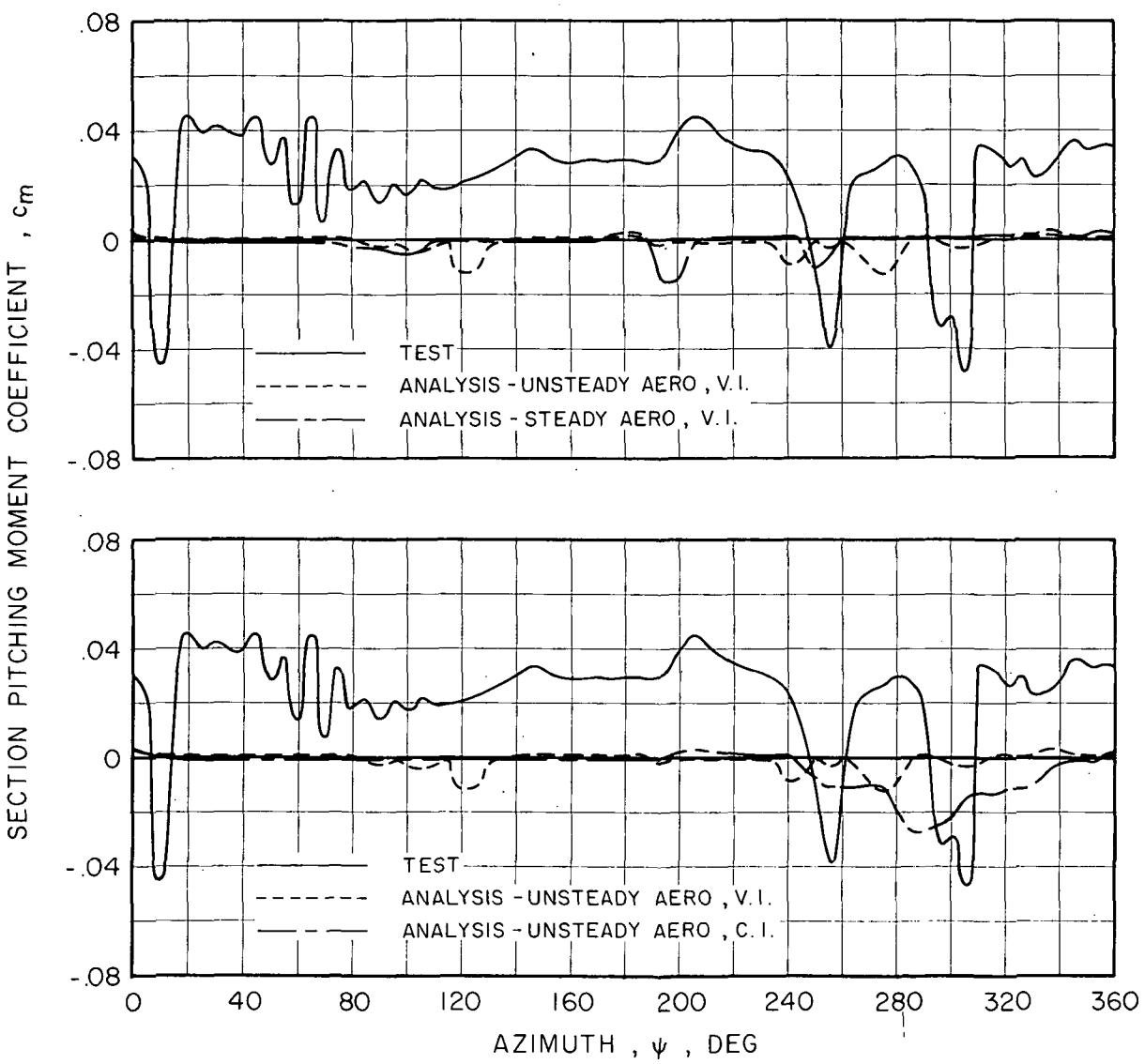

Figure 35.- Correlation of Section Pitching Moment Coefficient at r/R = 0.85 for CH-53A Case 41 TN.

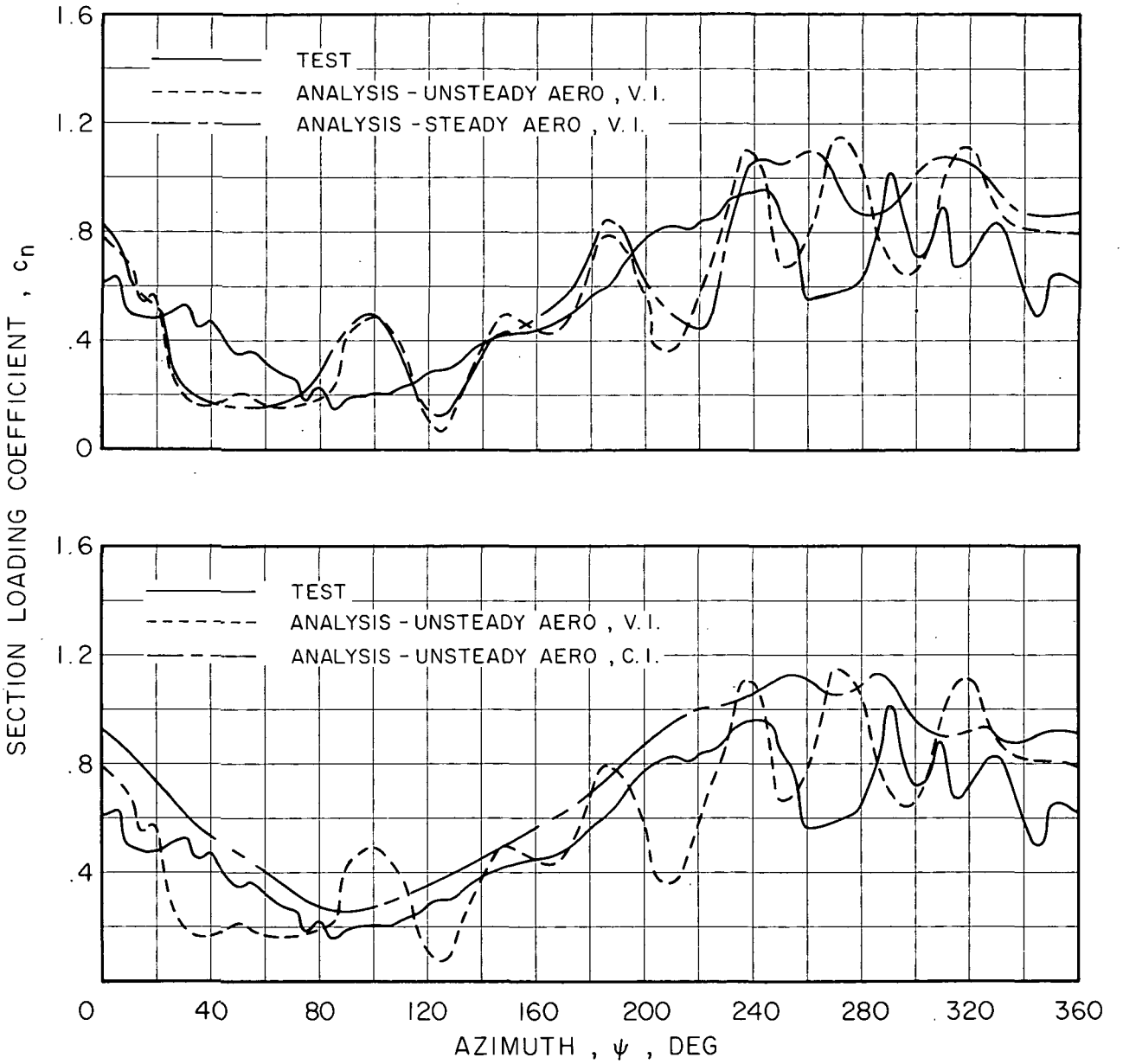

Figure 36.- Correlation of Section Loading Coefficient at r/R = 0.85 for CH-53A Case 41TN.

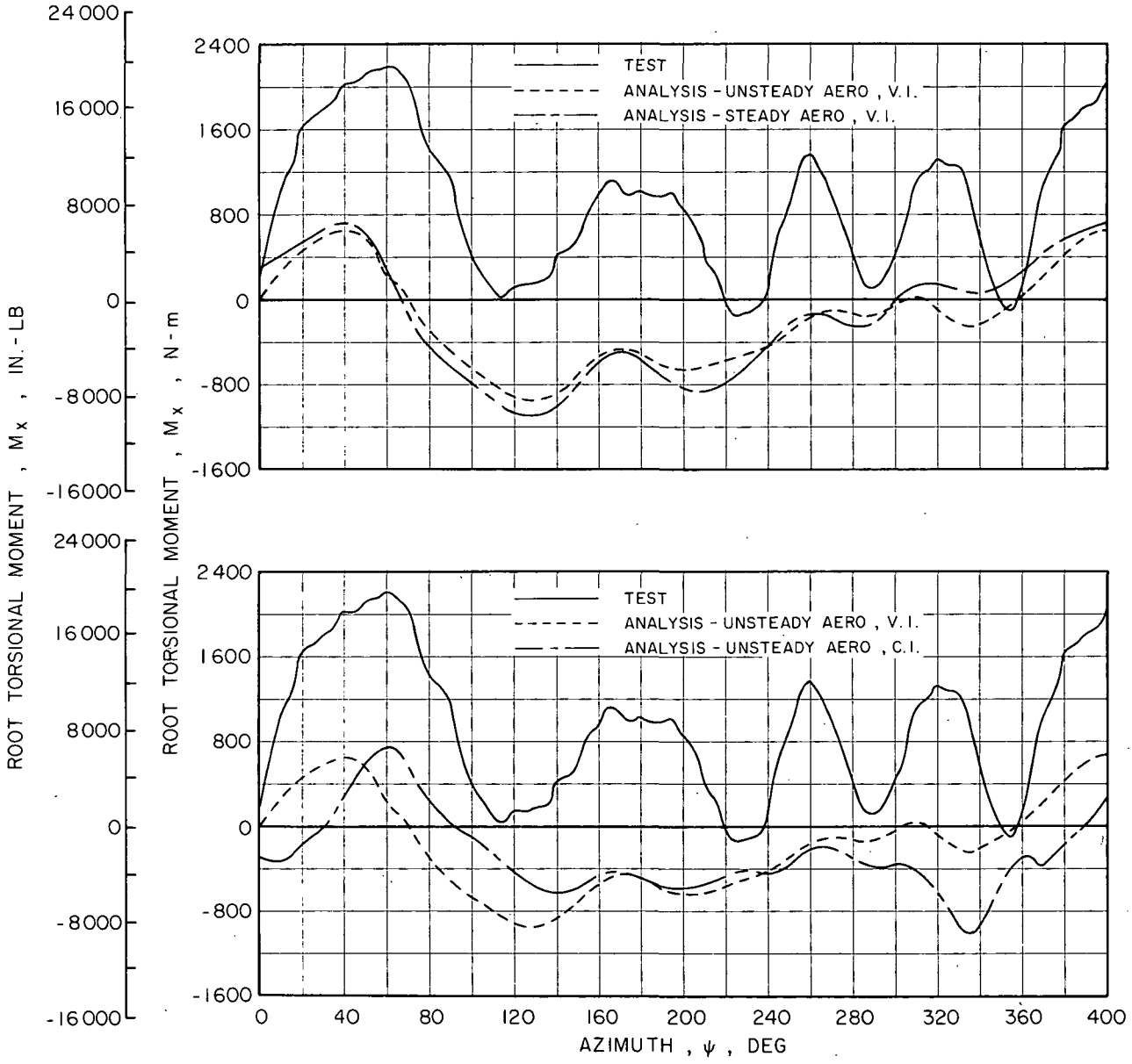

Figure 37.- Correlation of Root Torsional Moment for CH-53A Case 44.

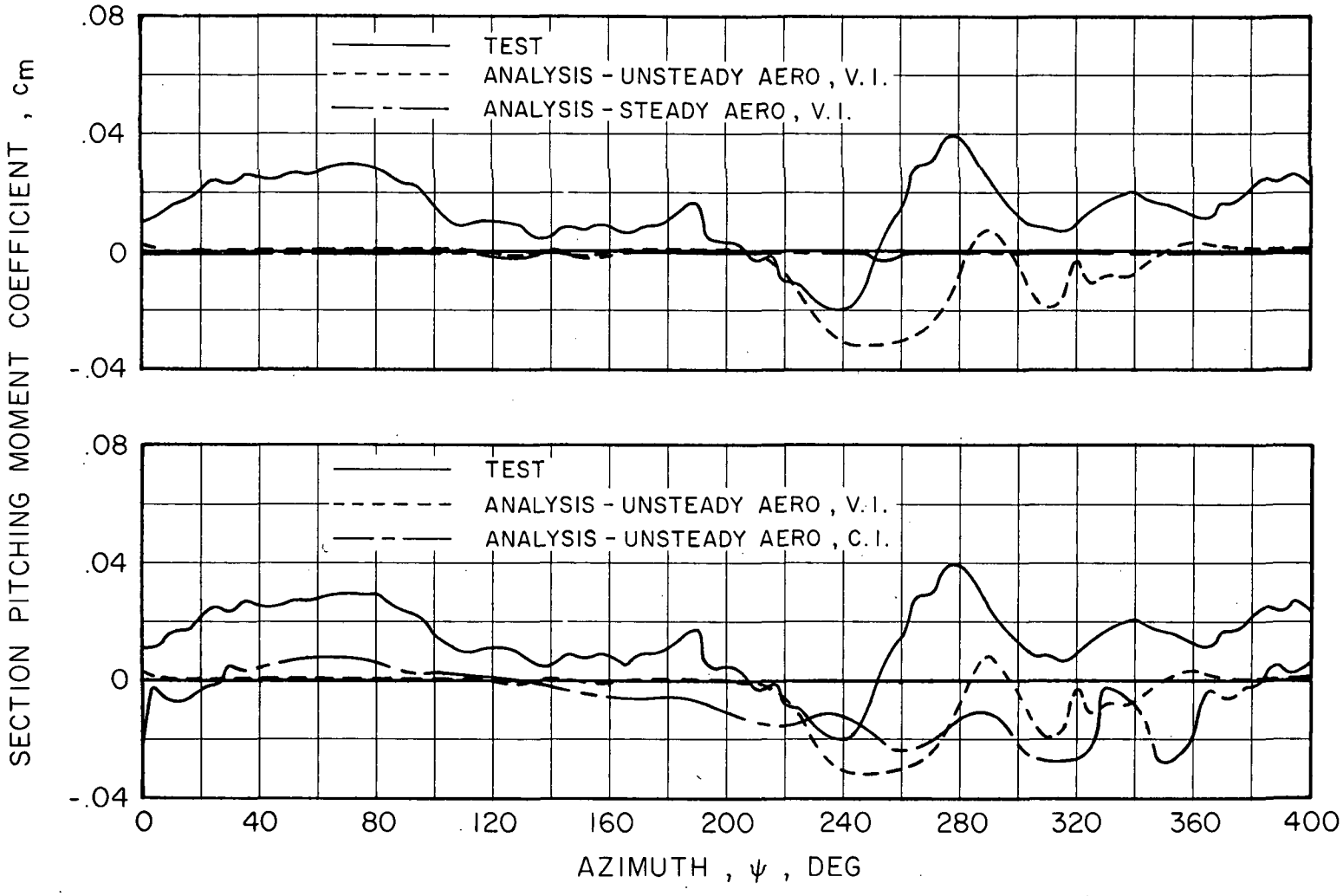

Figure 38.- Correlation of Section Pitching Moment Coefficient at r/R = 0.75 for CH-53A Case 44.

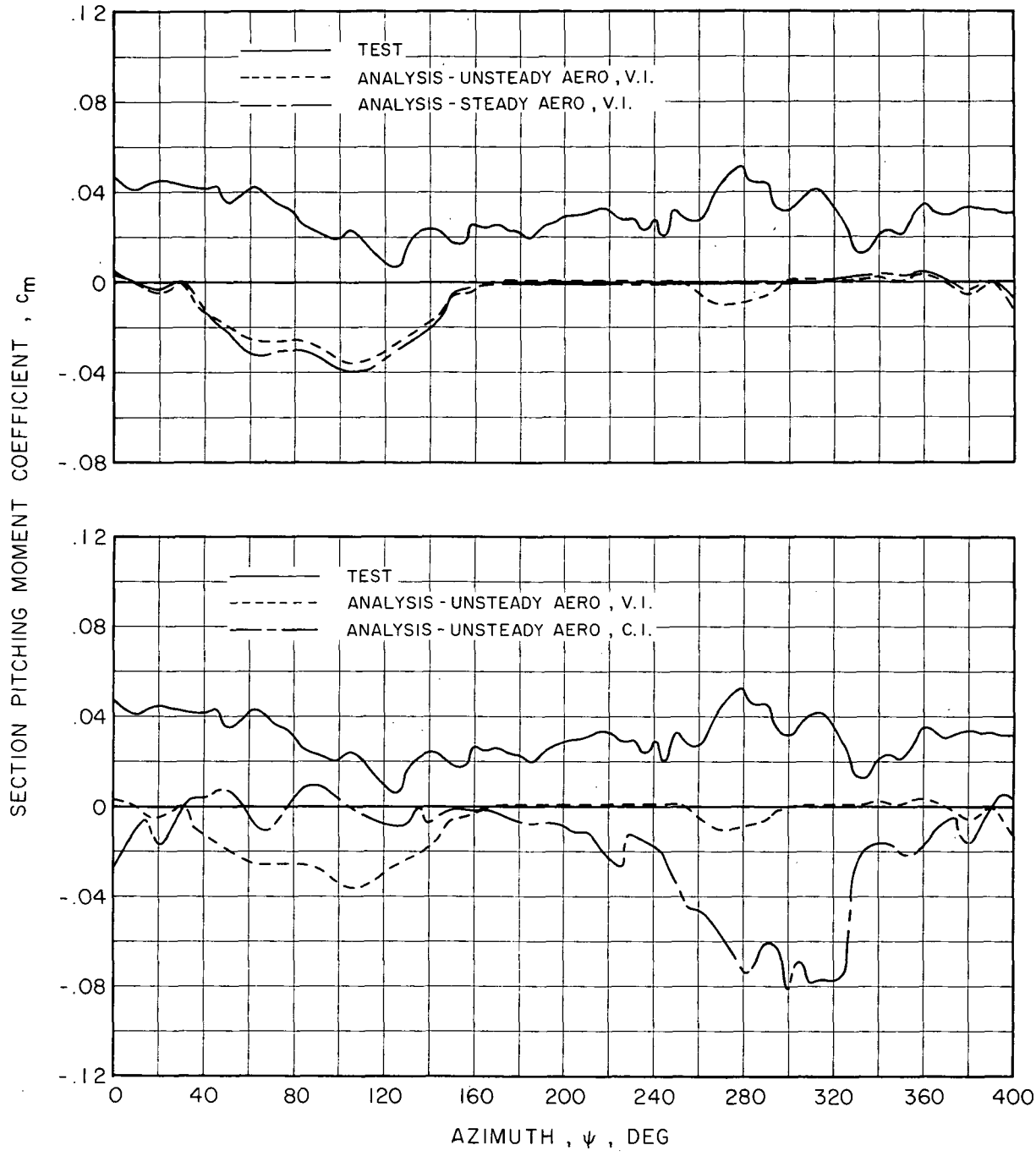

Figure 39.- Correlation of Section Pitching Moment Coefficient at r/R = 0.95 for CH-53A Case 44.

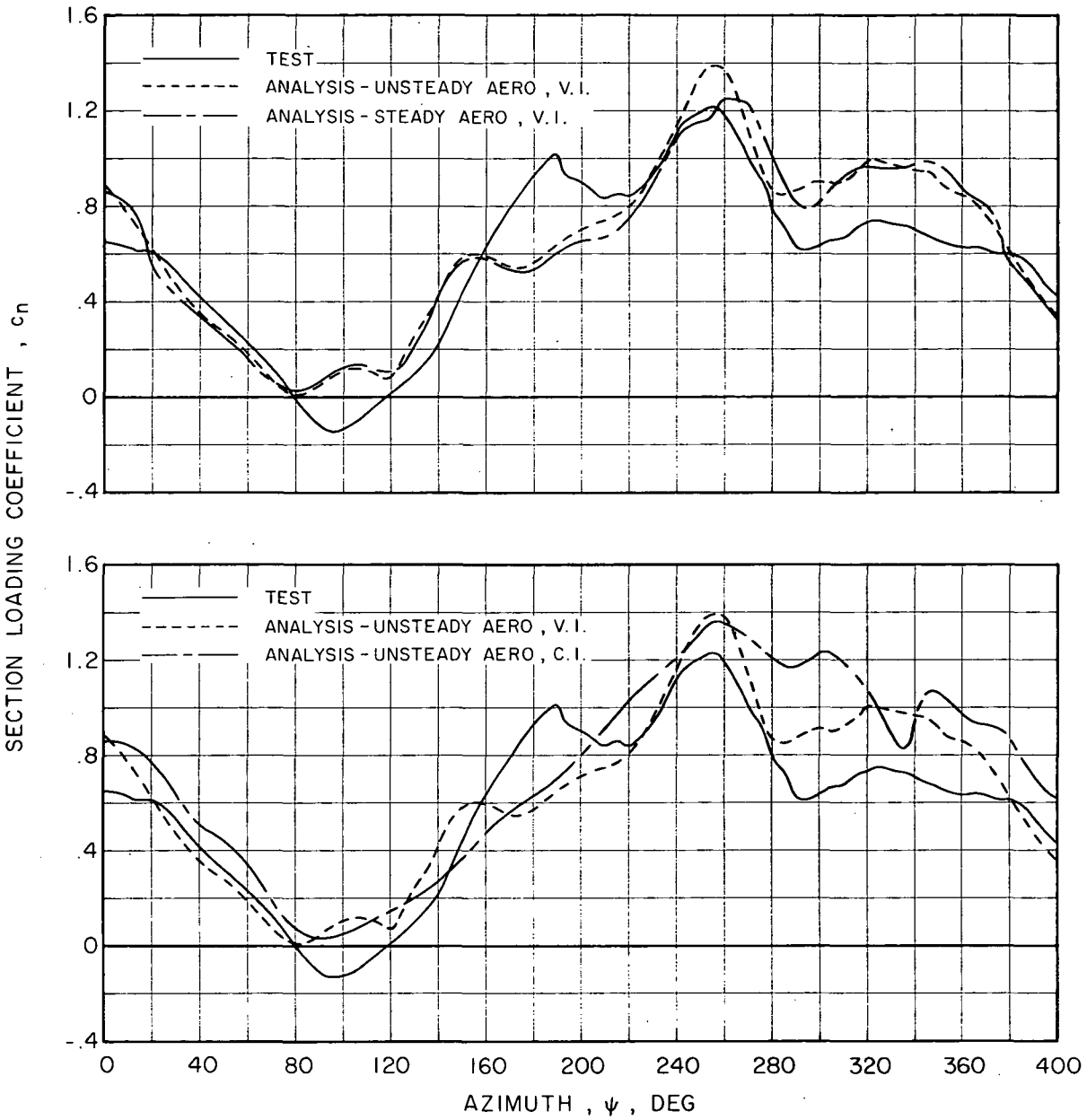

Figure 40.- Correlation of Section Loading Coefficient at r/R = 0.75 for CH-53A Case 44.

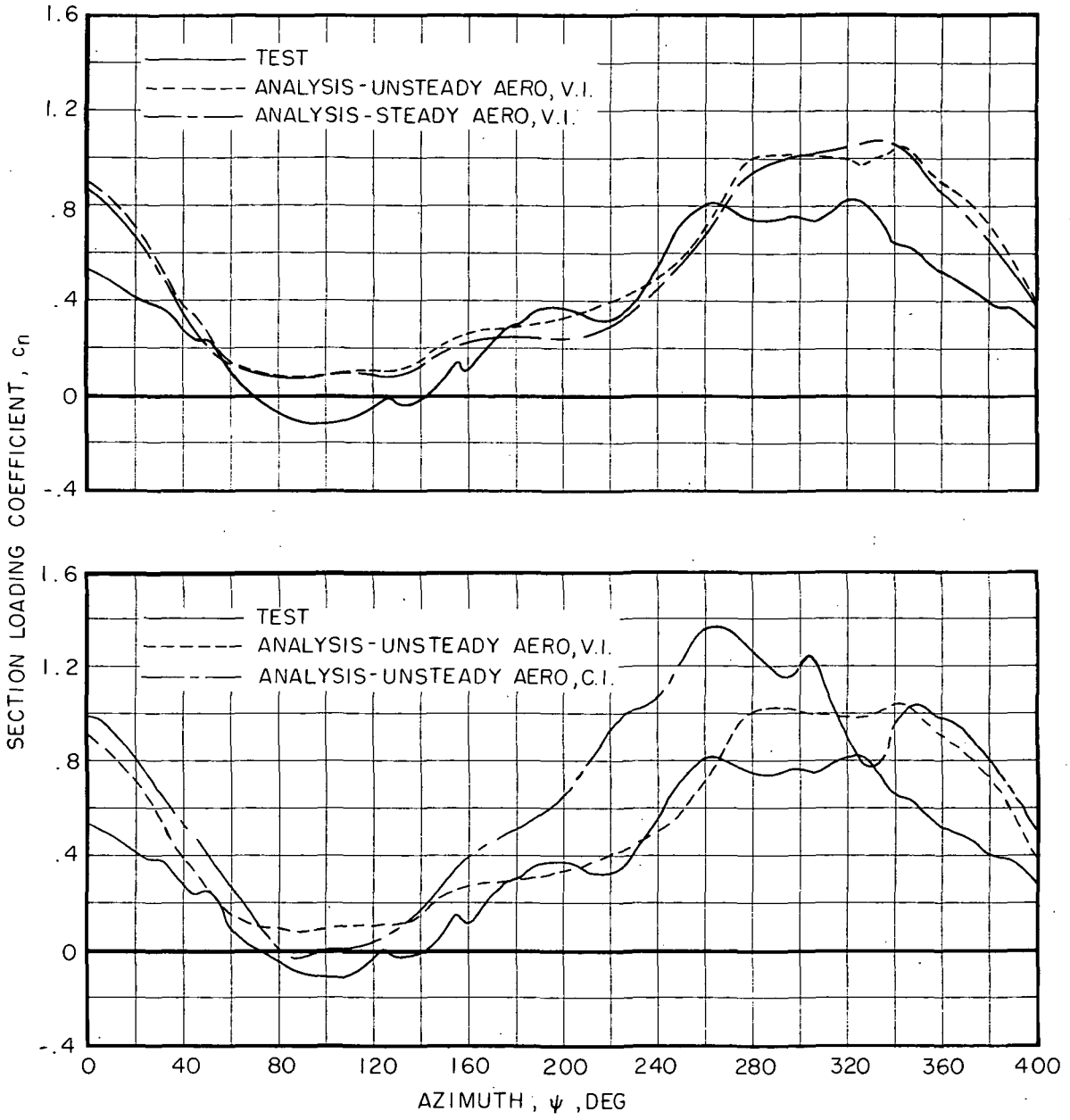

Figure 41.- Correlation of Section Loading Coefficient at r/R = 0.95 for CH-53A Case 44.

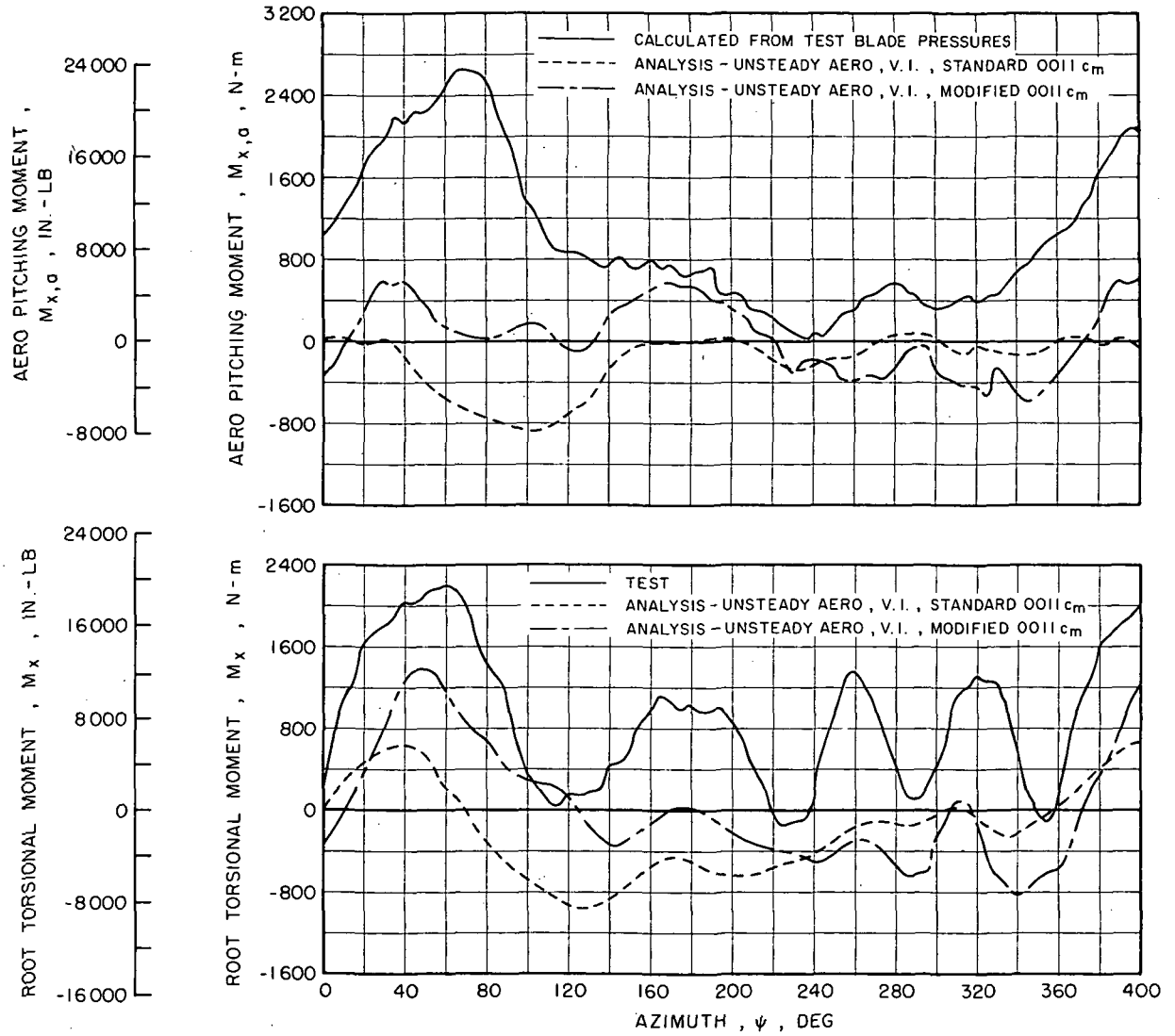

Figure 42.- Effects of Modifications to Analytical c_m Aerodynamic Data on Aerodynamic Pitching Moment and Root Torsional Moment for CH-53A Case 44.

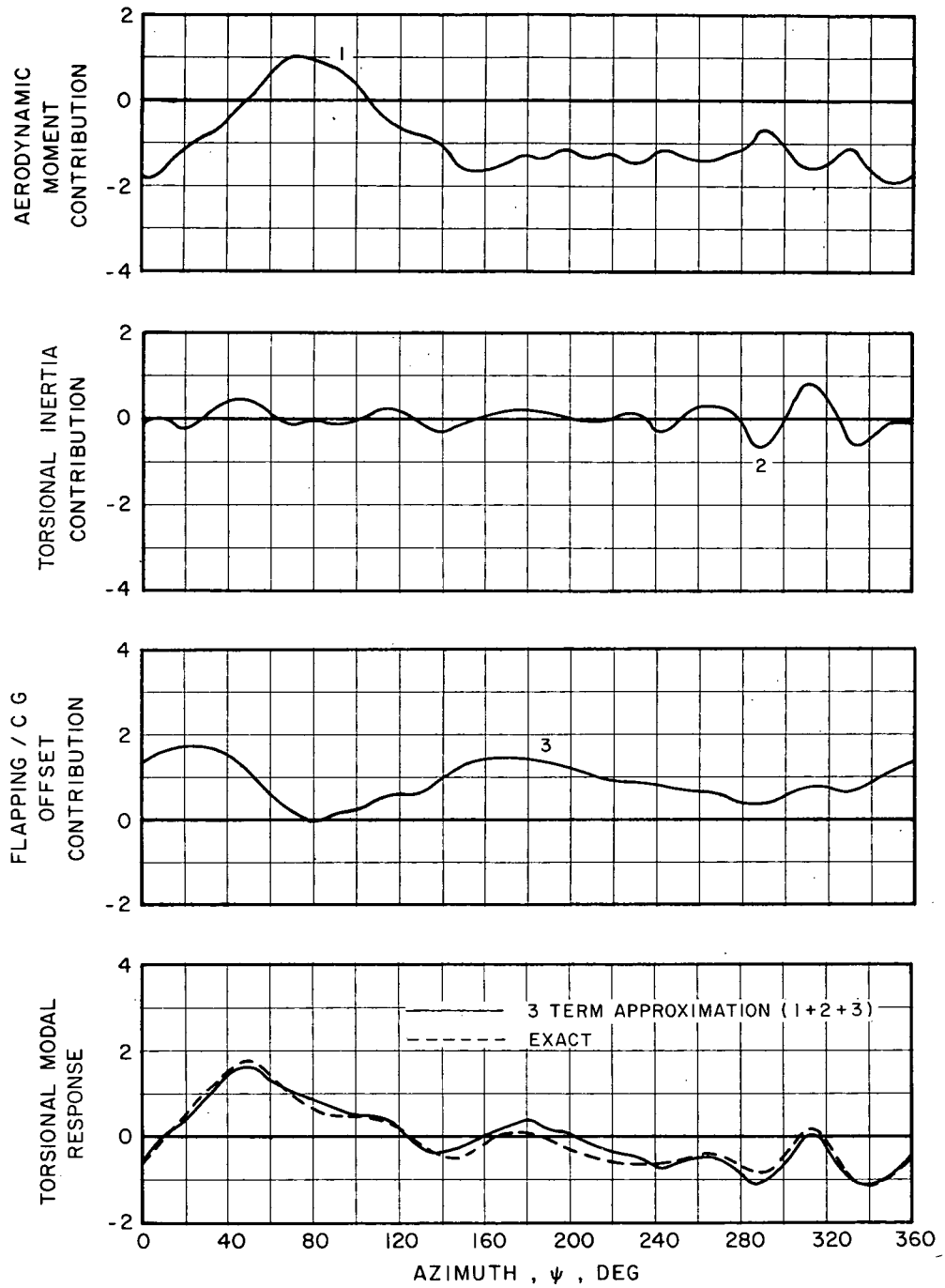

Figure 43.- Major Analytical Contributions to Nondimensional Blade Torsional Response for CH-53A Case 44 With Unsteady Aerodynamics, Variable Inflow, and Modified c_m Data.

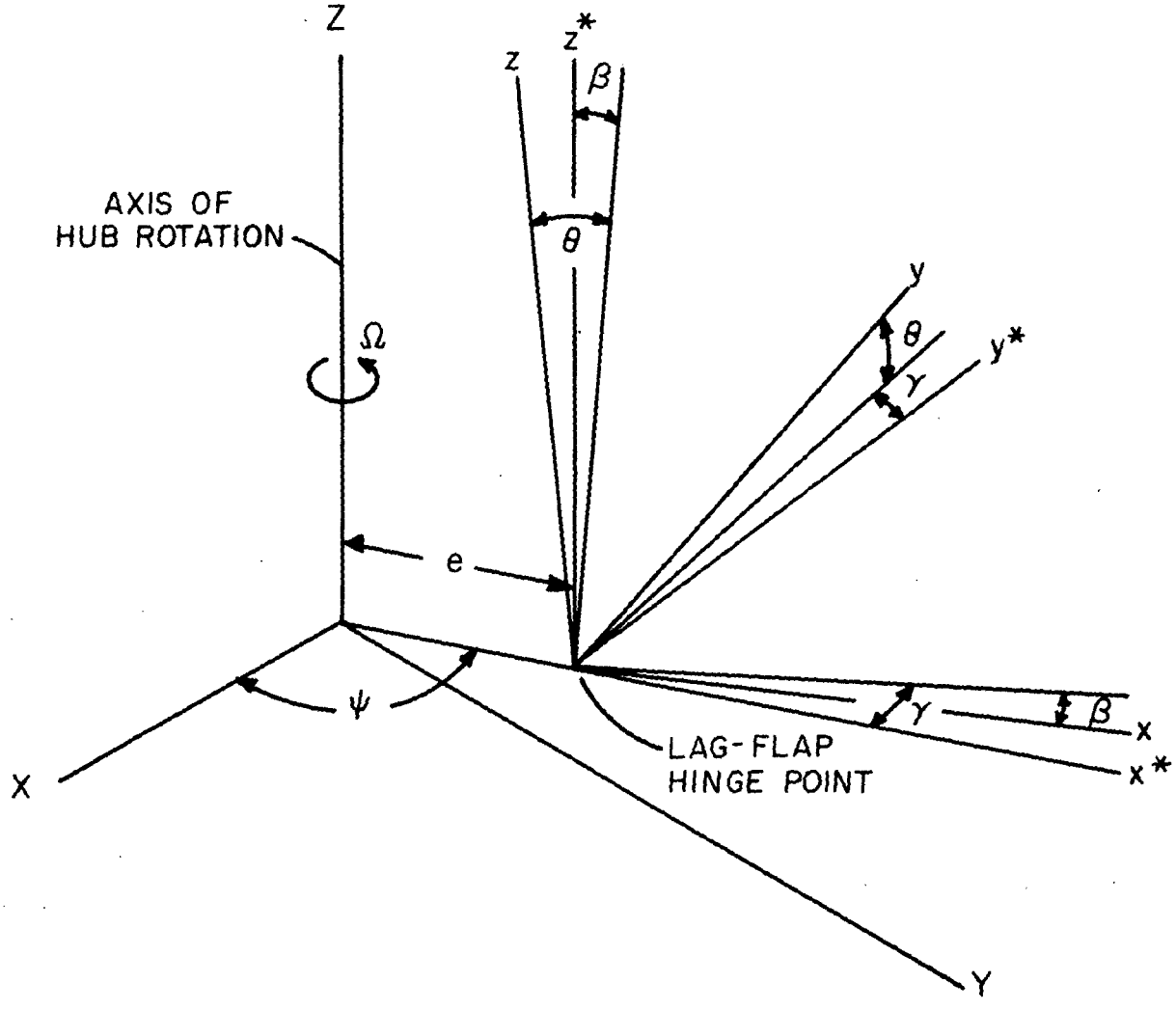

X ,Y,Z NON-ROTATING HUB AXES

x*,y*, z* ROTATING HUB AXES

x , y , z ROTATING BLADE AXES

Figure 44.- Rotor and Blade Axis Systems.

NOTE : COMPLETE DEFINITIONS OF THE SYMBOLIC TERMS (Y's) ARE GIVEN IN TABLE II.

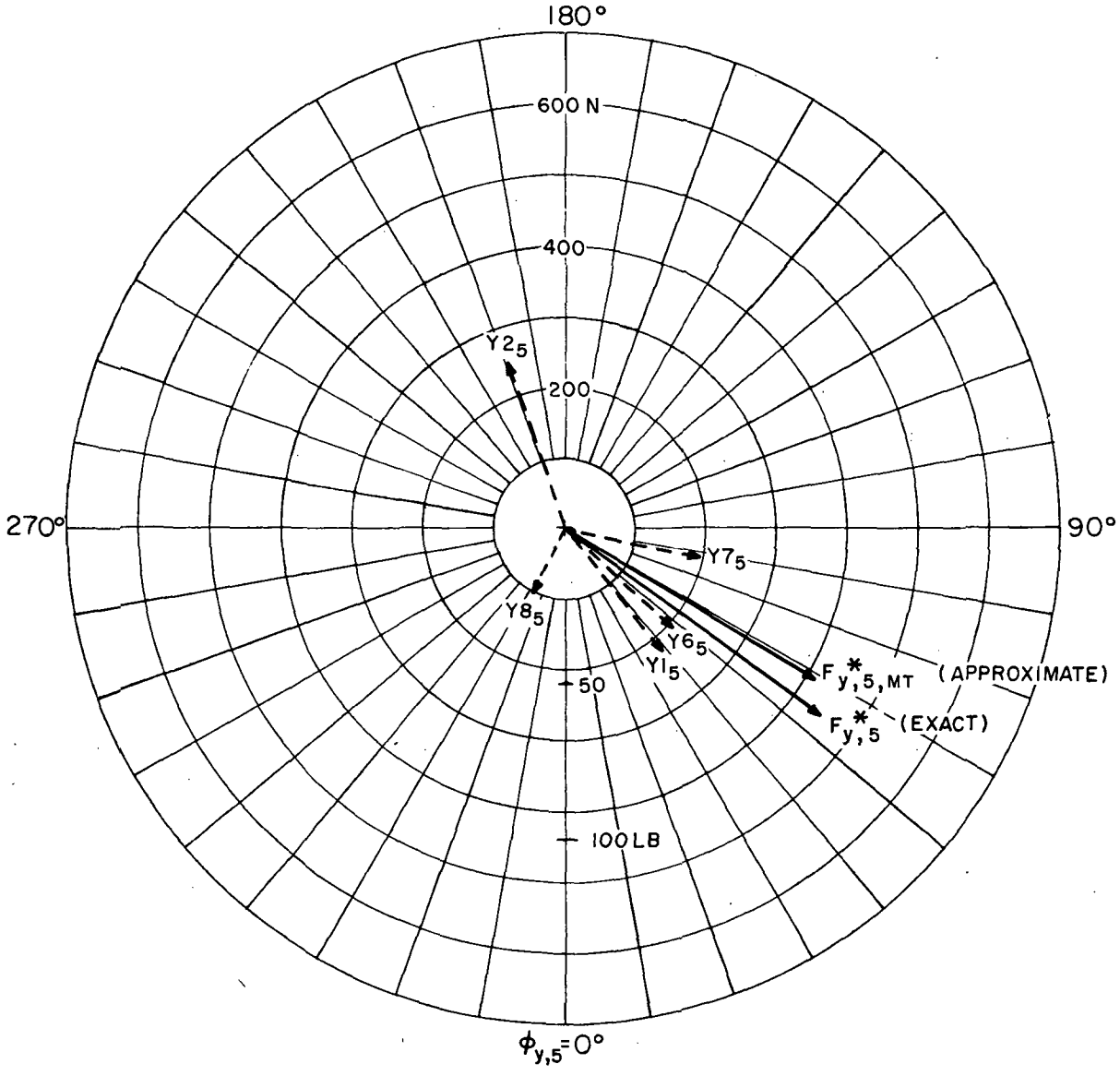

Figure 45.- Comparison of Approximate and Exact Calculations of the Fifth Harmonic of Edgewise Hinge Force, CH-53A, V = 78.4 m/sec (152.4 kn), μ = 0.36, $\frac{C_T}{\sigma}$ = 0.055.

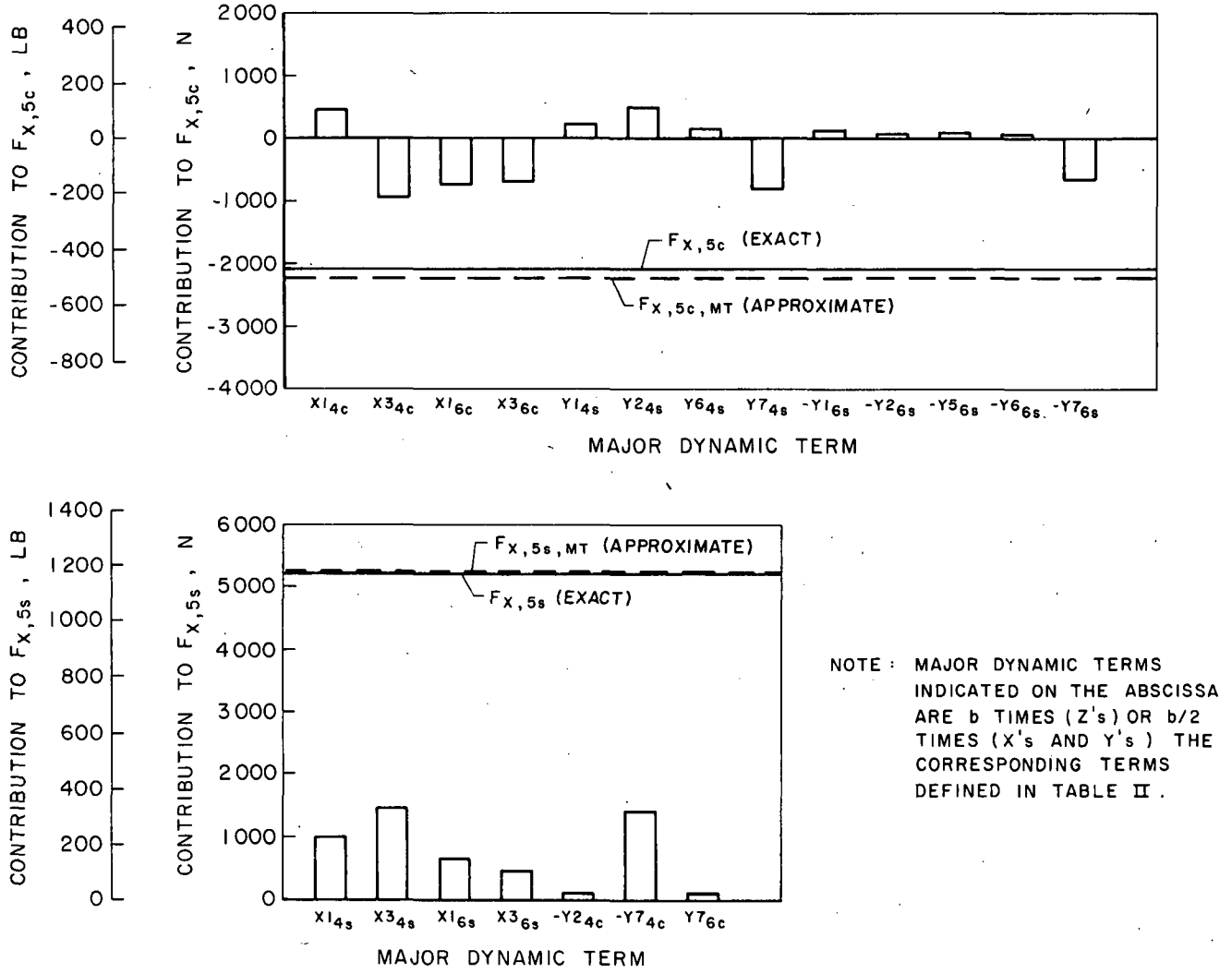

Figure 46.- Major b/Rev Longitudinal Hub Force Dynamic Terms, NH-3A, $\mu = 0.36$, $\frac{C_T}{\sigma} = 0.043$.

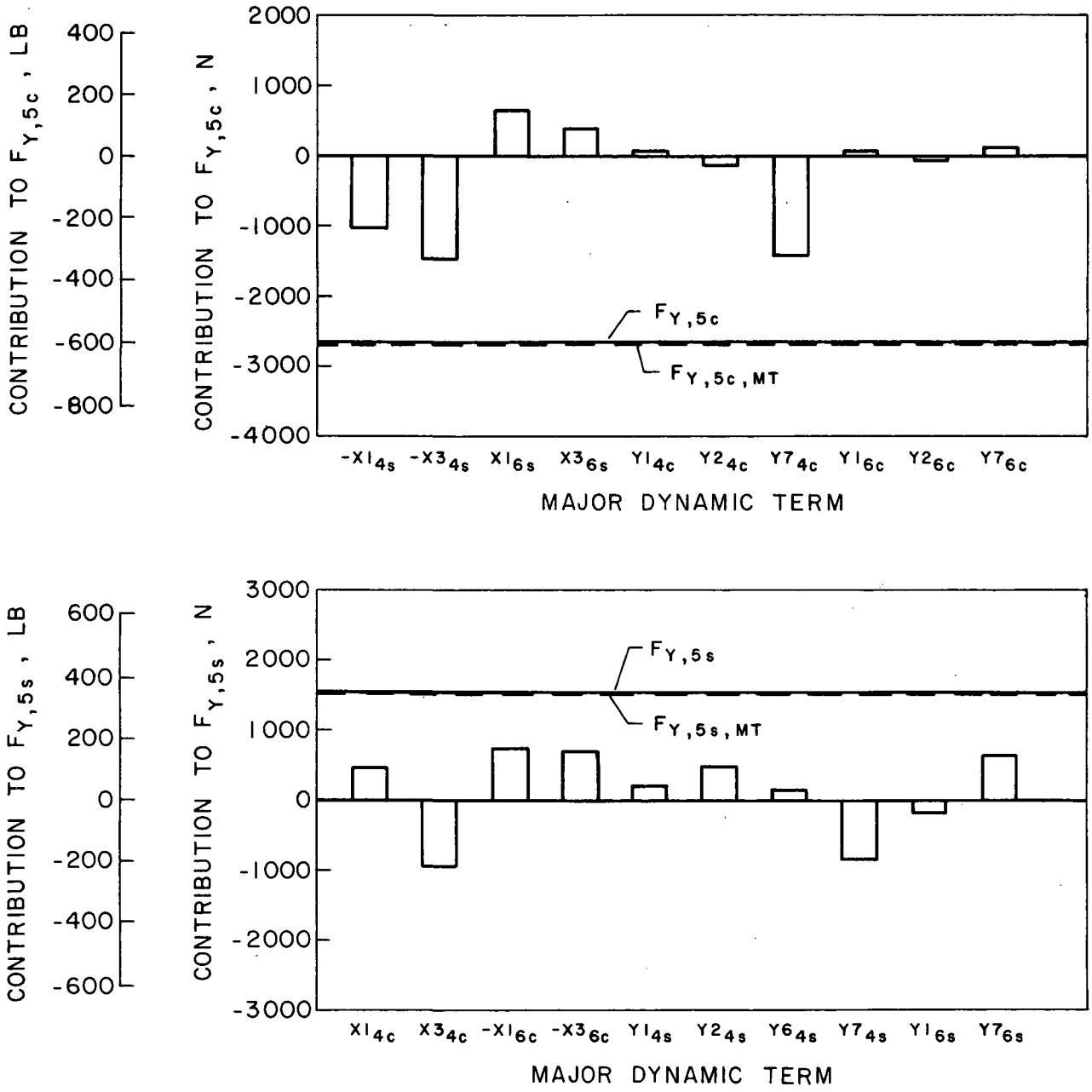

Figure 47.- Major b/Rev Lateral Hub Force Dynamic Terms, NH-3A, $\mu = 0.36$, $\frac{C_T}{\sigma} = 0.043$.

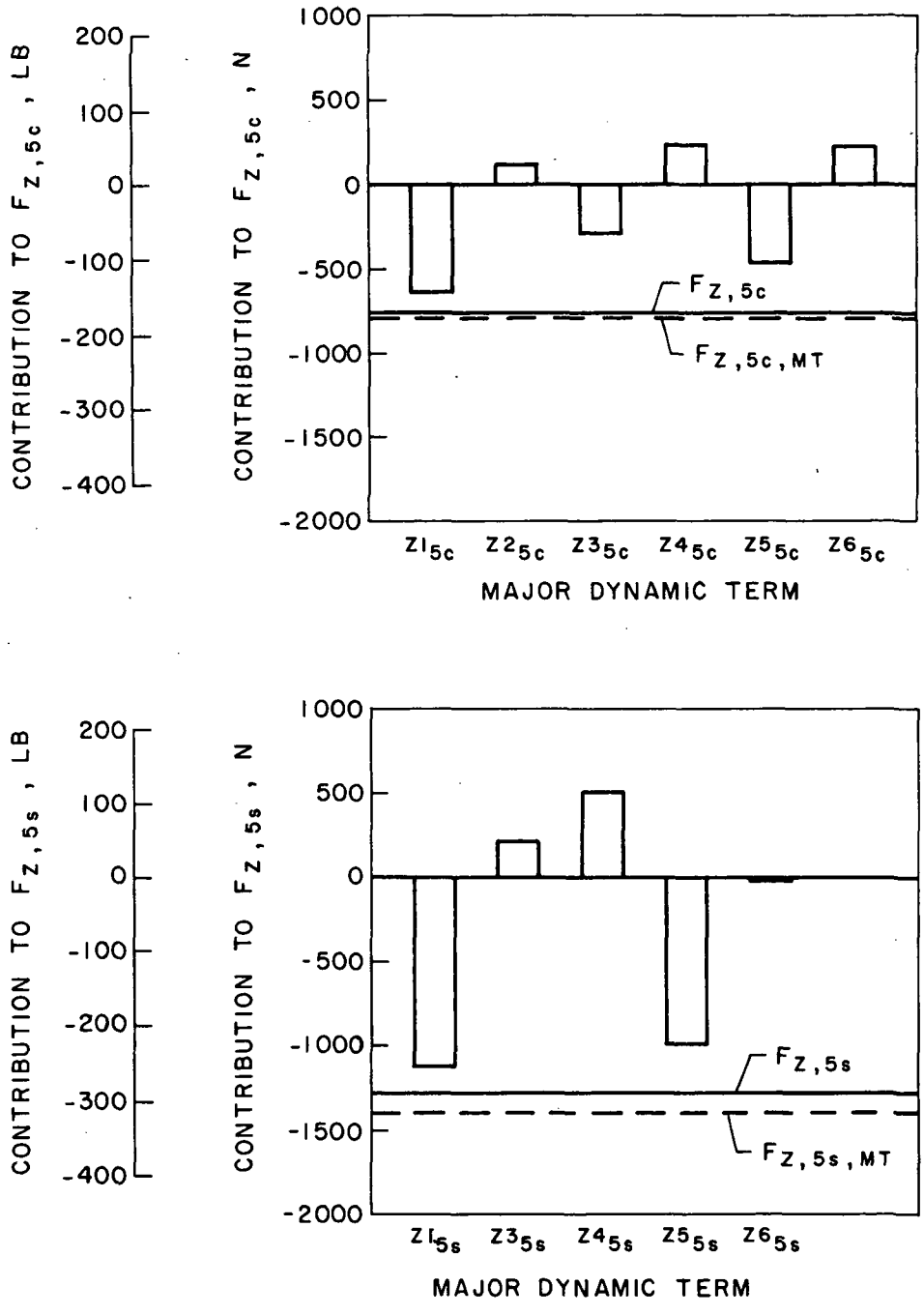

Figure 48.- Major b/Rev Vertical Hub Force Dynamic Terms, NH-3A, $\mu = 0.36$, $\frac{C_T}{\sigma} = 0.043$.

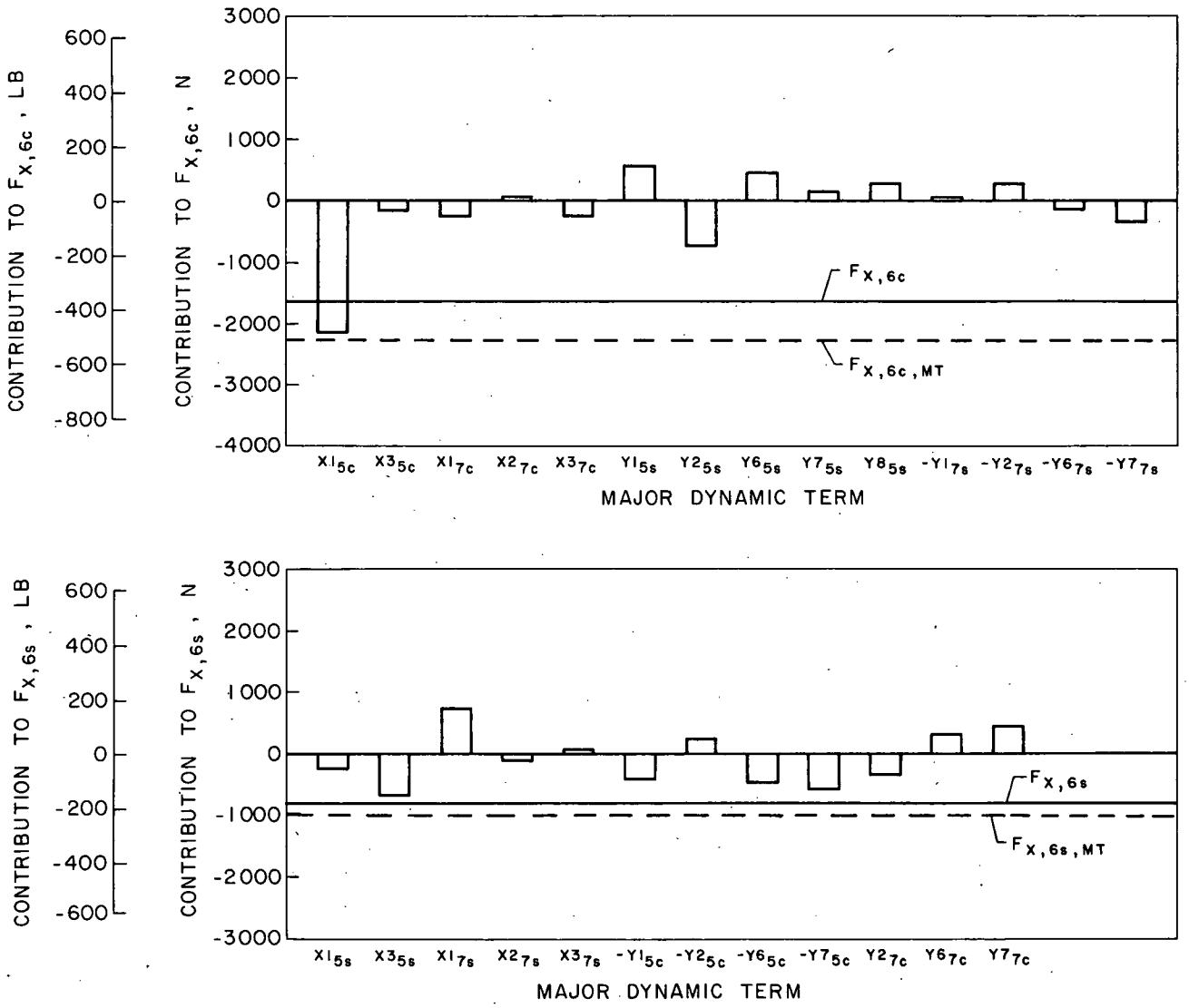

Figure 49.- Major b/Rev Longitudinal Hub Force Dynamic Terms, CH-53A, $\mu = 0.36$, $\frac{C_T}{\sigma} = 0.055$.

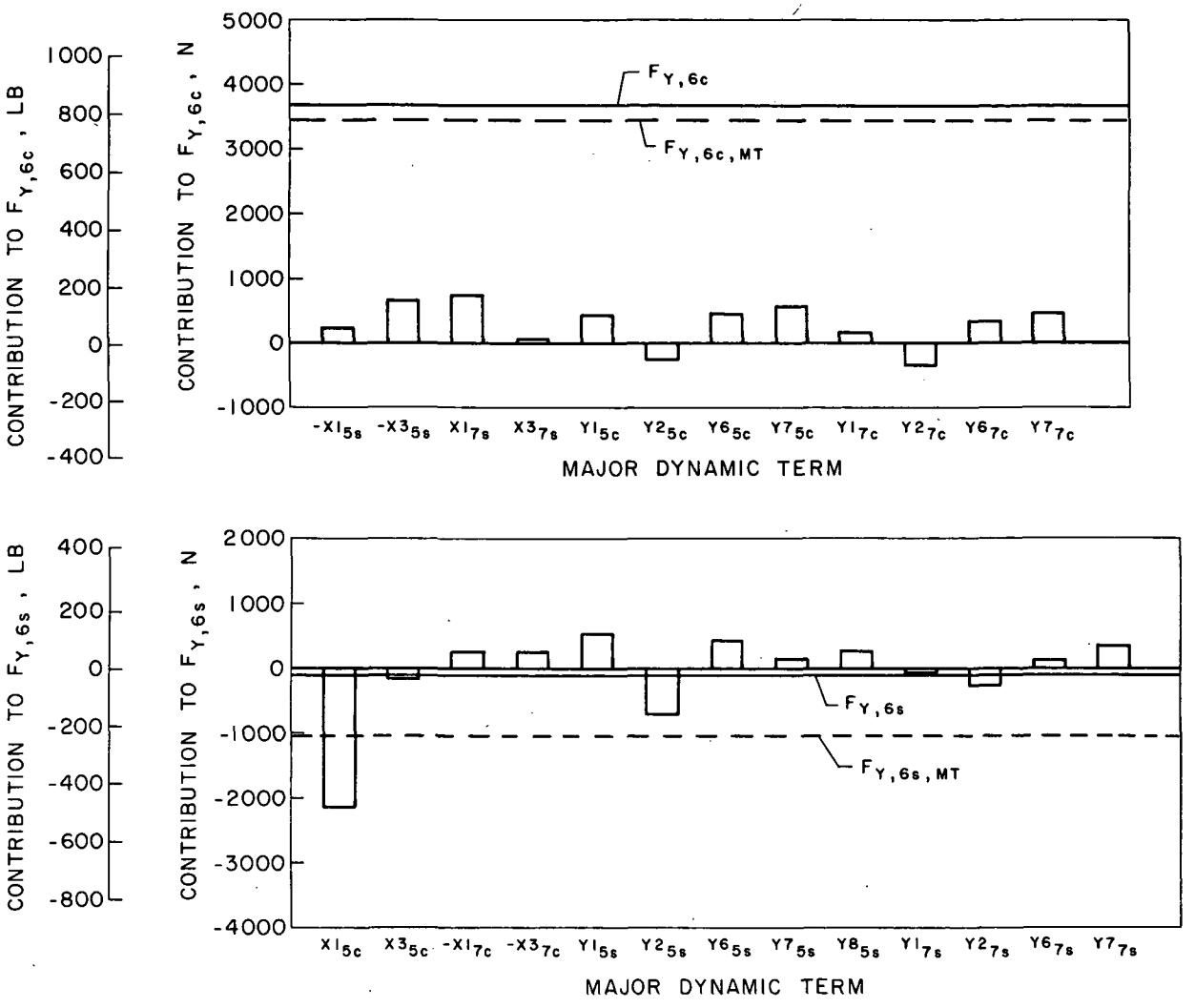

Figure 50.- Major b/Rev Lateral Hub Force Dynamic Terms, CH-53A, $\mu = 0.36$, $\frac{C_T}{\sigma} = 0.055$.

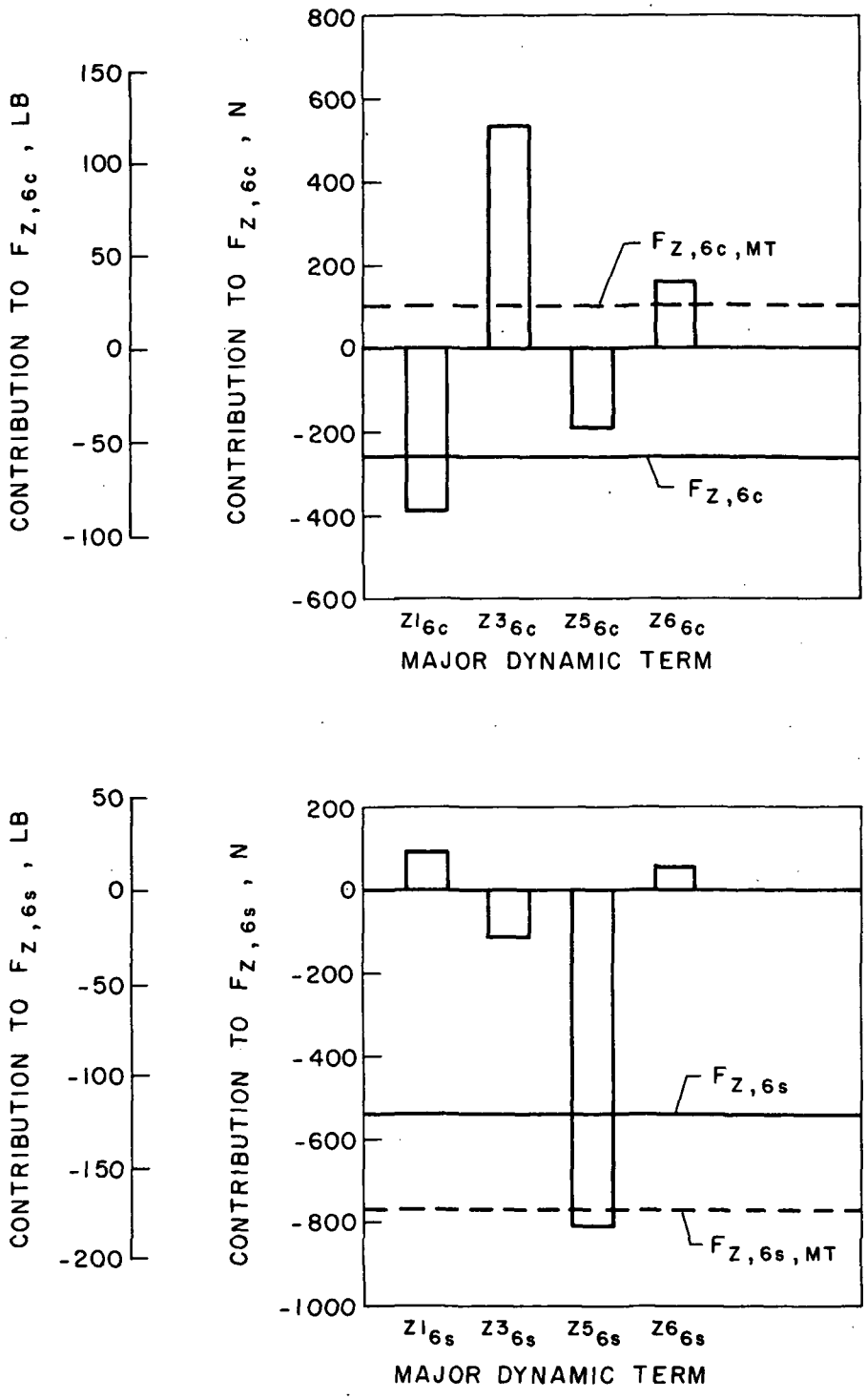

Figure 51.- Major b/Rev Vertical Hub Force Dynamic Terms, CH-53A, $\mu = 0.36$, $\frac{C_T}{\sigma} = 0.055$.

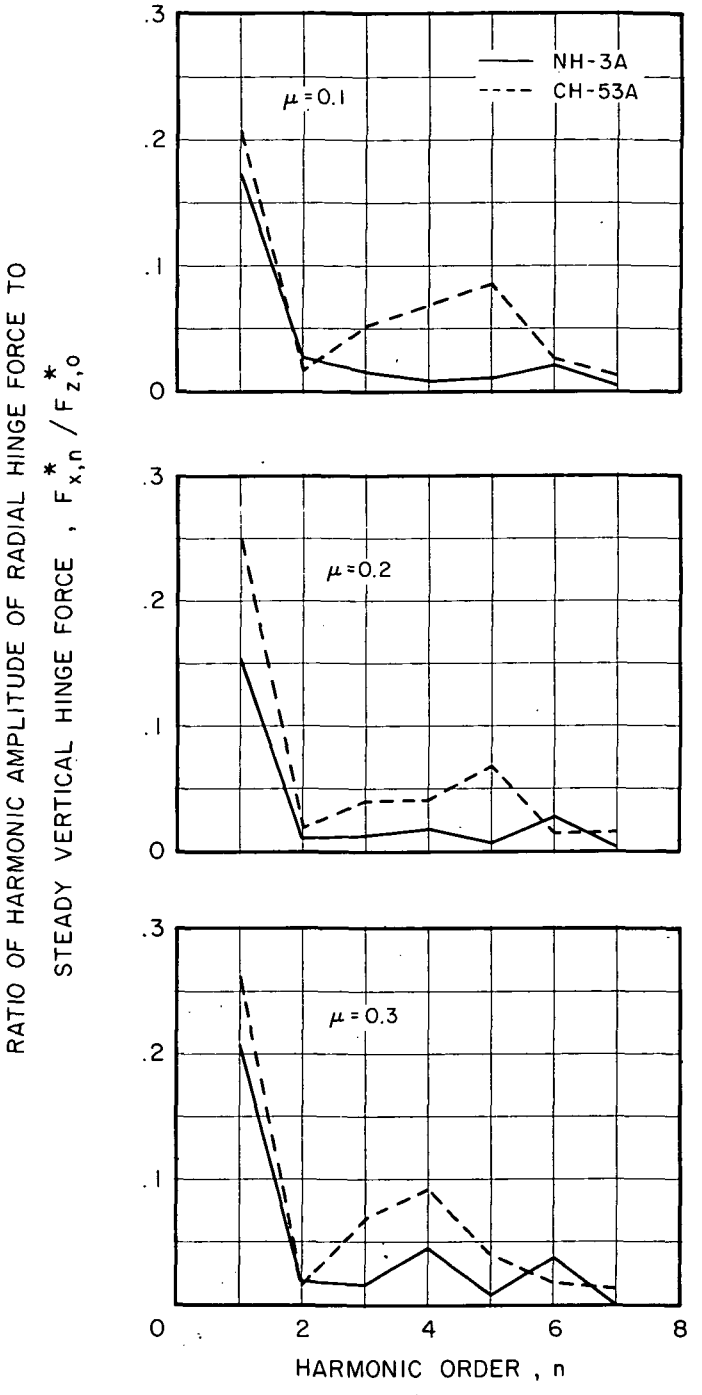

Figure 52.- Comparison of NH-3A and CH-53A Harmonics of Radial Hinge Force.

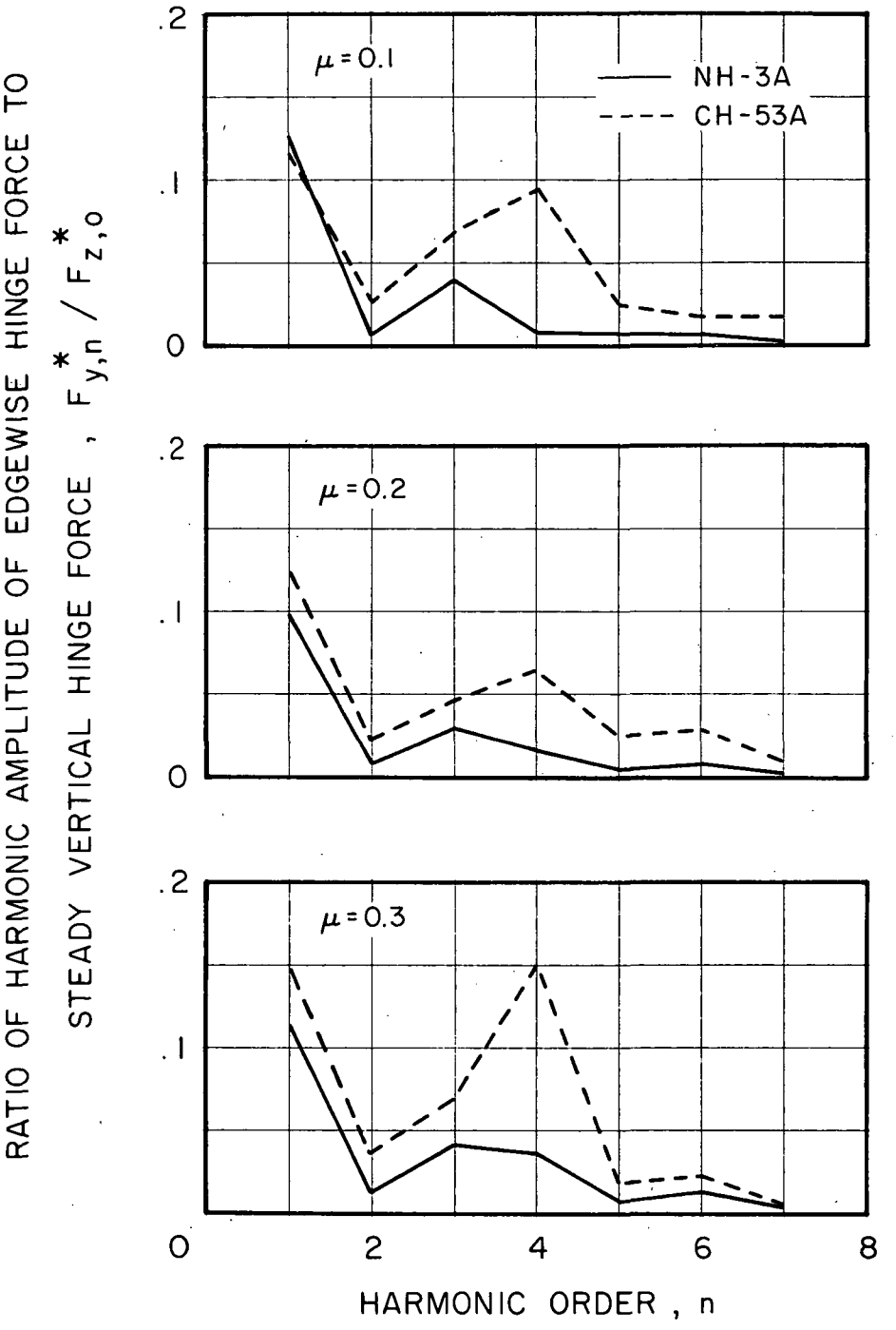

Figure 53.- Comparison of NH-3A and CH-53A Harmonics of Edgewise Hinge Force.

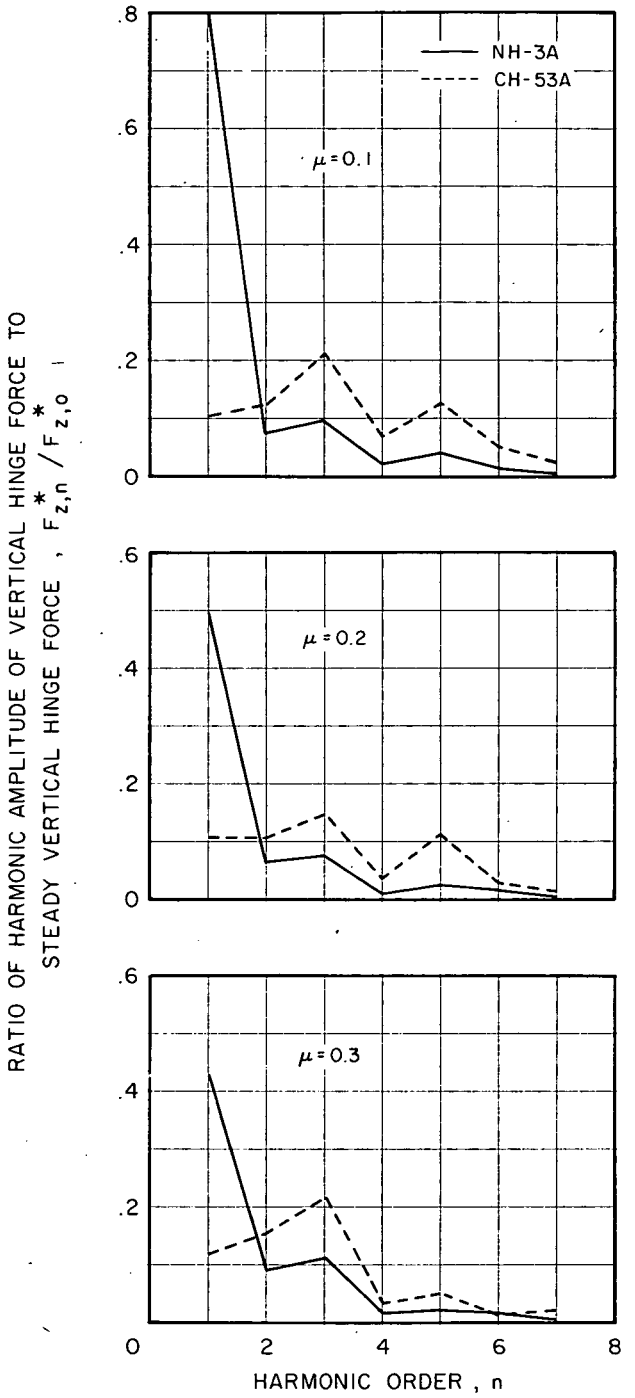

Figure 54.- Comparison of NH-3A and CH-53A Harmonics of Vertical Hinge Force.

"The aeronautical and space activities of the United States shall be conducted so as to contribute . . . to the expansion of human knowledge of phenomena in the atmosphere and space. The Administration shall provide for the widest practicable and appropriate dissemination of information concerning its activities and the results thereof."

—NATIONAL AERONAUTICS AND SPACE ACT OF 1958

NASA SCIENTIFIC AND TECHNICAL PUBLICATIONS

TECHNICAL REPORTS: Scientific and technical information considered important, complete, and a lasting contribution to existing knowledge.

TECHNICAL NOTES: Information less broad in scope but nevertheless of importance as a contribution to existing knowledge.

TECHNICAL MEMORANDUMS: Information receiving limited distribution because of preliminary data, security classification, or other reasons. Also includes conference proceedings with either limited or unlimited distribution.

CONTRACTOR REPORTS: Scientific and technical information generated under a NASA contract or grant and considered an important contribution to existing knowledge.

TECHNICAL TRANSLATIONS: Information published in a foreign language considered to merit NASA distribution in English.

SPECIAL PUBLICATIONS: Information derived from or of value to NASA activities. Publications include final reports of major projects, monographs, data compilations, handbooks, sourcebooks, and special bibliographies.

TECHNOLOGY UTILIZATION PUBLICATIONS: Information on technology used by NASA that may be of particular interest in commercial and other non-aerospace applications. Publications include Tech Briefs, Technology Utilization Reports and Technology Surveys.

Details on the availability of these publications may be obtained from:

SCIENTIFIC AND TECHNICAL INFORMATION OFFICE

NATIONAL AERONAUTICS AND SPACE ADMINISTRATION

Washington, D.C. 20546